ADAPTIVE INFORMATION PROCESSING DURING DETECTION AND DISCRIMINATION OF TACTILE SENSORY STIMULI

A Dissertation
Presented to
The Academic Faculty

by

Douglas Robert Ollerenshaw

In Partial Fulfillment
of the Requirements for the Degree
Doctor of Philosophy in the
Department of Biomedical Engineering

Georgia Institute of Technology
Emory University

December 2013

ADAPTIVE INFORMATION PROCESSING DURING DETECTION AND DISCRIMINATION OF TACTILE SENSORY STIMULI

Approved by:

Dr. Garrett B. Stanley
Biomedical Engineering
Georgia Institute of Technology
Emory University

Dr. Christopher J. Rozell
Electrical and Computer Engineering
Georgia Institute of Technology

Dr. Robert Liu
Biology
Emory University

Dr. Lena H. Ting
Biomedical Engineering
Georgia Institute of Technology
Emory University

Dr. Cornelius Schwarz
Systems Neurophysiology
Werner Reichardt Centre for Integrative Neuroscience
University of Tübingen

Date Approved: August 19, 2013

To Elliott and Adrienne

Acknowledgments

The work presented here wouldn't have been possible without the help of a group of very important people, and I'm grateful to each one.

First of all, thanks to all of my fellow graduate students in the Stanley lab, Daniel Millard, Clare Gollnick, He Zheng, Sean Kelly, Clarissa Shephard, and Peter Borden, for all of the great conversations about both science and life. Every one of them has been amazingly generous with their time to help this work along, and they've also made the long days in the lab fun. But more than anything, their own hard work and accomplishments have set a high bar that I've done my best to match. Being surrounded by such talented colleagues has forced me to push myself harder than I ever knew possible.

I have also had the pleasure of working with a great group of undergraduates and lab technicians that helped immensely with data collection, along with making a countless number of intellectual contributions. Jane Puntkattalee, Spencer Neely, Christopher Pace, and Elaina McLean all became experts at animal handling and training and helped collect some great data. But the one student that was involved almost from start to finish was Bilal Bari, who deserves special thanks. It was an honor getting to see such a gifted future scientist and physician at the beginning of what will be an amazing career. I was also extremely fortunate to be able to build my behavioral work on the solid foundation that Lauren Orr created during her year in the lab as a technician, and Beth Bosworth and Emilio Salazar were amazingly helpful in the latter stages.

I also owe a huge thanks to all of my committee members, Robert Liu, Chris Rozell, Cornelius Schwarz and Lena Ting for an incredible amount of help in directing the science and for helping me take the first steps toward a career after the Ph.D. I know how many demands are made of a faculty member's time, and I appreciate every bit that was given over to me. I owe Cornelius, along with his lab members, an additional debt of gratitude for hosting me in Tübingen during the summer of 2010. The quality of my work took massive steps forward after that trip, and none of the results presented here would have been possible without the training I received in Germany.

I was also fortunate to have what amounted to a second Ph.D. advisor during the majority of my time as a graduate student. Until leaving early this year for Columbia University, Qi Wang kept a watchful eye on almost every aspect of my project. I was constantly in awe of his technical skills and the patience he displayed in sharing his knowledge with others. On rare occasions when he wasn't in the lab himself, his office door was nearly always open. Qi provided a great example of how to be not just a good scientist and engineer, but also a good person.

And of course, I'll be forever indebted to my advisor Garrett Stanley. Garrett has been the ideal advisor, giving me enough space to both make my own mistakes and to feel that my project was my own, but also keeping a close watch on progress and making sure I stayed more or less on track. And despite the demanding schedule, the tight deadlines, and the constant pressure to keep the lab operating, Garrett always managed to convey

excitement about his work and to maintain a great balance with life outside of the lab. He's been a great role model in every respect.

But above all else, I owe a huge thanks to my wife Adrienne. She's been amazingly supportive, forgiving me for long hours at the lab and keeping me sane at times when I felt like I'd never make it through the process. But more importantly, she has been a wonderful mother to our new son Elliott. I hope that they can both be proud of the work I've done so far, and of the career that I'm about to embark upon. There could be no better measure of success.

Table of Contents

List of Figures

Summary

Our sensory systems provide us with our ability to perceive and ultimately act upon the world around us. However, the transformation from external stimulus to perception is more complex than the simple transduction of an event – an object touching the skin, photons striking the retina, sound waves entering the ear – into action potentials. Our perceptions are constantly modified as the brain extracts only certain bits of sensory information and ignores others, or interprets the information differently based on the context and past history of the system. For instance, changing task demands require different sensing strategies. One such example that will be studied in depth here is the ability to both detect the presence of external stimuli and to correctly identify the source of those inputs. It has long been held that the brain is capable of switching between processing modes that allow it to better perform these two types of tasks, detection and discrimination, depending upon the current demands on the system (Crick, 1984; Sherman, 2001a). In the detection mode, the system is thought to code for the presence of stimuli with a strong volley of action potentials that helps to ensure that the stimulus is detected. This type of information processing mode would be especially helpful at alerting the system to unexpected stimuli. Alternatively, in the discrimination mode, the system more faithfully transmits information about particular features of the stimulus using lower firing rates that more closely track small changes in the stimulus. In the simplest sense, this switch effectively represents a change in gain in the system: in the high gain mode, stimuli cause a strong but potentially indiscriminable burst of activity in the system, while in the low gain state, stimuli become more discriminable, but potentially at the expense of the ability to detect weaker inputs.

How the system might be capable of switching between these two processing states remains an open question. Top down processes, such as attention, undoubtedly play a large part, and there is a rich literature focused on exploring attention and its role in sensory processing (Posner and Petersen, 1990; Desimone and Duncan, 1995; Kandel et al., 2000; Kastner and Ungerleider, 2000; Gilbert and Li, 2013). For example, the activity of neurons in the visual cortex have been shown to be modulated depending only upon where in visual space the subject was attending, even when the eye remained fixed (Wurtz et al., 1982). Such attentional processes are thought to be modulated by areas such as the prefrontal cortex and form an important part of conscious awareness (Crick and Koch, 1990, 2003). While there is a huge amount yet to be explored regarding the role of attention on sensory processing, a more immediately tractable and no less important question concerns the contribution of bottom-up processes, or those dictated purely by the stimuli themselves, on subsequent neural processing. It has long been known that such bottom-up processes play an important role in modulating the switch between neural response modes (Sherman, 2001b; Moore, 2004). Furthering this idea is the fact that cortical responses can be shaped in a manner that would appear to make stimuli either more detectable or discriminable even in the anesthetized animal, for which top down processes have been effectively eliminated, and based solely on the recent history of the stimuli themselves (Sheth et al., 1998; Lesica and Stanley, 2004; Wang et al., 2010). The work presented here will focus predominantly on these bottom up, sensory driven changes in neural processing.

This change in neural processing due to stimulus history is a phenomenon known as sensory adaptation (Clifford et al., 2007). A simple and long observed example of sensory adaptation is the waterfall illusion, in which, after fixating on a waterfall for an extended period of time, then looking away, the visual world appears to be moving upward (Crane, 1988). More generally, sensory adaptation can be seen as the matching of the range of outputs of a sensory system to the currently relevant distribution of stimuli (Wark et al., 2007). Such an adaptive change in information processing would allow sensory systems to encode information much more efficiently than would be possible with a system that was designed with a range of outputs spread over the range of all possible sensory inputs (Barlow, 1961; Laughlin, 1989; Simoncelli, 2003). The effects of sensory adaptation on neural processing occur rapidly, tend to decay on a similarly short timescale on the order of a few seconds, and have profound impacts on the nature of sensory processing and perception (Chung et al., 2002; Tannan et al., 2006; Lesica et al., 2007).

The strategies employed by the organism, be it a lab animal or a human, also have a profound impact on the way sensory information is encoded. For instance, self-generated sensory events as a result of active sensation are encoded differently from those resulting from passively applied stimuli (Cullen, 2004), which allows externally generated events to be distinguished from those resulting from an organism's own motion. Hence our inability to tickle ourselves (Blakemore et al., 1998). In addition, different behavioral states such as inattentiveness, quiet attention, or active exploration are also applied with different neural processing states (Fanselow and Nicolelis, 1999; Ferezou et al., 2007;

Gilbert and Sigman, 2007; Poulet and Petersen, 2008; Niell and Stryker, 2010; McManus et al., 2011). Thus, the behavioral state and active sensing strategy of the subject also have important effects on neural coding and perception.

The vibrissa, or whisker, system of rats was chosen as a model system for the experiments described here for a number of reasons. The vibrissa system has become a very popular model for tactile sensation due to the fact that rats (along with mice and some other rodents) are capable of actively palpating their whiskers in a form of active sensation known as 'whisking' that is roughly analogous to a human moving their hands to feel an object (Kleinfeld et al., 2006). In addition, the vibrissae form a stereotyped array of rows and arcs that is conserved from animal to animal, making direct comparison of stimuli applied to each animal possible (Petersen, 2007). The discrete nature of the whisker system is conserved at each level of neural processing to at least the level of the primary sensory cortex (S1), where each whisker is represented by a separate barrel-shaped column of tissue that has led the area to be called the 'barrel cortex.' Each barrel in the barrel cortex receives its primary inputs from a distinct region in the thalamus known as a 'barreloid.' It is thus possible to record neural activity in either the thalamus or the cortex in response to the deflection of a single whisker. Finally, given the importance of pairing neural activity to behavior, the rat makes an ideal model system for the experiments described here due to the relative ease with which it can be trained to perform complex behavioral tasks (Carandini and Churchland, 2013). This allows us to more or less 'ask' the rat what it is feeling by training it to respond to stimuli in a characteristic way. While the vibrissa system is a highly specialized sensory system

unique to rodents, insights gained from work in this model system will provide more general insights into neural coding, sensory processing, and perception in other species, including humans.

The work presented in this thesis uses a combination of neural recordings in both the awake and anesthetized animal, combined with a series of behavioral tasks performed by awake rats, with the goal of understanding how sensory systems both detect and discriminate between stimuli. More specifically, the goal was to understand how the effects of sensory adaptation and the animal's own active sensing strategy affect its ability to perform sensory tasks, and how changes in neural coding ultimately drive these changes.

In a series of experiments detailed in Chapter 2, rats were trained to respond to brief puffs of air delivered to their vibrissa (whisker) array by licking a water spout in a brief interval following the stimulus. The animals were head-fixed to minimize variability in the applied stimulus and the experiments were carefully controlled to avoid the possibility that the animals could respond to cues other than the mechanical forces imparted at the whisker follicles as a result of the air puff stimulus. The strength of the stimulus was then varied to measure performance as a function of whisker deflection velocity, and high speed video was used to monitor the animals' own self-generated whisker motion prior to the delivery of the stimulus. When performance in the detection task was parsed based on pre-stimulus whisker motion, performance was shown to be significantly better when the animals avoided whisking and held their whiskers still. This result appears

counterintuitive at first in that an active sensing strategy - whisker motion - might be expected to improve the animals' chances of detecting the stimulus, much as a person might actively feel their way around a dark room to search for the light switch. However, whisker motion itself leads to activity in the pathway that could potentially overwhelm the activity caused by weak sensory inputs. It is also known that the brain is optimized for detecting weak stimuli when an animal is in a behaviorally quiescent state (Fanselow and Nicolelis, 1999; Ferezou et al., 2007). Thus, a better analogy might be to a person listening for a quiet sound - they are likely to limit their own motion as much as possible to maximize the possibility of hearing it.

In a further set of experiments also described in Chapter 2, neural recordings were obtained using voltage sensitive dye (VSD) imaging from the cortex of anesthetized rats receiving the same stimulus set as those in the behavioral task. VSD imaging allows the subthreshold membrane potential of layer 2/3 neurons to be recorded over a relatively large spatial extent (the majority of the barrel cortex), and with high temporal resolution (200 Hz, or 5 ms between captured images). The recorded neural data from the VSD imaging experiments was used to the input of a model of the decision making process that assumed that the animal was monitoring incoming sensory evidence and more heavily weighting recent data to form a decision about the presence or absence of an external stimulus. Such models, known as 'leaky integrators,' are thought to simulate the manner in which a higher brain area might monitor primary sensory data to ultimately form a decision about the presence of a stimulus (Gold and Shadlen, 2007). The output of

this model provided a very close match between the predicted and actual detection performance of the animals.

In contrast to asking how the animals' own self-motion affects sensory processing, as in Chapter 2, the experiments described in Chapter 3 explore the process by which an ongoing sensory input leads to changes in the ability to both detect and discriminate subsequent inputs through the process of sensory adaptation. Animals were first trained in a detection task similar to that used in Chapter 2, with two important changes: that an individual whisker was deflected with a much more repeatable stimulus delivered to a single whisker by a piezoelectric actuator, and that a subset of stimuli were preceded by an adapting stimulus that consisted of a 12 Hz sinusoidal deflection applied to the whisker. We first found that detection performance was reduced after the animal was exposed to the adapting stimulus. Further, we found that as the time interval between the end of the adapting stimulus and the deflection increased, giving the system more time to recover from the effect of adaptation, the detection performance became more similar to that seen in the non-adapted state. This reduced detection performance after adaptation could be analogous to that seen with self-motion in Chapter 2 - whether self-generated or externally applied, ongoing sensory activity leads to a reduced ability to detect subsequent stimuli.

However, beyond just a deleterious effect on detection ability, an important additional question is the extent to which the effects of adaptation could be beneficial to the animal. Previous work had indicated that adaptation could lead to a more constrained cortical

response (Sheth et al., 1998), which could lead to an improved ability to discriminate between nearby inputs (Moore et al., 1999; Moore, 2004). To test this, the rats were subsequently trained on a novel task in which they were asked to discriminate between inputs to two nearby, and potentially adjacent, whiskers, both in the presence and absence of a preceding adapting stimulus. Consistent with predictions, the animals displayed an improved spatial discrimination ability after exposure to the adapting stimulus.

Finally, in Chapter 4, neural recordings were made in the thalamus of awake behaving animals to attempt to better understand the changes in neural coding that lead to these changes in cortical processing and ultimately in task performance. Given its important role as the final input stage to the barrel cortex, the ventroposterior medial (VPm) nucleus of the thalamus was chosen as the site for these recordings. Recordings of spiking activity from collections of neurons in the VPm were obtained using chronically implanted microwire electrodes implanted on moveable arrays, allowing them to be moved into position in the VPm only after the animals had learned the necessary behavioral task. Consistent with previous findings in the anesthetized animal, it was found that the thalamic neurons responded to adaptation by firing fewer and less temporally precise spikes, both of which likely contribute to the decreased detectability and improved discriminability. The thalamus was found to recover from the effects of adaptation with a similar time course as was seen in the behaving animals in Chapter 3. When the measured changes in the firing statistics of the thalamus were used as the input to a spatiotemporal model of the thalamocortical circuit, the model predicted changes in cortical processing that were analogous to those measured in the brains of anesthetized animals in Chapter 3.

Together, these results implicate changes in neural coding in the VPm nucleus of the thalamus due to sensory adaptation as critical in driving both the changing cortical response properties and the resulting behavioral shift toward improved spatial discrimination ability at the expense of detection performance.

The results of this work will help us to better understand how our sensory systems naturally interact with the outside world, where constantly shifting task demands are placed on the system. Neither detection nor discrimination is done in isolation. Instead, the system must constantly switch between processing states. In addition, this work could add insights into multiple possible clinical problems. For instance, it has been shown that adaptation fails to alter discriminability of tactile inputs in autistic individuals, a finding that appears related to abnormalities in the cortical circuitry (Tommerdahl et al., 2007). Better understanding of the cortical effects of adaptation, and the related behavioral manifestations, could therefore lead to useful diagnostic tools for autism and related pathologies. In addition, sensory prostheses, from cochlear to retinal to thalamic and cortical implants, revolve around the ability to provide useful surrogate signals to sensory pathways, requiring a firm understanding of the manner in which sensory inputs are processed in intact pathways. Further, despite the recent progress toward cortical control of motor prostheses, the lack of tactile and proprioceptive sensory feedback limits the potential applicability (Gilja et al., 2011). However, the effect of adaptation is lost without ongoing peripheral inputs. A more complete understanding of sensory adaptation and its effect on the resulting percept is therefore absolutely critical for the clinical success of engineered interfaces.

Chapter 1 - Introduction

As we navigate the natural world, our sensory systems are faced with the challenge of extracting useful information from a noisy and constantly changing environment. This task is fundamentally a signal versus noise problem: the nervous system must be capable of detecting salient information amidst a constant barrage of activity resulting from both environmental and internally generated noise, then identifying the source or identity of the input. These two types of tasks, detection and discrimination, place competing demands on the system and require different neural coding strategies to be optimally performed (Crick, 1984; Sherman, 2001a).

However, no discussion of this subject is possible without first addressing the role of top down processing, most notably the role of attention, in driving changes in sensory processing that modulate detection and discrimination performance. It is well known that higher brain areas are capable of asserting top-down influences through attention that affect the way sensory information is ultimately processed (Wurtz et al., 1982; Motter, 1993; Frith, 2001; Sarter et al., 2001; Buschman and Miller, 2007). A commonly used example of this phenomenon is the classic 'cocktail party problem' (Cherry, 1953; Haykin and Chen, 2005), which refers to the ability of an individual to selectively attend to a single source of auditory input - a companion's conversation - amid a chaotic scene of similar and overlapping inputs in a busy room. More specific to the system being studied here, Pais-Vieira et al. (Pais-Vieira et al., 2013) recently demonstrated that neurons in both the thalamus and the cortex of behaving rats displayed anticipatory changes in firing rates just before contact with objects in a whisker mediated behavioral

task, and that these changes were correlated with task performance. In general, these attentional processes are thought to be modulated by areas such as the prefrontal cortex and form an important part of conscious awareness (Crick and Koch, 1990, 2003). While studies of consciousness and attention will ultimately be critical for a complete understanding of how the brain functions, such work is largely beyond the scope of that presented here. Instead, with the exception of the whisking/non-whisking analysis presented in Chapter 2, the focus will be on bottom up, or sensory driven, changes in sensory processing. Care was taken to design experiments to limit the effects of changing attention to the extent possible.

Sensory adaptation fundamentally changes the information conveyed by the circuit:

An important example of changes in information processing due to bottom up processes is sensory adaptation. As a sensory system is exposed to changing environments, the manner in which information is processed in the pathway also changes. Some common examples include moving from a dark to a light room, or from a quiet building to a loud street. In response to these environmental changes, the brain has evolved the ability to modify its operating characteristics to fit the range of currently relevant inputs. This modified response, generally called 'adaptation,' can be defined as changes in the operating properties of a neural system in response to changes in the environment (Clifford et al., 2007). It has long been posited that adaptation acts to enhance information flow in sensory pathways (Barlow, 1961; Simoncelli, 2003), and more recent work has begun to shed light on the transient changes in the statistical properties of the sensory signal that result from adaptation (Ahissar et al., 2000; Fairhall et al., 2001;

Chung et al., 2002; Maravall et al., 2007; Benucci et al., 2013). For example, the work of Fairhall et al. (2001) demonstrated that neurons in the visual system of the fly were capable of rapidly adapting to changes in the variance of visual inputs by adjusting the range of firing rates they used to encode visual information. Similarly, Gardner et al. (Gardner et al., 2005) used fMRI to demonstrate that the human visual system is capable of adapting its range of sensitivity to match the ambient ranges in contrast.

Further indicative of its pervasive nature, the perceptual effects of sensory adaptation have been reported in every sensory pathway (Clifford et al., 2007). In the somatosensory pathway, for example, human psychophysical studies have shown that adaptation enhances spatial acuity in the fingertip (Tannan et al., 2006). In that study, researchers asked human subjects to identify which of two sites on their fingertip was mechanically stimulated following either a long (5 seconds) or short (0.5 seconds) application of a 25 Hz vibrotactile adapting stimulus to the fingertip. Subjects reported up to a 2-fold decrease in the minimum spacing between input locations required to correctly discriminate the inputs after the longer period of adaptation. Though the neural basis for this improvement in performance is unclear, it has been hypothesized that the increased acuity could be linked to reductions in the spatial extent of cortical activation resulting from tactile inputs with adaptation (Vierck and Jones, 1970; Lee and Whitsel, 1992; Lee et al., 1992). Furthering this theory, intrinsic optical imaging studies in the anesthetized monkey (Simons et al., 2005, 2007; Tommerdahl et al., 2007) and rat (Sheth et al., 1998) demonstrated a more focal cortical response to tactile inputs following adaptation. Combined, these results demonstrate that adaptation leads to potentially important

changes in cortical processing in parallel with perceptual changes. Given that adaptation is likely to occur in parallel with active exploration of the environment, and specifically with whisking in the case of the rodent, these results led to the proposal that adaptation could lead to a specificity/sensitivity tradeoff (Moore et al., 1999; Garabedian et al., 2003; Moore, 2004), with better sensitivity in the non-adapted state and improved specificity after adaptation. In other words, sensory adaptation might serve to sharpen the contrast between inputs during exploration in exchange for a less robust response to any given input.

This large body of work indicates that adaptation is not merely a trivial effect of synaptic fatigue or some related mechanism, but instead reflects a fundamental change in the features to which the pathway is sensitive. Along these same lines, recent work from the Stanley lab using anesthetized rats demonstrated that adaptation led to a sharpened cortical response to inputs of both varying velocities and directions, a phenomenon attributed to a reduction in synchronous activity of the thalamocortical projecting neurons (Wang et al., 2010). From the perspective of an ideal observer of cortical activity, this implied that the animal's performance in a discrimination task would be improved in the presence of an ongoing adapting background stimulus, but at the expense of its detection performance, as suggested by Moore et al. (1999). However, this assertion has yet to be tested in the awake animal, and doing so forms an important aspect of the work presented here.

Controlled behavioral tasks allow the limits of sensory systems to be measured:

Though sensory systems are capable of extracting useful information from very complex environments, controlled experiments generally require a simpler and more repeatable set of inputs in order to make their study tractable. The fields of psychophysics and decision theory provide a framework upon which to build experiments for the study of sensory processing (see Carandini and Churchland (Carandini and Churchland, 2013) for a recent review of decision theory and psychophysics as applied to rodents), thus allowing us to directly test the effects of both sensory adaptation and the animal's active sensing strategy on their ability to perform detection and discrimination tasks. This type of framework also allows direct comparison of neural activity recorded during stimulus presentation, whether in the anesthetized animal, or more ideally in the awake animal, with the awake animal's behavioral output.

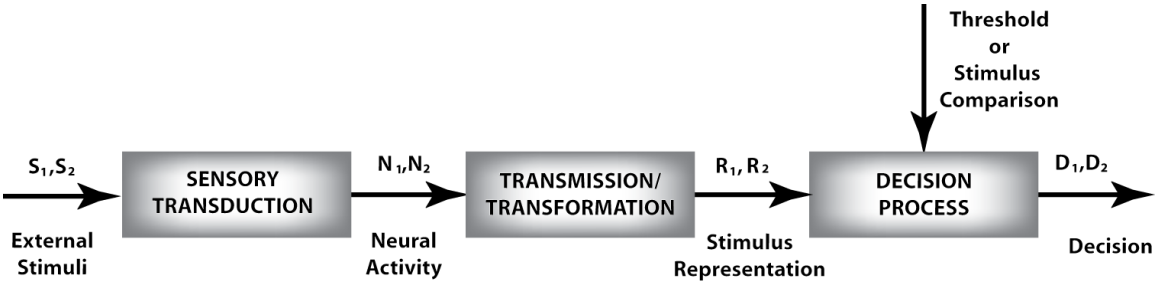

Figure 1-1 - *Schematic model of the sensory decision making process*. External stimuli are transduced by sensory organs into neural activity. The neural activity is transmitted through the sensory pathway and undergoes various transformations along the way. The final stimulus representation is compared against internal criteria in order to form a decision. (Figure adapted from Johnson, 1980)

Figure 1-1, which was adapted from Johnson (1980), shows a simple schematic of the steps in the decision making process in a basic laboratory task, though the general principles apply to sensory decision making in general. In this example, one of two possible stimuli (S_1 or S_2) is delivered to the subject on a given trial. S_1 and S_2 could be from two possible classes of stimuli, a type of problem that will here be referred to as a discrimination problem; or S_2 could be a stimulus that the animal is required to respond to while S_1 is simply noise, or the lack of a stimulus. This latter type of task will here be referred to as a detection task. In either case, the stimulus is transformed into a series of action potentials distributed across a potentially large number of afferent neurons - designated by N_1 and N_2 in **Figure 1-1** - by the sensory organ, be it the eye, the ear, the skin, or as will be the case throughout this body of work, the rodent whisker.

As the neural signal is transmitted through the early sensory areas and on to the cortex, it undergoes a series of transformations that lead from relatively simple representations at or near the periphery (a retinal ganglion firing action potentials in proportion the amount of light on a specific region of the retina, for instance (Masland, 2001)), to much more complex and often abstract representations in higher processing areas (a neuron firing in response to Jennifer Anniston's face, for instance (Quiroga et al., 2005)).

The final stimulus representation, R_1 or R_2, is then compared against internal criteria in order to form a decision about the proper action to take. As an example, in the case of detecting a stimulus amidst ongoing noise, the amount of neural activity on a given trial

could be compared against a threshold, above which the subject responds by indicating the presence of the stimulus. Alternatively, in the case of two possible types of stimuli, the amount or type of neural activity is compared against the stored representations of past stimuli in order to determine to which class the current stimulus belongs, followed by the appropriate behavioral response.

Understanding these transformations from sensory stimuli to neural data at various processing stages, and attempting to understand how they relate to our perceived representations of the outside world, forms an important part of sensory neuroscience (Stanley et al., 1999; Jacobs et al., 2009; Stüttgen et al., 2011). The neural representation of sensory stimuli, N_1 and N_2, can initially be distributed over a large population of neurons and potentially over extended periods of time. In Chapter 2 of this thesis a general model for spatially and temporally integrating this early sensory information into a single response variable, R, is introduced and the resulting predicted decisions and response latencies were compared to those of awake behaving animals performing a detection task. Similarly, in Chapter 3, the cortical response is integrated in space and time to form a set of response variables representing either whether a whisker was deflected (detection), or which whisker was deflected (discrimination), both in the presence and absence of sensory adaptation. The resulting response variables, R_1 and R_2, were again compared to the animals' response probabilities to help explain how the decisions D_1 and D_2 (go or no/go in this case) are made. Finally, in Chapter 4, recordings were made earlier in the pathway to better understand how transformations in the neural

data, N, leads to observed changes in the response variables and ultimately in the animals' decisions.

While these measurements would ideally be performed simultaneously in an awake, behaving animal, technical considerations have led to the majority of the electrophysiological results presented here being recorded in the anesthetized animal with corresponding behavior in the awake animal. In the final chapter, recent successful work in recording thalamic activity in the awake animal is also described and helps to bridge the gap between the anesthetized electrophysiological studies and the corresponding behavioral results. Under the signal detection theory framework, both detection and discrimination become similar problems: the ability to distinguish between stimuli (Green and Swets, 1966; Macmillan and Creelman, 2004).

In the case of detection, the stimulus might be a signal of varying strength which the participant must distinguish from background noise. The stronger the signal becomes, the more distinct it becomes from the background and the higher the probability of response for the animals. There are therefore two quantities of interest. The first is the false alarm rate, which is the probability of response given no stimulus. In the detection task designs presented here, we directly measure this by presenting a distractor stimulus that we call the S- stimulus. The false alarm rate is then P(R|S-), or the total number of responses divided by the number of S- trials. The other quantity of interest is the hit rate for a given stimulus strength, which is the probability of the animal responding in a fixed time window following the stimulus, which we define as the S+ stimulus. The hit rate is thus

P(R|S+). Performance can then be quantified in a couple of ways. If the false alarm rate remains consistent across experimental conditions, the hit rates can be compared directly. For instance, in many cases throughout the work presented here, the 'perceptual threshold' or 'detection threshold' is used as the quantity of interest. This is calculated by fitting a sigmoidal curve to all of the calculated response probabilities in a given condition, then measuring the point at which it crosses the halfway point between chance performance and maximum performance. Alternatively, if the assumption is made that both the signal and the noise are drawn from Gaussian distributions of equal variance, such as is shown in **Figure 1-2A**, performance can be measured as the distance between these two hypothetical Gaussian distributions. This quantity, d' is calculated as:

$$d' = z(P(R_{S+})) - z(P(R_{S-})) \quad (1)$$

where z represents the inverse cumulative normal distribution (Macmillan and Creelman, 2004).

Similarly, discrimination tasks require the participant to distinguish between two or more sensory inputs. In the simplest case, the discrimination task is mathematically identical to the detection task, with an S- and S+ stimulus and discrimination performance described using d' as in equation 1. As these inputs become more distinct and discriminable, the task becomes easier to perform and d' becomes larger.

In the case of both detection and discrimination, the simplest type of task, and that which is most easily trained in animals such as rats, is the 'yes/no' or 'go/no-go' task (Macmillan and Creelman, 2004; Schwarz et al., 2010; Carandini and Churchland, 2013), in which the subject is asked to respond to the presence of a stimulus during a detection task, or one possible class of stimuli in a discrimination task (the S+ stimulus in both cases), while withholding response to either the lack of a stimulus in the detection task, or for a second class of stimuli in the discrimination task (the S- stimulus in both cases), as shown in **Figure 1-2**. More complex tasks, such as the 'two alternative forced choice' (2AFC) task, in which the subject is given the option of choosing between multiple outputs, provide even higher levels of experimental control in that they allow hits and misses to be unambiguously separated from false alarms and correct rejections. However, the 2AFC paradigms come at the expense of increased complexity and extended training time. While it is unlikely that the 'go/no-go' paradigm can be made to match the 2AFC paradigm in the ability to separate response types, careful control of the experiments using catch trials, or trials in which no stimulus is presented, along with careful monitoring of subject motivation can lead to very good results using the 'go/no-go' paradigm (Stüttgen and Schwarz, 2008; Stüttgen et al., 2011; O'Connor et al., 2013).

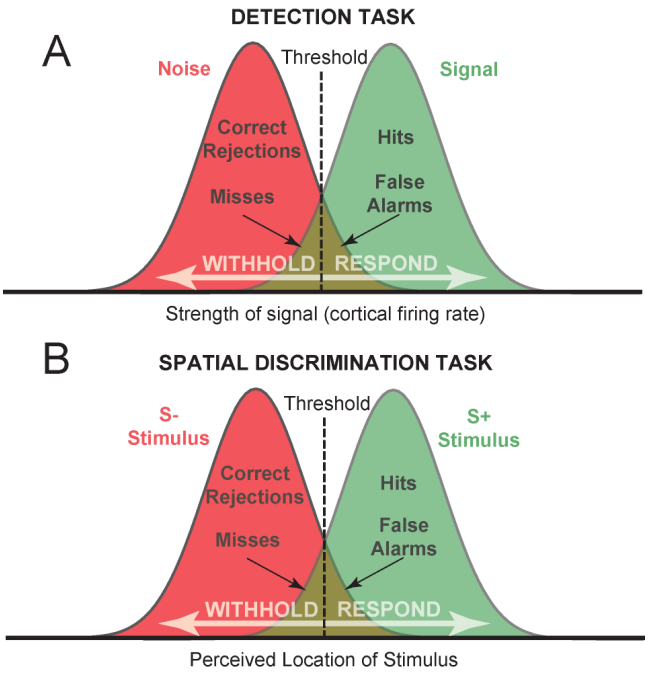

Figure 1-2 - *Schematic of 'go/no-go' paradigm for both a detection and a spatial discrimination task.* **A.** In a detection paradigm, the signal of interest varies in strength. As the stimulus becomes stronger, so too does the cortical response, creating more separation between the signal and noise distributions and making the detection task easier. **B.** In a 'go/no-go' spatial discrimination task, the two stimulus categories are the perceived locations of the stimulus. As the perceived locations become more separated, either through sharpening of the response distributions or by increasing the physical separation of the inputs, the discrimination task becomes easier. Note that for both detection and discrimination in the 'go/no-go' paradigms, correct responses are identical for correct rejections and misses (withhold), and for hits and false alarms (respond), preventing distinctions of these response types by the experimenter.

Detection and Discrimination are two fundamentally different types of tasks:

While detection and discrimination tasks can be described, at least in the simplest of cases, in an identical mathematical framework through signal detection theory, it has long been held that they are actually two distinct types of behavioral tasks that each place unique demands on the system (Crick, 1984; Sagi and Julesz, 1984; Guido and Weyand, 1995; Sherman and Guillery, 2002; Yu et al., 2009). This becomes especially apparent

when considering more than just two possible stimuli. In detection, the system is best served by being maximally responsive to inputs across a wide dynamic range, allowing novel stimuli to be identified against ongoing environmental and sensory noise, as shown in **Figure 1-3B**. During discrimination, performance is maximized by adjusting the dynamic range of the system to allow more subtle features of the stimulus to be discerned, though this could come at the expense of the detectability of weaker stimuli, as in **Figure 1-3D**. This would allow, for example, an animal to quickly detect the presence of something moving nearby, then to focus attention on that object to determine its identity.

It has been posited that these two processing modes require unique, parallel sets of neural circuitry (Sagi and Julesz, 1984; Xu, 2009; Straube and Fahle, 2011). However, perhaps more compellingly and completely in line with the results seen with adaptation, a long line of research suggests that the same circuitry may be capable of rapidly switching between these two processing states by taking advantage of the dynamic interplay between the thalamus and the primary sensory cortex (Güell et al., 1990; Steriade et al., 1993; Sherman and Guillery, 1996, 2002; McAlonan et al., 2008). Such a scheme would thereby allow the same piece of neural circuitry to perform both tasks, requiring only that the nature of the input place the system into the proper processing state. However, the mechanisms by which such a dynamically changing neural circuit might operate are only beginning to be understood.

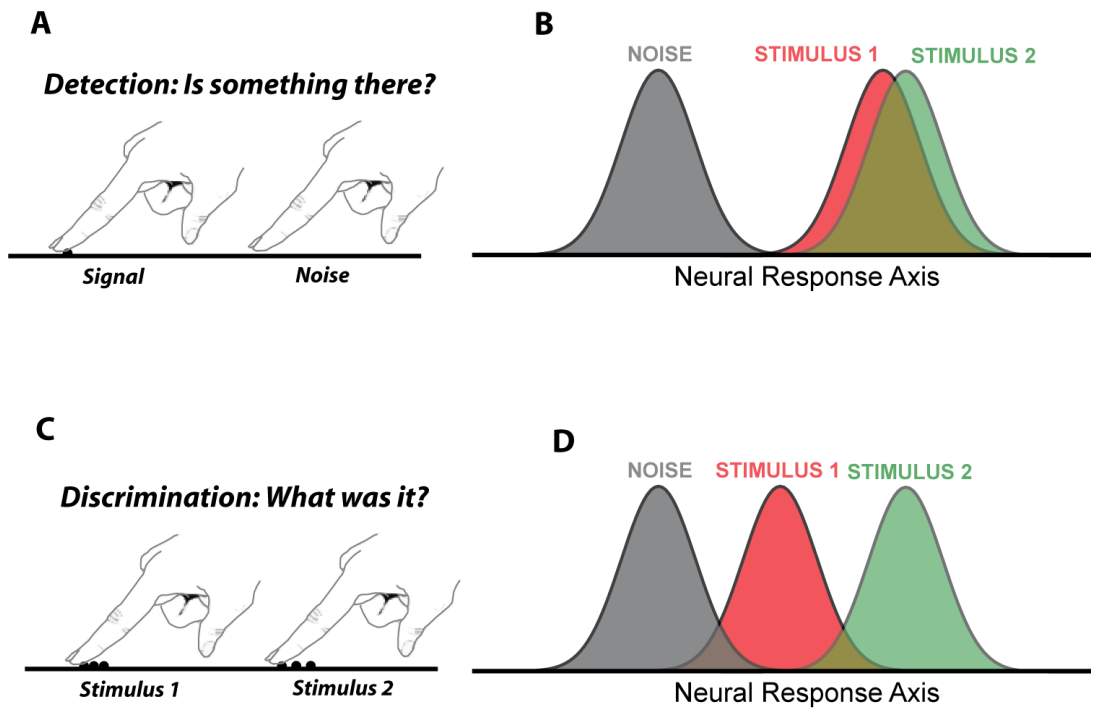

Figure 1-3 - *Cartoon showing idealized neural representations to favor feature detection or discrimination.* **A**. In a detection task, the goal of the system is to identify important signals against environmental and neural noise. **B**. A sensory system would be most effective at detecting inputs if it responded robustly to all inputs, placing the response as far as possible from noise. **C**. In a discrimination task, they goal of the system is to identify the nature of the stimulus to properly categorize it. **D**. In order to best discriminate between classes of possible inputs, the system should maximally spread out the responses to different inputs. However, in many cases this will serve to move the distribution of responses to some stimulus types closer to the noise. Improved discriminability is thus traded for degraded detectability.

The rodent vibrissae system is a powerful system in which to test this phenomenon:

While a great number of the perceptual studies to date have been performed in humans and non-human primates, the rat vibrissae system also provides a tempting additional target for such work and was used as the model system for the studies described here. As nocturnal animals, rats rely largely on their facial vibrissae, or whiskers, to navigate in

their natural environment, and the system has been the subject of active study for the past century (Vincent, 1912). By taking advantage of the exquisite sensitivity of the system, combined with the inherent intelligence of the animals themselves (Davis, 1996), researchers have been able to train rats and other rodents to perform complex whisker mediated detection and discrimination tasks (Carvell and Simons, 1990; Krupa et al., 2001, 2004; Mehta et al., 2007; Diamond et al., 2008a; Ritt et al., 2008; Jadhav et al., 2009; Gerdjikov et al., 2010; O'Connor et al., 2010b).

Further, beginning with the work of Harvey and colleagues (Harvey et al., 2001), a limited number of laboratories have begun training rats and other rodents to perform these behavioral tasks under head fixation (Stüttgen et al., 2006; Butovas and Schwarz, 2007; Bryant et al., 2009; O'Connor et al., 2010a; Stüttgen and Schwarz, 2010). Head fixation has been a common strategy in primate research for decades, and its use in rodents provides the promise of much more carefully controlled experiments to probe both behavior and its neural correlates (Schwarz et al., 2010). As the Stanley laboratory had no experience in working with the head-fixed rat at the outset of this project, a significant amount of effort was expended to get the paradigm up and running in the laboratory. The work was done in close coordination with the Schwarz Lab in Tübingen, Germany, and was greatly accelerated in the summer of 2010 when the lab graciously offered to host me for three weeks to learn surgical and training techniques.

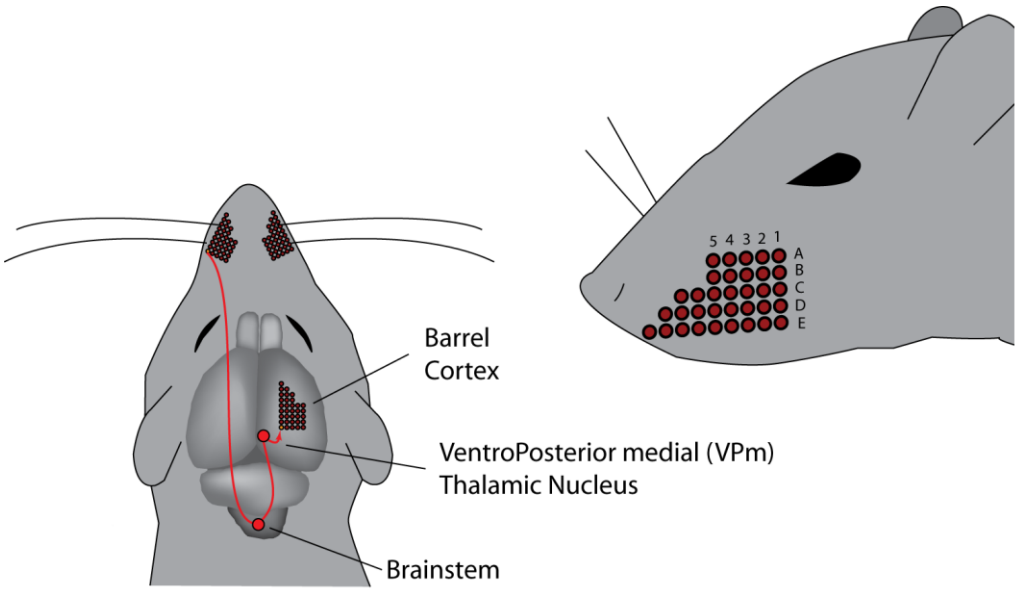

Figure 1-4 - *Anatomy of the rodent vibrissa pathway*. The vibrissae form a stereotyped pattern of 5 rows, lettered from A-E from top to bottom, and 5-9 arcs, numbered in ascending order in the posterior-to-anterior direction. Not shown are the four "greek" or "straddler" whiskers, which lie just posterior to first arc and between each of the five rows. Each whisker terminates in a densely innervated follicle on the face. Receptors in each follicle project to the brainstem, then to the VPm nucleus of the thalamus, and on to the barrel cortex. At each stage of processing, a discrete representation exists for each individual whisker. (Figure adapted from Diamond et al. 2008)

Finally, the anatomy of the system itself, shown in **Figure 1-4**, makes pairing behavioral studies with electrophysiology especially convenient. The rat's whiskers, each of which terminate in a densely innervated follicle on the animals snout (Ebara et al., 2002), form a stereotyped pattern of rows and arcs on the animal's snout. Each whisker is represented in discrete cortical columns known as "barrels," whose characteristic appearance lent the barrel cortex its name (Woolsey and Van der Loos, 1970; Petersen, 2007; Diamond et al., 2008b; Fox, 2008). One processing stage prior to the cortex, the thalamus is also somatotopically laid out into discrete representations for each whisker known as "barreloids," which consist of elongated, or "ellipsoid" representations with the largest

anatomical representations devoted to the more caudal (largest numbered) and more ventral (higher lettered) whiskers (Pierret et al., 2000; Haidarliu and Ahissar, 2001; Temereanca and Simons, 2003). This allows precise measurement of the neural response to a single whisker deflection at multiple processing stages and makes direct comparison across animals feasible.

Primary sensory signals provide the evidence upon which percepts are built:

The results presented here depend partially on signals recorded from the primary sensory cortex of anesthetized animals to draw inferences regarding the processes by which behaving animals make decisions about the presence and identity of sensory stimuli. This is based on results from an active subfield of neuroscience performing research into the neural basis of decision making (Romo and Salinas, 2001; Gold and Shadlen, 2007). This work presumes that sensory evidence in the form of activity in primary sensory areas is constantly monitored by higher cortical areas to form a so-called decision variable (DV). The DV is then compared to a threshold, which can be set based on factors such as motivation, cost/benefit analyses, etc. While most researchers are concerned with recording from prefrontal and parietal areas to locate cells encoding the DV itself, it is often assumed that the DV represents a leaky time integral of primary sensory information with a time constant of tens to hundreds of milliseconds (Cook and Maunsell, 2002). A schematic of this type of 'accumulating evidence' model is shown in **Figure 1-5**. Here, three different stimulus strengths were modeled by creating Gaussian distributions of equal variance with increasing means. At each point in time, a new piece of evidence was drawn and added to the accumulator until it crossed a threshold. This is

meant to model a higher brain area, often thought to be the parietal or prefrontal cortices, which monitors and accumulates incoming sensory evidence that ultimately leads to a decision to act. Stronger stimuli create more robust responses in the primary sensory cortex, which leads to faster evidence accumulation. The differences between the times at which the accumulator arrives at threshold for various stimulus strengths can help to explain the faster reaction times that are often seen for stronger stimuli. Such a model can also be extended to a two-choice discrimination task by creating thresholds in both the positive and negative direction and allowing evidence to accumulate in both directions.

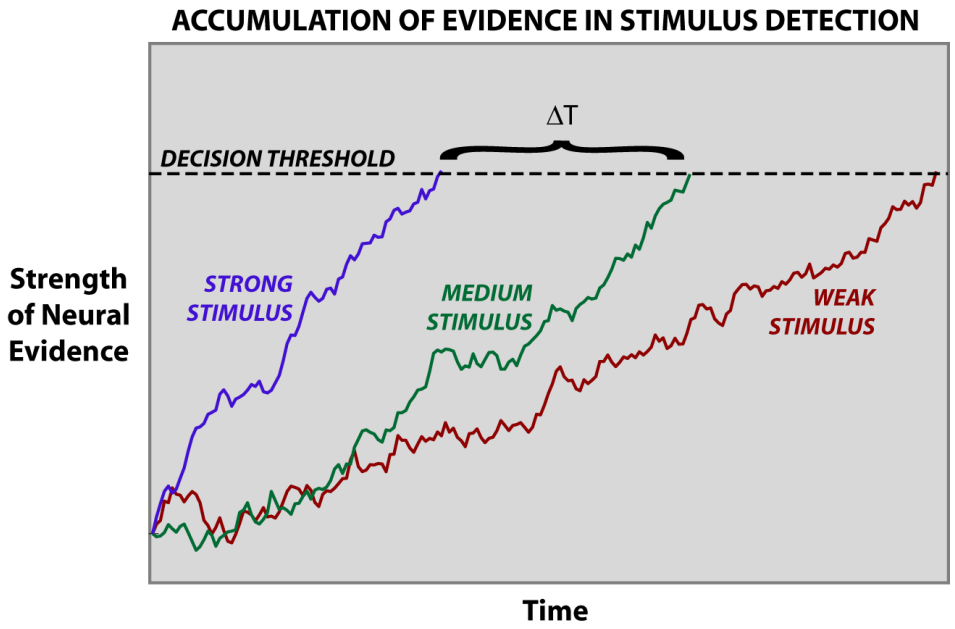

Figure 1-5 - *Schematic of an accumulating evidence model as it would apply to a go/no-go detection task.* Here, three different stimulus strengths are modeled as the inputs to an accumulating evidence model, which is assumed to represent a higher brain area such as the parietal cortex that is monitoring and accumulating sensory evidence from S1. By virtue of activating S1 more robustly, the strong stimulus allows evidence to accumulate more quickly toward a threshold, at which time a motor response is initiated. The differences between the times at which the accumulator arrives at threshold for various stimulus strengths, ΔT, can help to explain the faster reaction times that are often seen for stronger stimuli (figure adapted from Gold and Shadlen (2007) and Cook and Maunsell (2002))

However, in using recorded neural data from the primary sensory cortex as input to a decision making model, it must be true that the animal is actually using this information during the task in question. In a recent study by O'Conner et al. (2010a), the primary sensory cortex was reversibly inactivated during a vibrissa based object localization task, which eliminated the animals' ability to perform the task. This study confirmed that, at least for this particular subtype of task, the primary sensory cortex was indeed required.

Using this basic decision making framework, parallel experiments were performed in collaboration with other lab members to record population activity from the primary sensory cortex of anesthetized animals using voltage sensitive dye (VSD) imaging. VSD imaging is technique in which a fluorescent dye is allowed to diffuse into the exposed brain of an anesthetized animal, which allows the dye molecules to bind the external surface of cell membranes. The dye then fluoresces in direct proportion to the membrane potential of the neurons to which it is bound, allowing population neural activity to be optically recorded over a relatively large region of cortex with high temporal resolution (Jin et al., 2002; Grinvald and Hildesheim, 2004; Lippert et al., 2007). While the VSD signal represents primarily subthreshold activity in L2/3 of cortex (Grinvald and Hildesheim, 2004; Berger et al., 2007), this activity likely results from spiking activity one synapse earlier in the cortical input layer 4. The signal can therefore be modeled as the initial sensory evidence upon which the animal ultimately builds a decision about the presence of a stimulus. This framework has proven to be predictive of both the animals' response probabilities and reaction times, which tend to be significantly slower for

weaker stimuli. While there will clearly be changes in the processing state of anesthetized versus behaving animals (Steriade et al., 1993; Friedberg et al., 1999; Greenberg et al., 2008; Constantinople and Bruno, 2011), our results demonstrate that the acute studies capture information about the cortical response to stimuli that is relevant for the task performance in these relatively simple contexts.

Thalamocortical transformations and the gating of information flow to the cortex

Given its strategic location in the sensory pathway, combined with the large degree of feedback from cortex, the important role that the thalamus itself plays in information processing has long been appreciated (Crick, 1984; Sherman and Guillery, 2002; Sherman, 2007). Depending on the level of depolarization/hyperpolarization that is present in the thalamus prior to the arrival of a sensory stimulus, the thalamus is capable of responding with different types of responses known as 'burst' or 'tonic' modes, which convey fundamentally different types of information (Guido and Weyand, 1995; Sherman, 2001a, 2001b; Swadlow and Gusev, 2001; Beierlein et al., 2002; Lesica and Stanley, 2004; Lesica et al., 2006; Marsat and Pollack, 2006). These different processing modes fundamentally change the synchrony with which the population of thalamic neurons form excitatory post synaptic potentials (EPSPs) in their downstream cortical targets, leading to changes in the probability of response of the target neurons (Alonso et al., 1996; Bruno, 2011). The relatively weak synaptic connections between any given thalamic neuron and its cortical target (Bruno and Sakmann, 2006) make the system particularly sensitive to these changes in timing synchrony. The level of synchronous firing of the thalamic input neurons thus forms a sort of gain control mechanism for

cortex: highly synchronous inputs lead to a robust response in the cortex - the high gain state, while a decrease in synchrony results in a more graded cortical response which is better at transmitting stimulus detail - the low gain state. Many of these changes in processing result from factors such as attentional modulation and are controlled via feedback connections from L6 of cortex which act on inhibitory cells in the thalamic reticular complex (Crick, 1984; Bourassa and Deschênes, 1995; Guillery et al., 1998; Thomson, 2010; Olsen et al., 2012). However, important coding changes have also been measured in the thalamocortical circuit of anesthetized animals as a result of changing stimulus characteristics (Temereanca and Simons, 2003; Wang et al., 2010). In these studies, the existence of anesthesia rules out the possibility of factors such as attention leading to the observed coding changes, indicating that the changing features of the stimulus alone, or bottom up processes, are enough to drive changes in the information processing characteristics of the pathway.

All of this points to the importance of recording activity from the thalamus in order to better understand the observed changes in cortical processing, and such recordings form the basis of the final chapter of this work. The recordings from the thalamus were combined with a model of thalamocortical processing to help explain the mechanism by which changes in thalamic firing properties could lead to a sharpened cortical response the corresponding improvements in spatial discrimination performance. Combined with behavioral studies from the awake animal and the VSD recordings from the anesthetized animal, this body of work helps us to better understand the neural and behavioral

consequences resulting from both different active sensing strategies and adaptation to ongoing sensory stimuli.

Chapter 2 - Detection of tactile inputs in the rat vibrissa pathway

---

A modified version of this chapter was originally published as an article in the *Journal of Neurophysiology*:

Ollerenshaw DR, Bari BA, Millard DC, Orr LE, Wang Q, Stanley GB. *Detection of tactile inputs in the rat vibrissa pathway*. Journal of neurophysiology 108: 479-90, 2012.

Portions of this work were presented in poster form at the following:

Ollerenshaw, DR, Wang, Q, Bari, BA, Millard, DC, Orr, LE, Zheng, HV, Stanley, GB, *Tactile detection and discrimination: behavioral predictions from VSD imaging of cortex* Abstract for Poster Presentation, Computational and Systems Neuroscience (Cosyne) meeting, Salt Lake City, UT, February 2011

Ollerenshaw, DR, Bari, BA, Millard, DC, Orr, LE, Wang, Q, Zheng, HV, Stanley, GB, *Linking Evoked Cortical Activity to Detection Psychophysics in the Vibrissa System* Abstract for Poster Presentation, The Neural Basis of Vibrissa-Based Tactile Sensation, HHMI Janelia Farm Research Campus, Ashburn, VA, April 2010

Ollerenshaw, DR, Bari, BA, Millard, DC, Orr, LE, Wang, Q, Zheng, HV, Stanley, GB, *Detection of Whisker Deflections in Awake Behaving Rats,* Abstract for Poster Presentation, Joint South East Nerve Net and Georgia/South Carolina Neuroscience Consortium Conference, Emory University, Atlanta, GA, March 2010

2.1 Abstract

The rapid detection of sensory inputs is crucial for survival. Sensory detection explicitly requires the integration of incoming sensory information and the ability to distinguish between relevant information and ongoing neural activity. In this study, head-fixed rats were trained to detect the presence of a brief deflection of their whiskers resulting from a focused puff of air. The animals showed a monotonic increase in response probability and a decrease in reaction time with increased stimulus strength. High speed video analysis of whisker motion revealed that animals were more likely to detect the stimulus during periods of reduced self-induced motion of the whiskers, thereby allowing the stimulus-induced whisker motion to exceed the ongoing noise. In parallel, we used voltage sensitive dye (VSD) imaging of barrel cortex in anesthetized rats receiving the same stimulus set as those in the behavioral portion of this study to assess candidate codes that make use of the full spatiotemporal representation and to compare variability in the trial-by-trial nature of the cortical response and the corresponding variability in the behavioral response. By applying an accumulating evidence framework to the population cortical activity measured in separate animals, a strong correspondence was made between the behavioral output and the neural signaling, both in terms of the response probabilities and the reaction times. Taken together, the results here provide evidence for detection performance that is strongly reliant on the relative strength of signal versus noise, with strong correspondence between behavior and parallel electrophysiological findings.

2.2 Introduction

Understanding how the brain integrates sensory information, and how it ultimately uses that information to initiate a motor response, are among the most important questions facing the field of sensory neuroscience. Given that most rodents are nocturnal and rely heavily on their facial whiskers for navigation and survival, the rodent vibrissa system has evolved into an incredibly sophisticated sensorimotor system (Petersen, 2007; Diamond et al., 2008b). Recent studies have shown that the vibrissa system is capable of a wide range of sensory tasks, such as whisker contact detection (Stüttgen et al., 2006; Stüttgen and Schwarz, 2008), object localization (Hutson and Masterton, 1986; Shuler et al., 2002; Mehta et al., 2007; O'Connor et al., 2010a), texture, pattern, and vibrotactile discrimination (Guić-Robles et al., 1989; Carvell and Simons, 1990; Brecht et al., 1997; Heimendahl et al., 2007; Ritt et al., 2008; Wolfe et al., 2008; Gerdjikov et al., 2010; Adibi and Arabzadeh, 2011; Adibi et al., 2012), and aperture width discrimination (Krupa et al., 2001, 2004), but how this information is extracted by the neural circuitry is still largely unknown.

Between the arrival of a stimulus-induced neural signal in the primary sensory cortex and the subsequent motor response, the brain must evaluate the available evidence to determine whether the activity constitutes an important event, or is instead environmental or internal noise (Gold and Shadlen, 2007). Although the decision process is likely mediated in brain regions that are not purely sensory in nature, by assuming the role of an ideal observer of cortical activation, we can learn much about what information is

available to downstream structures and evaluate possible candidate codes upon which the computation might actually be based (Jacobs et al., 2009; Wang et al., 2010). Although behavioral outcomes are ultimately linked to the concerted supra-threshold neuronal activity, much of what we currently understand is limited to measurements of single neurons or small groups of neurons, upon which neurometric comparisons to psychometric performance are made (Britten and Shadlen, 1992; Shadlen and Newsome, 2001; Stüttgen and Schwarz, 2008).

In their natural environments, rats and other rodents actively move their whiskers to palpate their surroundings (Gustafson and Felbain-Keramidas, 1977; Carvell and Simons, 1990; Brecht et al., 1997; Bermejo et al., 2002; Berg and Kleinfeld, 2003). The resulting sensory input to this pathway is a complex combination of both the macro- and micro-motions of the whisker that relate to the properties of the objects being palpated (Hartmann et al., 2003; Neimark et al., 2003; Knutsen et al., 2005; Birdwell et al., 2007; Ritt et al., 2008; Wolfe et al., 2008) and the self-induced movement of the whisker (Kleinfeld et al., 2006; Curtis and Kleinfeld, 2009; Stanley, 2009; Jenks et al., 2010). Tactile sensing thus explicitly requires the disassociation of self-induced motion from the exogenous sensory input. It has been shown that the pathway encodes information directly related to whisker motion, even when the whiskers are not in contact with an object (Yu et al., 2006; Leiser and Moxon, 2007; Khatri et al., 2009a). How this might affect the animal's ability to detect an exogenous stimulus in the presence of endogenous, self-generated "noise" has not been well studied.

In this study, head-fixed rats were trained to detect the presence of a brief deflection of their whiskers resulting from a focused puff of air. The animals showed a monotonic increase in response probability and a subsequent decrease in reaction time with increased stimulus strength. High speed video analysis of whisker motion was used to measure both the stimulus-induced as well as self-generated motion of the vibrissae, with evidence indicating that animals were more likely to detect the stimulus during periods of reduced self-motion of the whiskers, thereby allowing the stimulus-induced whisker motion to exceed the ongoing noise. In parallel to the behavioral detection experiments conducted here, we used VSD imaging of barrel cortex in anesthetized rats receiving the same stimulus set as those in the behavioral portion of this study to assess candidate codes that make use of the full spatiotemporal representation and to compare variability in the trial-by-trial nature of the cortical response (Petersen et al., 2003b) and the corresponding variability in the behavioral response. By applying an accumulating evidence framework to the population cortical activity measured in separate animals, a strong correspondence was made between the behavioral output and the neural signaling, both in terms of the response probabilities and the reaction times.

2.3 Methods

Five Long-Evans rats (Charles Rivers Laboratories, Wilmington, MA; 7 weeks of age, ~250g at the beginning of the study) were used in the behavioral portion of this study and two Sprague-Dawley rats (Charles River Laboratories, Wilmington, MA; 200-350g) were used in the acute voltage sensitive dye (VSD) experiments. Animals were housed on a 12 hour light/dark cycle with all experimental sessions occurring during the light phase. All procedures were in accordance with protocols approved by the Georgia Institute of Technology Animal Care and Use Committee.

Procedure to implant head post

All animals used in the behavioral task were habituated to human contact for a minimum of five days prior to the surgical procedure to implant the head post. The head post consisted of a stainless steel machine screw implanted with the threaded end facing upward. All surgical procedures adhered to aseptic principles. Anesthesia was induced with isoflurane at 4-5% in the home cage and was subsequently maintained at 1.5-3% using a nose cone. The depth of anesthesia was monitored through toe-pinch reflexes and a non-invasive continuous measurement of heart rate and blood oxygenation. The scalp was shaved and cleaned of hair using depilatory cream. Animals were then placed in a stereotactic device using non-penetrating ear bars and the eyes were covered in ophthalmic ointment to prevent drying. Atropine (0.05 mg/kg, SC) and saline (10 mL/kg, SC) were administered. The body temperature was thermostatically maintained at 37°C throughout the procedure. The scalp was cleaned with alcohol and a 10% povidone-

iodine solution, followed by an injection of lidocaine prior to making an incision. After clearing the skull of connective tissue, 6-8 holes were drilled, and 1.4mm diameter stainless steel screws were inserted to anchor the head post to the bone. The head post was then held over the midline, and dental cement was applied over the base of the post and the skull screws. The wound was treated with antibiotic ointment and closed using metal wound clips. Bupronorphine (Buprenex, 0.03 mg/kg, SC) was provided as an analgesic, and antibiotics (Baytril, 5 mg/kg, IM) were administered for a minimum of three days postoperatively. Animals were given a minimum of ten days of recovery before commencing behavioral training.

Water restriction schedule

Water restriction was implemented after a minimum of ten days of recovery from head post implantation. Training and data recording sessions took place Monday through Friday, daily, and animals did not have access to water in their home cages on those days. Correct responses in the behavioral task were rewarded with 75-100μL aliquots of water, and animals were allowed to continue performing the task until sated. The weight of the animal was tracked daily and, when necessary, water supplements were provided after the daily experimental session in order to maintain the weight of the animal within 90% of its age-adjusted value. Water was provided *ad libitum* from Friday afternoon through Sunday afternoon of every week, and for one full week every two months.

Behavioral apparatus

The behavioral apparatus is illustrated in **Figure 1-2A** and was contained in a standard

operant conditioning chamber (Lafayette Instruments, Model 80003, Lafayette, IN) placed inside a sound and light attenuating cubicle (Med Associates, ENV-014, St. Albans, VT). A 6cm aluminum extension was attached to the animals' head post prior to each behavioral session using a set screw. This head post extension was then held rigidly with a stainless steel clamp extending from the side of the operant conditioning chamber. The body of the animal was contained in a custom built body restraint box designed to prevent excessive movement while head-fixed. A moveable plate at the front of the restraint box provided a location for the animal to rest its forepaws while head-fixed. The body restraint box was rigidly attached to the floor of the operant conditioning chamber. A stainless steel water spout was directly in front of the animal and served both to deliver water rewards and to measure licking responses. As described by Hayar et al. (2006), the positive lead of an A/D converter was attached to the stainless steel spout and the negative lead was attached to the aluminum floor of the body restraint box. Contact of the animal's tongue with the water spout resulted in an approximately 600mV potential change across the two leads. This potential was converted to a binary value, time-stamped, and stored in the data file, thus allowing the onset and offset of each lick of the water spout to be recorded. Water was fed through the spout by a peristaltic pump (Lafayette Instruments, Model 80204M, Lafayette, IN). A tone generator (Lafayette Instruments, Model 80223M, Lafayette, IN) and a stimulus light (Lafayette Instruments, Model 80221M, Lafayette, IN) were installed directly above the water spout. A white noise masking stimulus was delivered through speakers installed in front of the animal, one to either side.

Stimuli consisted of brief, 150 ms puffs of air delivered to the vibrissa array on one side of the face (Ahissar et al. 2000; Derdikman et al. 2003; Sosnik et al. 2001). The air puffs were delivered through a custom-built air nozzle constructed from stainless steel hypodermic tubing (Smallparts Inc., 19 gauge, 0.0325in ID at tip). The air puff nozzle was aligned 15 degrees from the longitudinal axis of the animal and aimed such that the air stream impacted the vibrissae approximately halfway between the follicle and the tip, but away from the face. The pressure of the air puff was adjusted using a computer controlled voltage regulator (Proportion Air, Part number QPV1TFEE015CXL, McCordsville, IN) and varied from 0 to 15psi. The duration of the air puff was controlled by a miniature normally-closed solenoid valve (Mcmaster-Carr, Part number 5001T332, Atlanta, GA). Both the solenoid and the pressure regulator were placed outside of the sound attenuating chamber to prevent auditory confounds. A second air puff nozzle with identical dimensions was placed adjacent to the stimulus nozzle, but aimed such that it did not result in deflections of the whiskers. This second nozzle, referred to as the 'distracter nozzle', was programmed to release a puff of air intermittently on a 0-5s uniform distribution and was designed to prevent the animal from cueing off of the sound of the air puff during the behavioral task.

Control of the behavioral task and data logging were performed using custom software written in Microsoft Visual Basic 6. The interior of the behavioral chamber was illuminated with infrared light (Lorex Technology Inc., model VQ2121, Markham Ontario) and the animal's behavioral state during the task performance was monitored using a low speed CCD camera (The Imaging Source, LLC, model DMK 21BF04,

Charlotte, NC).

Training and behavioral task

After the animal was placed on a water restriction schedule, it was systematically habituated to head fixation and trained to perform the full detection task. The first step was to train the animal to lick the response spout in order to receive a water reward. In this stage of training, the animal was allowed to freely roam the operant conditioning chamber and approach the water spout at will. Water was dispensed on a 1 second interval as long as the animal continued to lick the spout, and the animal was allowed to drink until sated. The animals quickly learned to voluntarily enter the body restraint box to approach the water spout. After 2-3 days, a rubber version of the head post extension was clamped onto the head post and held by hand while the animal drank from the water spout. After the animal was able to tolerate manual fixation without signs of distress, the rubber head post extension was affixed in the head post clamp, allowing a limited degree of mobility. The length of time that the animal was affixed in the head clamp was gradually increased, as was the delay between water rewards.

After the animal was capable of tolerating head fixation for a minimum of 5 minutes, with a 4 second delay between water rewards, the rubber head post extension was replaced with the aluminum version and the animal was moved to the next stage of training, in which lick responses were conditioned on the air puff stimulus. In this stage of training, the animal was placed on a modified version of the task in which premature licks were not penalized. Thus, the animal was able to lick the spout freely, but only the

first lick within a maximum of 2 seconds following a 15 psi puff of air to the whiskers was rewarded with a water drop. The window of opportunity following the air puff was gradually decreased to 500 ms over a number of days. Simultaneously, a delay was added if any licks were detected within a 1 second window preceding the scheduled stimulus delivery time. This delay was gradually increased to 1.5 to 5.5 seconds randomly chosen on a uniform distribution. The animals quickly learned to withhold licking until the stimulus was detected. Finally, the white noise masking stimulus and the distracter puffs were added. Training and habituation procedures were based off of those described in Schwarz et al. (2010).

In the full version of the task, described schematically in Fig. 1B, a 500 ms tone signaled the start of a new trial. The white noise masking stimulus was muted during presentation of the tone. On S+ trials, or those in which the animal was expected to respond, the stimulus delay was drawn from a 1.5 to 5.5 second uniform distribution. To prevent random licking, any licks occurring within 1 second of the scheduled stimulus resulted in a further 1.5 to 5.5 second delay. A trial was categorized as a 'hit' if the animal licked the water spout within 500 ms of the air puff stimulus and a 'miss' otherwise. Hits were rewarded with a 70-100 μL aliquot of water (activation of the peristaltic pump for 1-1.5 seconds) and misses were not penalized. On each trial, one of eleven possible stimulus strengths was randomly chosen (0 psi, 0.375 psi, 0.75 psi, 1.125 psi, 1.5 psi, 1.875 psi, 2.25 psi, 3 psi, 4.5 psi, 7.5 psi, 11.25 psi). The resulting angular deflection velocities of the whiskers were measured using high speed video analysis of an anesthetized animal undergoing the same range of stimulus strengths, as shown in **Figure 2-1**. On every fifth

trial, a test stimulus consisting of the maximum air pressure (15 psi) was presented to probe the attentional/motivational state of the animal. The test stimulus was repeated if the animal failed to respond, and the session was halted if the animal failed to respond to three consecutive test pulses. Catch trials (labeled S-) were interleaved on 10-20% of trials. S- trials were identical to S+ trials with the exception that only the distracter air puff nozzle was fired at the scheduled stimulus delivery time, thus probing the animal's probability of responding by chance or as a result of potential auditory confounds. Responses on S- trials were labeled as 'false alarms' and were penalized with a 5 to 10 second timeout in which the stimulus light was turned on. 'Correct rejections,' or S- trials on which the animal did not respond in the window of opportunity, were not rewarded. All trials were preceded by a 1 second period designed to ensure separation between individual trials and to ensure that animals had sufficient time to consume the water reward from the previous trial.

Animals generally performed one session per day and were allowed to work until sated. In cases in which two sessions were performed in a day, the first session was halted after 15 to 20 minutes and the animal waited a minimum of one hour before starting the second session. Well trained animals generally performed 100+ correct trials per day. Across all five animals, over 10,000 total trials were performed (including test pulses and S- trials), with each animal being presented each of the 11 possible stimulus strengths an average of 81 times.

Behavioral data analysis

To prevent the inclusion of trials in which the animal was not highly motivated, trials were excluded from analysis if the animal did not correctly respond to the subsequent test stimulus. Thus, a pair of successful responses to test stimuli bracketed each five-trial block. This relatively conservative criteria resulted in the exclusion of approximately 10% of all trials. Psychometric curves were constructed from the measured behavioral response rates by fitting a sigmoidal curve of the form: $P(V) = 1 - (1 - \alpha)e^{-(V/\beta)^{\gamma}}$, where V is the whisker deflection velocity and α, β, γ are free parameters that were calculated using a nonlinear least squares regression algorithm in Matlab. The combined psychometric curve was constructed by pooling the behavioral data from all five animals. Error bars represent 95% confidence intervals. Response times were calculated as the mean time between stimulus onset and the first emitted lick within the response window, limiting the longest possible reaction time to 500 ms. Error bars for the latency data points represent the standard error of the mean.

High speed videography

High speed video was used both to map the known air pressure of the chosen range of stimuli to the resulting angular deflection velocities as well as monitor the effect of whisker motion on detection performance in the awake animal. To prevent self-motion of the animal's whisker pad from affecting the measured velocities resulting from the air-puffs, this analysis was performed on an animal under isoflurane anesthesia. While all of the reported behavioral results were obtained using animals in which the full vibrissa array was intact, the vibrissae were subsequently trimmed, leaving only the C row intact

in order to facilitate imaging. High speed video was acquired using an infrared CMOS camera (Fastec InLine 1000 with 1GB onboard memory). The camera was mounted directly above the animal's head and focused on the whiskers of interest. Backlighting was achieved using two infrared LED arrays (Lorex Technology Inc., model VQ2121, Markham Ontario) placed ~10cm below the region of interest. 3/16" opaque white plastic was placed directly above the LEDs to act as a diffuser and to improve the contrast of the whiskers. All video was recorded at either 440x330 or 640x238 pixels/frame at a temporal resolution of 500 frames/s with exposure time limited to 0.665 ms per frame. The spatial resolution of the region of interest was 7.0-8.5 pixels/mm (Jenks et al. 2010).

All whisker tracking was implemented using a custom routine written in Matlab. The whisker tracking routine was based on that described by Knutsen et al. (2005), which was subsequently made available online (http://code.google.com/p/whiskertracker/). On a subset of videos, results using our custom tracking routine were compared and provided similar results. In the tracking program, three points were chosen on each whisker of interest, one defining the base of the whisker at its junction with the facial pad, one defining a point ~20 mm from the base which defined the length of the whisker that was tracked, and a third intermediate point about which a vertical search was performed on each frame to locate the new position of the whisker. In each frame, a search algorithm was performed in both the positive and negative x (medial-lateral) directions from the new intermediate point to define the new x and y position of each pixel representing the whisker between two user-defined extremes. Note that this algorithm does not prevent the base of the whisker from moving in the y-direction (rostral-caudal), as it clearly does

during self-induced motion of the whisker pad in awake animals. These new x and y locations were then fit with a second order polynomial in each frame. Example frames of the high speed video with a polynomial fit to the C2 whisker are shown in **Figure 2-2C**. The local whisker angle, in degrees, was computed in each video frame by taking the first spatial derivative of the polynomial at the whisker base. Angular velocity was calculated as the change in whisker angle from the previous frame to the current frame, divided by the temporal resolution of the video (2 ms per frame). All results were filtered using a 2nd order Butterworth low pass filter with a cutoff frequency of 50 Hz.

Whisker tracking in the anesthetized animal

In order to calibrate the known stimulus strengths, in pounds per square inch of air pressure, to a more behaviorally relevant range of deflection velocities, the full range of air puff stimuli was applied to an anesthetized animal four times per stimulus, with the results shown in **Figure 2-1A**. We reasoned that the whisker with the maximum velocity would likely dominate the cortical signal, and thus defined the velocity for a given air puff strength as the maximum deflection velocity observed across all whiskers. In every case, the maximum velocity was measured in the C2 whisker. The maximum velocity for each of the four trials was averaged and a second order polynomial was fit to the resulting maximum velocities to convert between the known air pressure of the stimulus and the velocity imparted at the follicle, as shown in **Figure 2-1B**.

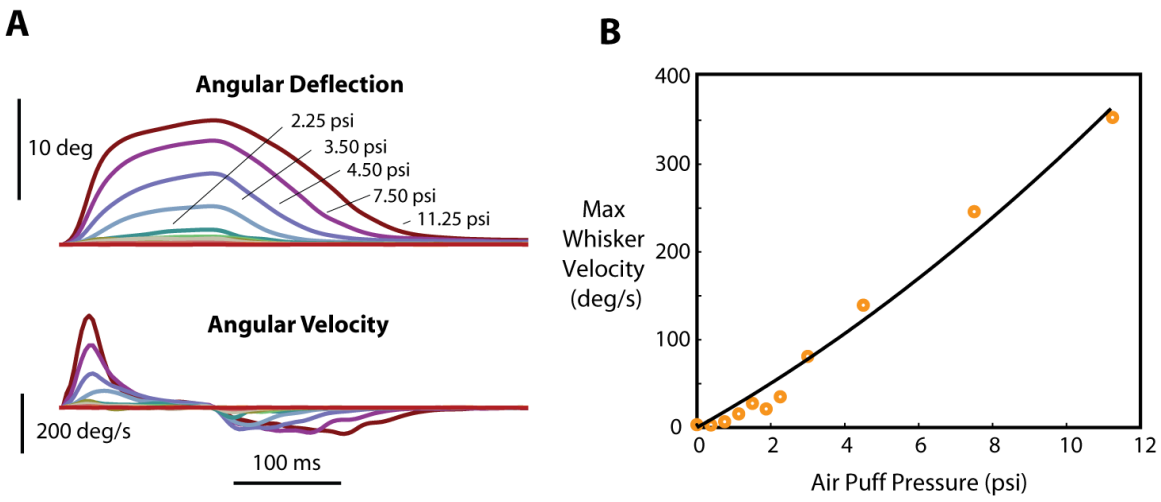

Figure 2-1 - *Summary of whisker tracking results for calibration between air puff pressure and angular velocity* **A.** Angular deflection and angular velocity as a function of time for the maximally deflected whisker in an anesthetized animal. Each curve represents the mean of four repeated deflections. **B.** The maximum angular velocity for each of the air puff pressures used during the behavioral task. A 2nd order polynomial was fit to the data points and used to convert between the known air puff pressure and the imparted angular velocity during the behavioral task.

Whisker tracking in the awake animal

After completion of data collection with the full whisker array intact, two animals were continued in the behavioral task with all whiskers excluding the C row trimmed. Analysis was confined to trials in which a 121 deg/s stimulus was delivered. This value was chosen because it was near the animals' behavioral detection threshold, meaning the animals tended to successfully detect the stimulus on approximately 50% of the trials. The camera was triggered on stimulus onset and was programmed to record an interval of 500 ms before and after the stimulus presentation. A total of 57 trials were collected across two animals.

In the subsequent analysis, the deflection angle as a function of time was measured for the C2 whisker. In all cases, the C2 whisker underwent a larger deflection than other C-row whiskers, and analysis was therefore confined to that whisker alone. For each of the 57 trials, the mean whisker angle in the 150 ms prior to stimulus onset was subtracted from the measured angle, and the discrete Fourier transform of the whisker angle was calculated over the same time interval in Matlab. Trials were categorized as being either 'whisking' or 'nonwhisking' trials based on the total power in the 0-15 Hz frequency band, with a hard threshold manually chosen to provide maximum separation. The behavioral response probabilities for these two categories of trial types were compared to assess how the animals' own self-generated whisker motion affected the probability of detecting the stimulus.

Voltage Sensitive Dye Imaging

Layer 2/3 population activity resulting from whisker deflections was measured in separate animals using voltage sensitive dye imaging, which primarily measures subthreshold membrane voltage fluctuations with high temporal and spatial resolution (Petersen et al., 2003b; Grinvald and Hildesheim, 2004; Ferezou et al., 2006; Berger et al., 2007). Two female Sprague-Dawley rats were used for VSD imaging experiments. Surgical procedures were similar to those described above. Anesthesia was induced with isoflurane, then followed by an injection of sodium pentobarbital (Nembutol, 50 mg/kg, IP), and a steady depth of anesthesia was maintained throughout the procedure with a continuous delivery of sodium pentobarbital (Nembutol, 12.5 mg/kg/hr, IV) through the tail vein. After clearing the skull of connective tissue, a 3x3 mm craniotomy centered at

~2.5 mm caudal to bregma and ~5.5 mm lateral to the midline (Paxinos and Watson, 2007) was performed over the barrel cortex, with extreme care taken to avoid heat buildup during the drilling process. An approximately 1 mm tall dam was constructed around the craniotomy using dental cement to facilitate the staining process. The bone fragment was then carefully lifted and the dura was washed with Ringer's solution, then dried with a gentle air blow for about 10-15 minutes or until it had a "glassy" appearance (Lippert et al., 2007). Voltage sensitive dye (VSD RH1691, Optical Imaging, Inc.) was diluted in Ringer's solution to 2 mg/mL. The dye solution (~200 μL) was carefully circulated over the cortical surface using a micro-pipette and was circulated and replenished with a micropipette every 5 minutes over a total of two hours, allowing ample time for the dye to diffuse into the cortex. During the entire staining process, the craniotomy was covered whenever possible to avoid premature photo bleaching of the dye. After staining, the surface was washed with saline, which was also periodically reapplied during the imaging process to avoid drying.

Imaging was achieved using a 150 W halogen lamp to illuminate the brain surface. The excitation light source was filtered at 621-643 nm, and the fluorescence signals were collected with a MiCam02 camera system (SciMedia Inc., Costa Mesa, CA), which was focused 300 μm below the surface of the cortex, primarily imaging the activity of layer 2/3 neurons. The camera had a frame rate of 200 Hz with a resolution of 192x128 pixels comprising a field of view of approximately 4 mm x 2.5 mm at 0.63x magnification.

The air puff nozzle was placed in the same position as during the behavioral task and

stimuli were presented to the full whisker array in pseudorandom order for a total of 20 trials at each of the 11 deflection velocities. On each trial, 40 frames (200 ms) and 160 frames (800 ms) were collected before and after stimulus presentation, respectively. The raw fluorescence values at each pixel for each individual trial were recorded using the Scimedia software and exported to Matlab for further analysis.

Voltage Sensitive Dye Data Analysis

All VSD analysis was performed using custom written scripts in Matlab. Prior to further analysis, the raw fluorescence data output by the imaging hardware was converted to a normalized value. For each trial, the first 39 frames prior to stimulus onset were averaged together to obtain an average level of background fluorescence, F0. The background fluorescence was then subtracted from each of the 200 frames in a particular trial to obtain the differential fluorescence, ΔF, then normalized by the background fluorescence to obtain the standard VSD measure of $\Delta F/F0$.

Occasionally, large spontaneous waves of activity were observed before stimulus onset that subsequently prevented post stimulus activation. To prevent the inclusion of these trials in the analysis, the activity for the 200 ms prior to stimulus onset was averaged across the entire frame, and any trials in which this pre-stimulus activity varied by more than 3 standard deviations from the mean were discarded from the analysis.

Additionally, for visual presentation purposes only, the frames were smoothed with a 3x3 boxcar filter, all data below a threshold defined as 10% of the maximum $\Delta F/F0$ value

were removed, and the resulting fluorescence image was superimposed on a background image of the cortical surface. All quantitative analyses were performed on the raw VSD images.

We modeled an observer of cortical activity that was assumed to represent a higher cortical area that may be monitoring primary sensory data to form a decision variable (DV) regarding the presence of a sensory stimulus (Cook and Maunsell, 2002). The observer was assumed to have access to activity across a wide area of barrel cortex. To model this, we found the center of mass of activation in the peak frame (generally 40-45 ms after stimulus onset), and, for each frame, averaged the $\Delta F/F0$ values in a circular region with a radius of 1 mm surrounding this point. Given a barrel diameter of approximately 300-400μm, this corresponds to an area of cortex containing the majority of the whisker representations. To account for slow, non-neural changes in the VSD signal, a linear function was fit to the averaged data in this spatial region over the first 200 ms prior to stimulus onset. This linear trend was then subtracted from the entire one second trial (Chen et al., 2008).

Accumulation of sensory evidence was modeled by temporally integrating the spatially averaged signal using a leaky window that weighted data from one at the current time and decayed exponentially to zero for past evidence with a time constant of τ. Thus, the immediate signal was given the highest weight and past evidence decayed over time. This model was applied to the measured VSD signal from each individual trial, and the means and standard deviations were calculated for each deflection velocity. To calculate the probability that a stimulus with a particular deflection velocity would be detected by the

observer, a detection threshold was chosen, with the response probability measured as the probability of the integrated output crossing that threshold, assuming that the distribution of signals was normal. For a given integration time constant, a range of thresholds were tested to search for the one that produced the lowest mean squared error between the predicted response probabilities and those observed behaviorally. The neurometric decision latency was modeled by generating 1000 simulated trials based on the mean and standard deviation of the measured responses, with the latency defined as the time at which each integrated response crossed the threshold. Trials in which the signal did not reach the threshold were not included in the latency calculation. These subthreshold trials would correspond with behavioral trials in which insufficient evidence existed to trigger a response, and thus no behavioral latency would exist. The analysis was repeated for a range of time constants from 1 ms up to 1000 ms, with a new optimal threshold value calculated for each integration time constant.

2.4 Results

We trained a total of five head-fixed male Long-Evans rats to perform a go/no-go detection task in which they were required to respond by licking a water spout within a 500 ms window following the onset of a brief puff of air delivered to their full whisker array (Stüttgen et al. 2006; Stüttgen and Schwarz 2008). The strength of the stimulus was varied in each trial to determine how the deflection velocity affected both the probability of response and the reaction time of the animals. The behavioral task is described in detail in the Materials and Methods section and is shown schematically in Figs. 1A and 1B. Great care was taken to avoid visual, auditory, and non-whisker mediated tactile cues. The task was performed in a sound and light attenuating cubicle with a white noise masking stimulus designed to prevent the animal from cueing on the sound of the air-puff stimulus. In addition, an air puff was emitted from a second nearby 'distracter nozzle' on a uniform 0-5 second random interval. This distracter stimulus was intended to decouple the sound of the air puff and the water reward in case the masking stimulus was not sufficient to fully prevent auditory cues. Catch trials were interleaved to directly measure the chance performance of the animals. The stream of air was carefully aimed to avoid impinging on the animal's face or body. In addition, occasional short sessions were undertaken in which the primary air puff nozzle was aimed slightly above the whisker array. During these sessions, which were kept very short to avoid frustrating the animals, the animals failed to reliably respond to the stimuli, further indicating that they had learned to fully rely upon whisker deflections to perform the task.

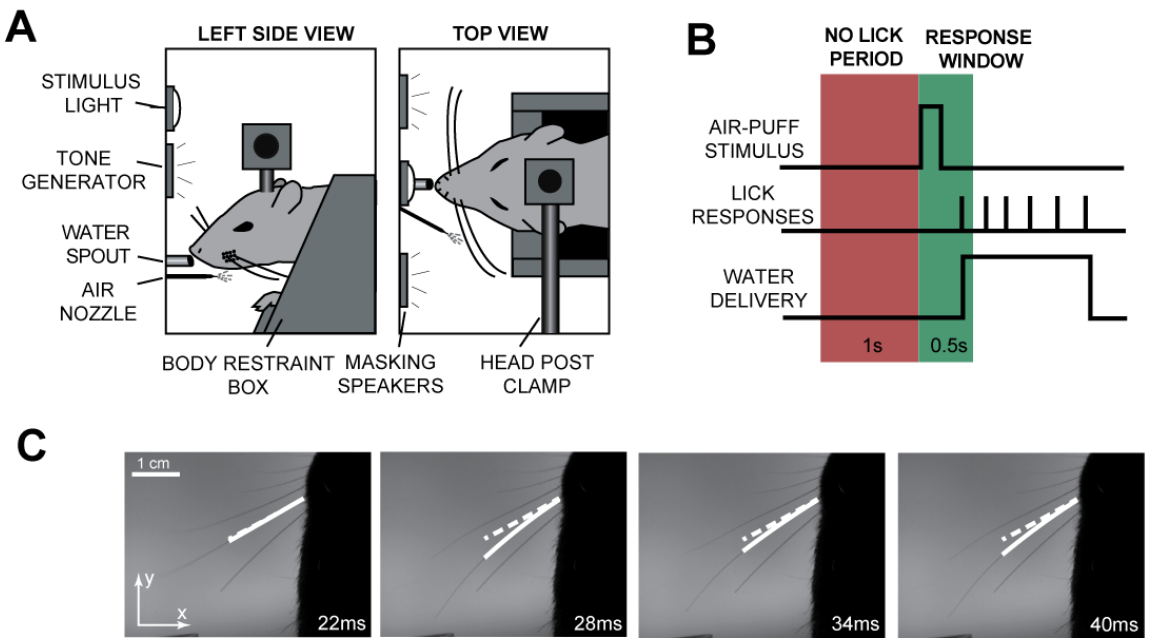

Figure 2-2 - *A Go/No-go behavioral detection task was used to probe the sensitivity of head-fixed animals to brief whisker deflections.* **A.** Schematic of the behavioral apparatus. Head-fixed animals were trained to respond to air-puff stimuli delivered to their whiskers by licking a response spout. **B.** Timeline of the behavioral task. Following a tone, the tactile stimulus was presented at a random time, where the duration between the tone and the stimulus was drawn from a uniform distribution on 1.5 to 5.5 ms. To discourage guessing, a "No Lick Period" was imposed, where any licks within 1 second prior to the forthcoming stimulus resulted in an additional delay of the stimulus. Animals had a 500 ms window in which to respond by licking the spout after the delivery of a stimulus. Responses to air puffs (S+) trials were rewarded with a 70-100 uL drop of water. Catch trials (S-) were interleaved on 10% of trials, where a distracter nozzle (positioned near the air nozzle, but not aimed at the vibrissae) was activated to test for chance response probability. Responses on S- trials were penalized with a 5-10 second timeout in which the stimulus light was activated. Failure to respond on S+ trials was not penalized and correctly withholding on S- trials was not rewarded. **C.** To quantify the strength of the air-puff stimulus, high speed video was recorded while the stimulus was delivered to an anesthetized animal with only a single row of whiskers remaining. Shown are four frames from a representative video with a tracking polynomial overlaid on the C2 whisker, which was the whisker that was deflected maximally by the air puff. Though multiple whiskers were deflected, only the maximally deflected whisker was considered for tracking purposes. The polynomial fit to the whisker is designated by the solid white line, while the dashed white line indicates the initial position of the whisker. The coordinate system used in the tracking algorithm is shown in the first frame.

Detection performance in the go/no-go task

The five animals in the behavioral portion of the study performed a total of over 10,000 trials during the course of the study. Each animal received an average of 81 presentations of each of the 11 possible stimuli, with the balance of trials consisting of test pulses and catch trials. **Figure 2-4** shows lick response rasters and corresponding histograms for three of the tested velocities for a single animal. The light grey section in the lick rasters and histograms designates the enforced no-lick period, during which any licks emitted by the animal resulted in an additional randomized delay of the stimulus. This no-lick period was designed to prevent the animals from licking impulsively. The dark gray section of lick rasters and histograms represents the 500 ms response window, during which the animal was required to respond to receive a water reward. Each tick mark in the lick raster represents the time of contact of the animal's tongue with the water spout. The first lick after the stimulus but within the 500 ms response window resulted in a water reward for the animal and is highlighted (rewarded lick, black). Subsequent licks were generally a result of the animal consuming the water reward (unrewarded lick, gray). The animals' licking responses were clearly periodic and subsequent analysis (not shown) indicated an average licking frequency of approximately 8 Hz.

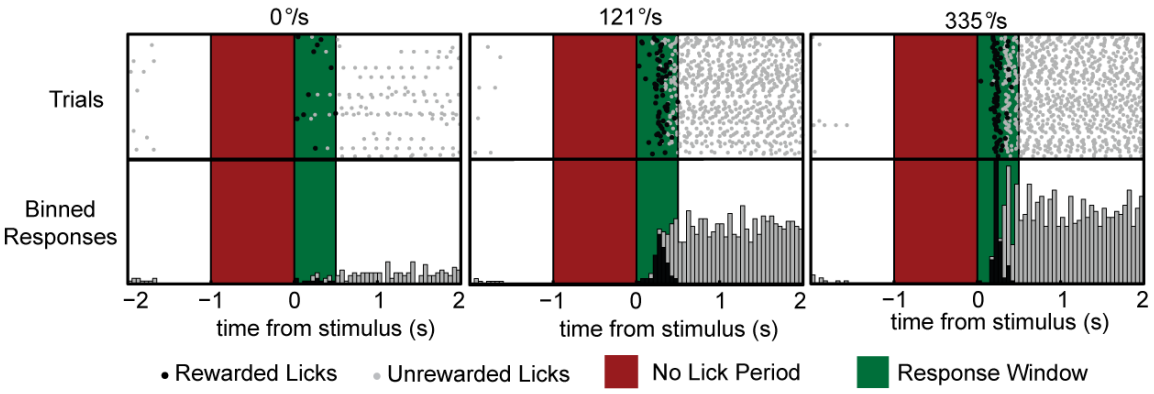

Figure 2-3 – *Lick response rasters from the detection task*. Data is from a single animal for three deflection velocities. The red region indicates the enforced no-lick period and the green region indicates the 500 ms response window. Each tick mark in the lick raster indicates a contact of the tongue with water spout, with all first licks falling within the response window highlighted in black (rewarded lick). The responses are divided into 50 ms bins in the accompanying histograms, with first licks again highlighted in black.

Figure 2-4A shows the individual response probabilities as a function of deflection velocity for each of the five animals in the study. Each of the five animals showed a maximal response probability of approximately 90% for the highest velocity and responded to approximately 10% of the 0 deg/s stimuli, in which no stimulus was applied. It should be noted that the 0 deg/s stimuli were distinct from the catch trials, which are described in detail below, in that the primary stimulus solenoid was opened on 0 deg/s trials, but there was no air pressure present in the line.

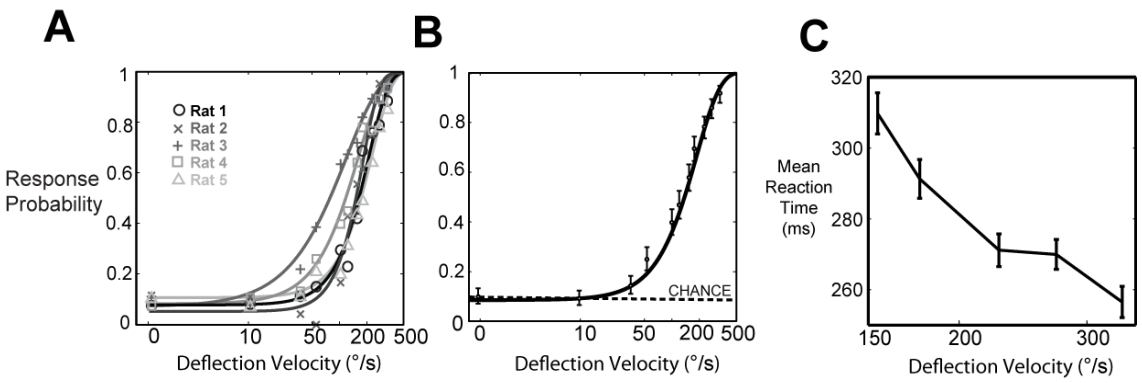

Figure 2-4 - *Response probability increased and reaction time decreased with increasing stimulus strength.* **A.** Psychometric curves for each of the five individual animals. Solid lines represent sigmoidal fits to the response probabilities at each of the 11 tested deflection velocities (see Methods). Individual mean response probabilities are shown for each of the five animals. **B.** The psychometric curve for all five animals combined. Each data point represents the response probability at a particular deflection velocity with data pooled across all five animals. The solid line is the sigmoidal fit to the data and the dashed horizontal line represents the response probability on catch trials, which is the experimentally derived measure of chance performance. The average detection threshold, which is defined as the deflection strength at which the animals detect the stimulus 50% of the time, was approximately 125 degrees/second. **C.** The mean reaction times for all five animals for the five highest deflection velocities. There is a 52 ms decrease in the reaction time from the fifth highest deflection velocity to the highest ($p<0.005$, two sample t-test).

Figure 2-4B shows the psychometric curve for the combined data among all five animals. The dashed horizontal line labeled as 'chance' in **Figure 2-4B** represents the averaged response probability on catch trials, which were trials in which no tactile stimulus was delivered, but in which the distracter nozzle was fired at the time of the stimulus. Responses on catch trials were considered false alarms and were penalized with a 5-10 second timeout period in which the stimulus light in the behavioral chamber was turned on. The average response rate for all catch trials was 9.74% (13.66%, 11.39%, 8.70%, 12.77% and 6.67% for animals 1-5, respectively), which corresponded well with the response rate on 0 deg/s trials (9.69%), further indicating that the animals were not

using auditory cues to detect the presence of a stimulus. Assuming that the animals' tendency to guess at the presence of a stimulus remained constant throughout the duration of the trial, a theoretical chance response rate can be calculated by dividing the length of the response window (500 ms) by the overall duration in which a correct guess could result in a reward, which was 4.5 seconds. This yields an expected chance performance level of 11.11%, which also corresponds well with the experimentally measured chance performance.

Figure 2-4C shows the mean reaction times for the highest five velocities tested for all five of the animals in this study. The mean reaction time at the threshold velocity, 154 deg/s, was 309 ms and the reaction time steadily decreased with increasing stimulus strength. The reaction time at the highest velocity, 335 deg/s, was 257 ms. This 52 ms difference between the strongest deflection velocity and the threshold level deflection velocity was statistically significant ($p < 0.005$, two sample t-test). Reaction times for subthreshold deflection velocities, in which the animals tended to respond on less than half of the trials, were much more variable and were therefore not plotted.

Detection in the presence of self-motion

Rats and other rodents possess fine control over the motion of their whiskers, and often explore their environment using a rhythmic sweeping of their vibrissae known as whisking. Multiple studies have shown that whisking corresponds with changes in the processing state of cortex, leading to a reduction in the cortical response to passively applied stimuli (Fanselow and Nicolelis, 1999; Castro-Alamancos, 2004; Crochet and

Petersen, 2006; Ferezou et al., 2006, 2007). Through use of high speed video, we sought to explicitly determine whether self-induced whisker motion affected the animals' probability of detecting the externally applied stimulus. After the completion of data collection with the full vibrissa array intact, two animals continued to perform the task with only the central C row of whiskers intact and all others trimmed at skin level, in order to facilitate imaging. The whiskers were backlit with infrared LEDs (Jenks et al. 2010), and the camera was positioned directly above the head of the animal. The angle at the base of the whisker was subsequently evaluated using a custom Matlab routine (see Materials and Methods for details on the videography and whisker tracking).

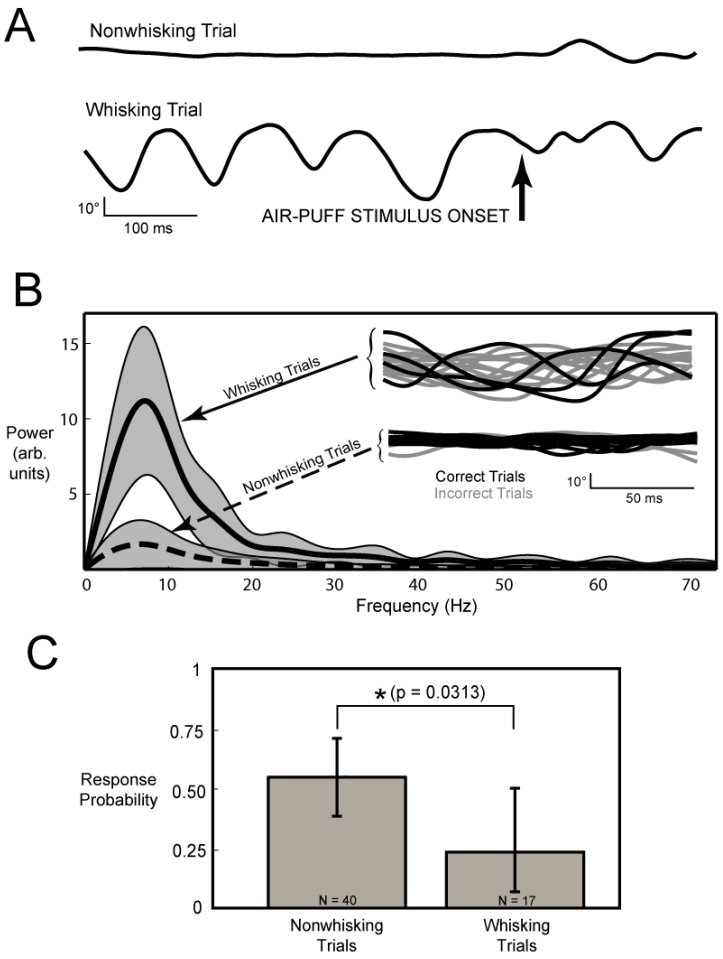

Figure 2-5 - *Self motion of whiskers degrades detection performance.* In a subset of behavioral trials, the whiskers were trimmed, leaving only the C row to facilitate imaging. High speed video was collected during presentation of the 121 deg/s stimulus, which corresponded to the velocity at which the animals responded correctly on 45% of the trials with the full vibrissa array intact. **A.** Whisker angle at the base was measured using custom tracking software and trials were categorized based on the total power in the 0-15Hz frequency band. Shown are representative examples of both a nonwhisking and a whisking trial. **B.** The average power for all of the whisking (solid line) and nonwhisking (dashed line) trials in the 150 ms prior to stimulus onset, with the shaded region representing one standard deviation about the mean. The inset shows all of the whisking trials at top, and all of the nonwhisking trials at bottom. Behaviorally correct and incorrect trials are black and gray, respectively. **C.** The response probability was significantly higher during periods of reduced self-motion prior to the arrival of the stimulus. Response probabilities for the two conditions were 0.55 and 0.24, respectively. Error bars represent 95% confidence intervals. The asterisk indicates statistical significance between the response probabilities under the two conditions ($p = 0.0313$, Wilcoxon rank sum test).

To maximize the possibility of recording both correct and incorrect trials, the camera was only triggered on presentation of 121 deg/s stimuli, which was just below the behavioral detection threshold (response probability with full vibrissa array intact = 46.58%). A total of 57 trials were recorded across the two animals. Trials were separated into two categories based on the amount of whisker motion in the 150 ms epoch prior to stimulus delivery: those with high power in the 0-15 Hz range, which were categorized as whisking trials, and those with low power in the 0-15 Hz range, which were categorized as nonwhisking trials. **Figure 2-5A** shows an example of both types of trials, from 450 ms prior to stimulus onset to 200 ms after stimulus onset. **Figure 2-5B** shows the mean +/- 1 standard deviation of the power from 0-75 Hz for all of the whisking and nonwhisking trials and clearly demonstrates a distinct separation between the two categories in the 0-15 Hz range. The inset of **Figure 2-5B** shows the angle vs. time traces for the 150 ms prior to stimulus onset for all of the whisking and nonwhisking trials, with trials in which the animal correctly detected the stimulus shown in black and those in which the animal failed to detect the stimulus shown in gray. The behavioral response probabilities for both types of trials are shown in **Figure 2-5C**, demonstrating that the animals had a significantly higher response rate on trials in which whisker motion was suppressed in the 150 ms prior to the arrival of the stimulus ($p = 0.0313$, Wilcoxon rank sum test). To verify whether or not the change in response probabilities represents a change in the signal or noise distributions, a change in the animals' response criterion, or some combination of these factors, both the hit rate and the false alarm rates must be considered. While we did not record high speed video during presentations of catch

stimuli to directly measure false alarm probability on these trials, an alternative measure of the animals' response criterion is their propensity to emit an anticipatory lick prior to stimulus presentation, resulting in a subsequent delay of the stimulus. The animals emitted an anticipatory lick on 3 out of 17 (17.6%) of the whisking trials and 4 out of 40 (10.0%) of the non-whisking trials, representing a non-significant difference in the rate of anticipatory licking across the two trial types ($p = 0.4340$, Wilcoxon rank sum test). This suggests that the reduced response probabilities represented a change in the way the stimulus was perceived in the whisking and non-whisking conditions, as opposed to a change in the attentional or motivational state of the animals.

Voltage sensitive dye imaging of cortical activation

In additional experiments in the anesthetized rat, voltage sensitive dye (VSD) imaging was used to characterize the population cortical response resulting from the range of whisker deflection velocities applied during the behavioral task. Voltage sensitive dye imaging has previously been shown to capture primarily subthreshold membrane potential fluctuations in layer 2/3 pyramidal neurons (Berger et al. 2007; Ferezou et al. 2006; Petersen et al. 2003a). **Figure 2-6A** shows a schematic of the VSD imaging setup. The air puff nozzle was positioned as in the behavioral task and deflections were applied to the entire vibrissa array. Images of the resulting layer 2/3 cortical activation were captured at 200 Hz with each stimulus applied 20 times in pseudorandom order. **Figure 2-6B** shows sample frames for five of the applied deflection velocities from 15 ms to 55 ms after the stimulus presentation. The images represent the average of all 20 stimulus presentations at each deflection velocity, and the activity was thresholded at 10% of the

peak fluorescence value, smoothed, and overlaid on an image of the cortical surface for visualization purposes. All subsequent quantitative analyses used the raw VSD signal. In the case of the higher velocity stimuli, activity was initially seen to be present by the 25 ms frame, though it appeared 5-10 ms later for the weaker stimuli. In all cases, the signal initially grew in both magnitude and spatial extent before slowly decaying back to baseline. The spatiotemporal dynamics of the VSD signal, as well as the relationship between increasing signal strength and response magnitude, were largely consistent with previous VSD imaging literature (Berger et al. 2007; Petersen et al. 2003a; Petersen et al. 2003b).

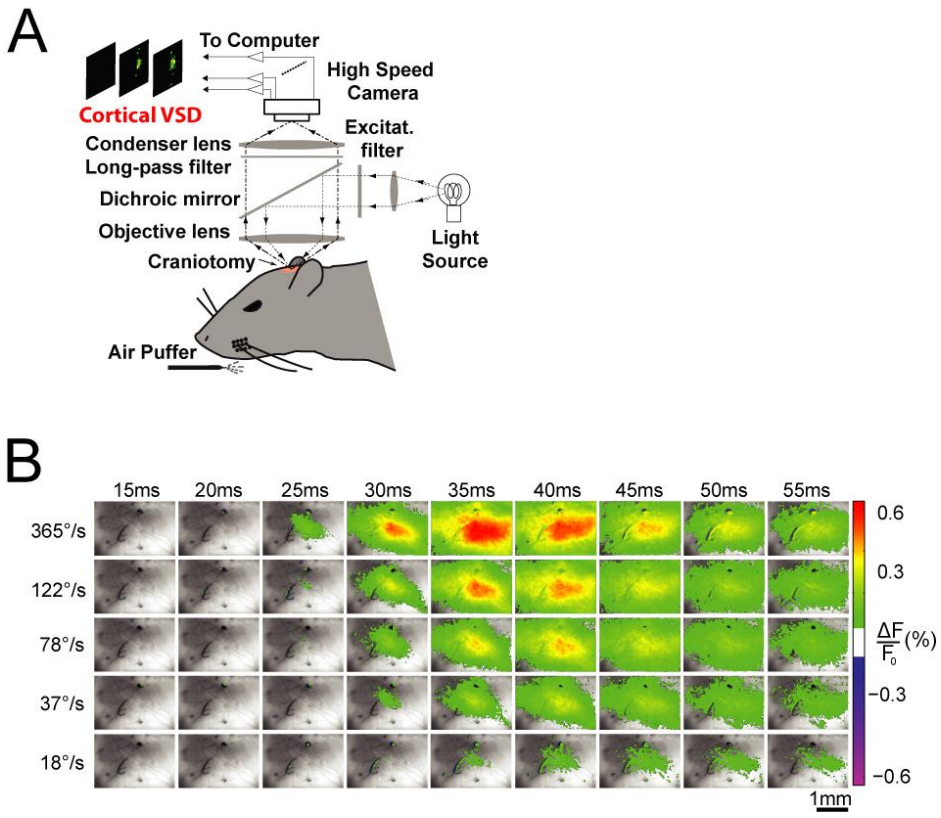

Figure 2-6 - *VSD Imaging was used to characterize the layer 2/3 cortical population response to the air-puff stimuli.* **A.** Schematic of the VSD system. After performing a craniotomy over the barrel cortex, RH1691 voltage sensitive dye was allowed to diffuse into the cortex. A high speed camera was subsequently focused 300μm below the cortical surface and images of cortical surface were captured every 5 ms. **B.** Image frames showing the spatiotemporal evolution of the signal during the 55 ms after stimulus onset for five stimulus strengths. Frames representing the initial 15 ms are not shown. The background image shows the region of cortex being imaged. Responses were smoothed with 3x3 boxcar filter and any response less than 10% of the maximum value was excluded for visualization purposes.

Past studies have indicated that sensory detection can be well modeled as a thresholding of the spatial and temporal integration of ongoing, noisy sensory information (Schall and Thompson, 1999; Gold and Shadlen, 2001, 2007; Cook and Maunsell, 2002; Roitman and Shadlen, 2002; Mazurek et al., 2003; Carpenter, 2004; Smith and Ratcliff, 2004; Huk and Shadlen, 2005; Chen et al., 2008; Stüttgen and Schwarz, 2010; Fridman et al., 2010).

Spatially, we integrated the VSD signal within a 1 mm radius of the center of mass of activity in the peak frame, resulting in an area of the primary sensory cortex containing the representation of the majority of the barrel cortex. **Figure 2-7A** shows the trial-by-trial activity inside the included region of the barrel cortex with the averaged frames from 15 ms to 90 ms shown above. In the averaged frames, only the activity within the 1 mm radius is shown. While precise details of the temporal integration process vary somewhat among studies, most have modeled the accumulation of sensory evidence using a leaking integrator with a time constant in the range of tens to hundreds of milliseconds. Here, we systematically evaluated a range of window sizes and shapes, but found that the results were largely invariant to the shape of the window. We therefore utilized the conventional exponentially decaying window with time constant, τ. **Figure 2-7B** shows the output of the integrator with a time constant of 20ms for two deflection velocities, with the blue being the highest velocity (335 deg/s) stimulus and the green being the 154 deg/s, near threshold level stimulus. The solid lines represent the means of the integrated outputs and the shaded regions represent one standard deviation about the mean. A neurometric detection threshold was chosen and the probability of response for a particular deflection velocity was calculated as the probability that the integrated signal crossed this threshold. A range of detection threshold values was systematically tested with the goal of finding the threshold that minimized the mean squared error between the predicted and behaviorally observed response probabilities. The optimal threshold is shown as a dashed line in **Figure 2-7B**.

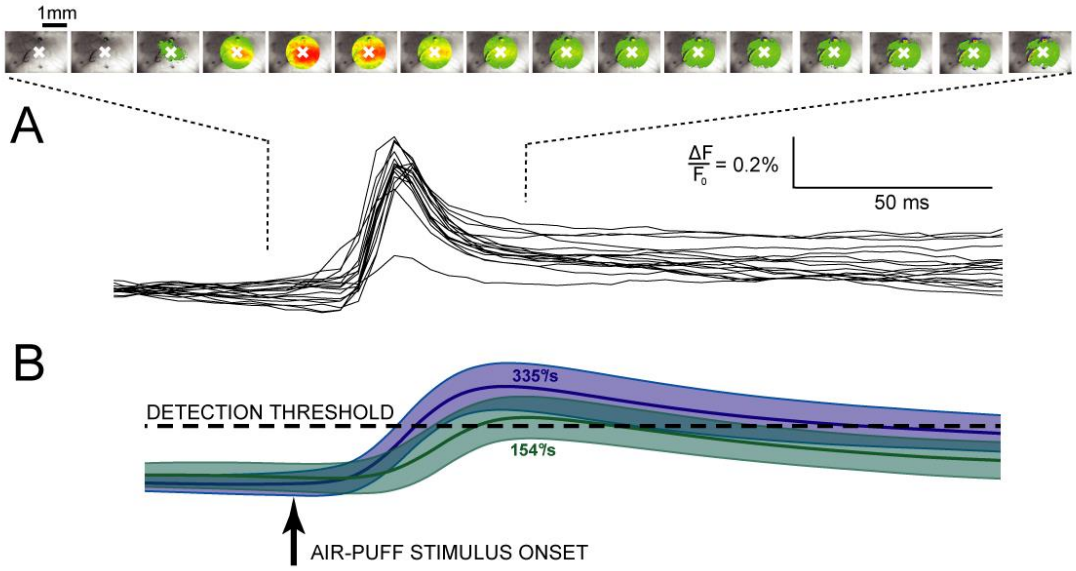

Figure 2-7 - *Neurometric performance based on an accumulating evidence model of the VSD signal* **A.** A circular area with a radius of 1mm centered at the center of mass of the peak signal, designated with a white X, was treated as the input to the accumulating evidence model. Shown are the averaged responses to the strongest air puff stimulus from 15-100 ms, with only the signal inside the region of interest shown. Below is the spatial average of these frames for each of the individual trials**. B.** The neurometric signal is generated from leaky integration of the VSD signal from A. Specifically, the VSD signal was convolved with an exponential window with a time constant of 20 ms. Shown is the mean and standard deviation of the integrated response for the strongest (335 deg/s, shown in purple) and the fifth strongest (154 deg/s, shown in cyan) velocities. For a given detection threshold, the probability of crossing that threshold was calculated for each of the 11 deflection strengths. The value of the threshold was chosen to minimize the mean squared error between the calculated response probabilities and those measured behaviorally (**Figure 2-4C**).

Figure 2-8A shows the predicted detection probabilities, shown as open circles, for all 11 of the whisker deflection velocities used in the behavioral study, averaged across the two animals in the acute portion of the study. The behaviorally observed detection probabilities (from **Figure 2-4C**) are again shown as for comparison. The black curve is the sigmoidal fit to the behavioral response probabilities and the red curve is the

sigmoidal fit to the predicted response probabilities. After determining the optimal detection threshold for each integration time constant, the neurometric decision latencies were modeled as the threshold crossing times generated from the distribution of the integrated VSD signal (see Methods). Trials in which the signal did not cross the threshold were excluded from the latency calculation. **Figure 2-8B** shows the predicted neurometric response latencies using an integration window with a 20 ms time constant. **Figure 2-8C** shows that, as expected, the latencies of the VSD threshold crossing times were significantly shorter than the corresponding behavioral reaction times (**Figure 2-4C**), and the absolute difference in latencies between the strongest stimulus and the threshold stimulus was significantly smaller than that of the behavioral reaction time (7 to 8 ms, versus 40 to 50 ms). However, the relative changes in the corresponding latencies induced by the strongest stimulus and the threshold stimulus were also evaluated for both the VSD recordings and the behavior. As shown in the bottom panel of **Figure 2-8C**, despite the differences in absolute measures between the psychometric and neurometric latencies, the relative measures were much more consistent between the cortical recordings and behavior.

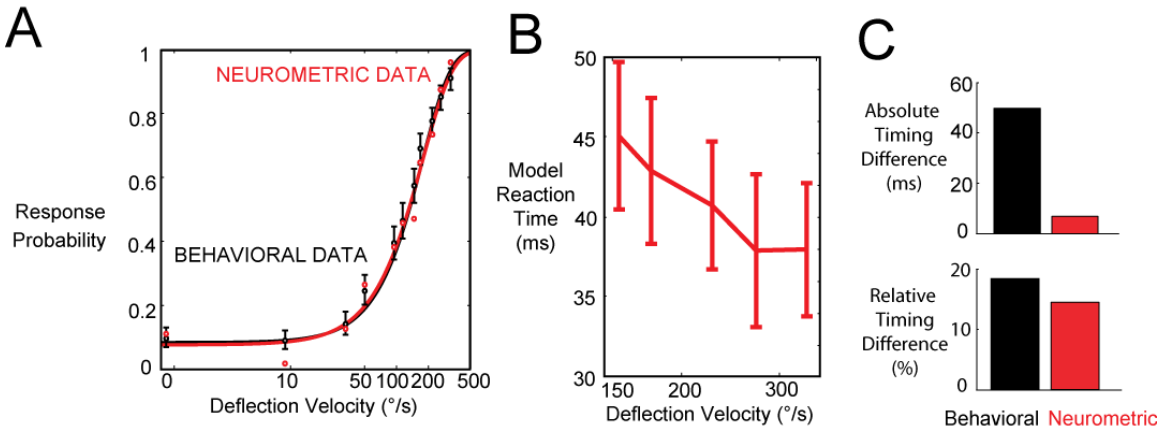

Figure 2-8 - *Results from the neurometric model closely predict psychometric performance* **A.** The neurometric/psychometric match using the optimized threshold values. The neurometric data points represent the average across two animals. **B.** The neurometric latencies were measured as the time that each integrated population response crossed the optimized threshold. Note that responses that fail to reach the threshold are not included in the measured neurometric latency. **C.** A comparison of both the total change in latencies and the percent change in latencies from the strongest presented stimulus to the threshold level stimulus. The black bars represent the values measured from the behaving animals and the red bars represent the output of the accumulating evidence model. The absolute change in neurometric latency is not reflective of the absolute change in the animals' reaction times, but the relative change provides much closer correspondence.

2.5 Discussion

The present study was designed to allow us to address four primary issues. First, in a head-fixed behavioral detection task in which multiple whiskers were deflected, we sought to determine the relationship between whisker deflection velocity and the probability that the animal could successfully detect the applied stimulus. Simultaneously, by allowing the animals to respond as quickly as possible, we were able to demonstrate a relationship between the stimulus strength and the mean reaction times of the animals in the task. The animals were then allowed to continue the task with only a single row of their whiskers remaining, allowing us to collect high speed video of their vibrissae during presentation of threshold level stimuli to determine the effect that whisker motion prior to stimulus onset had on the probability of detecting the stimulus. Finally, VSD imaging of the barrel cortex was used to characterize the population cortical response to the whisker deflections used in the behavioral task and to explore a candidate neural coding scheme that could explain both the observed response probabilities and reaction times.

Detectability of velocity transients in tactile input

In the tasks utilized in this study, the behavioral performance was reported in terms of the angular velocity of the vibrissae as calibrated through high-speed video under controlled conditions in anesthetized animals. When an object makes contact with a rodent's whisker, the motion of the whisker is transmitted to the densely innervated follicle at the whisker base, giving rise to complex mechanics that have only recently been investigated

in detail (Birdwell et al., 2007; Towal et al., 2011). Electrophysiological studies at the thalamic and cortical levels have largely focused on the neuronal responses to velocity and amplitude of simple tactile stimuli (Lee and Simons, 2004; Temereanca et al., 2008; Boloori et al., 2010; Wang et al., 2010). Though both the amplitude and velocity of a whisker deflection can co-vary, multiple studies have indicated that it is primarily the velocity of the whisker deflection that is ultimately encoded at the level of the primary sensory cortex (Pinto et al., 2000; Boloori et al., 2010). As a first step, we have therefore focused on the velocity of the applied stimuli when measuring the animals' response probabilities and reaction times, though both velocity and amplitude were seen to increase with increased stimulus strength and other dynamical measures are also possibly important. This analysis yielded a detection threshold, defined as the velocity at which the animals responded with 50% probability, of approximately 125 deg/s. This threshold value is approximately half of that measured in a very similar head-fixed detection task in which only a single whisker was deflected using a piezoelectric actuator (Stüttgen and Schwarz 2008). This difference can largely be accounted for by the fact that our stimuli were applied to the entire intact vibrissa array, allowing multiple whiskers to encode the stimulus simultaneously, which has previously been shown to increase the magnitude of the cortical response to a given stimulus in anesthetized animals (Mirabella et al., 2001). It should be noted that although the central data reported here corresponds to the full vibrissa array, it is our observation that the nozzle used to deliver the air puff stimulus produced a fairly focused stream of air that was largely limited to a single row of vibrissae, and thus the data obtained from vibrissa arrays trimmed to a single row were not significantly different from data obtained with the intact array. Further, in an aperture

discrimination task, in which animals were freely moving, the ability of rats to discriminate between apertures of similar widths was severely degraded when less than 8-12 whiskers on a given side of the face were intact (Krupa et al. 2001), and animals performing a texture discrimination task required at least two whiskers per side to accurately perform the task (Carvell and Simons, 1995), suggesting that integration across the vibrissa array could account for the lower detection threshold we observed here.

Suppression of self-motion improves detection performance

When rats are engaged in active exploration of their environments, or are trained in a task that requires active palpation of an object, they generally engage in a 5-15 Hz rhythmic sweeping motion of their whiskers known as whisking (Gustafson and Felbain-Keramidas, 1977; Carvell and Simons, 1990; Brecht et al., 1997; Bermejo et al., 2002; Berg and Kleinfeld, 2003). However, in some behaviors or tasks, self-generated whisker motion may actually be detrimental in providing accurate tactile feedback. For example, rats in locomotion-based aperture discrimination tasks (Krupa et al. 2001; Krupa et al. 2004), engaged in wall following (Milani et al., 1989; Jenks et al., 2010), or performing passive detection tasks under head fixation (Stüttgen et al. 2006), have been anecdotally reported to avoid self-motion of the whiskers.

Here, using video analysis of the whisker motion while rats were engaged in the detection task, we demonstrated that rats not only held their whiskers still during a majority of trials, but that their probability of accurately detecting the stimulus was actually decreased on trials in which they engaged in active motion of the whiskers.

This result corresponds well with other studies showing that the cortical response to peripheral inputs is attenuated when the animal is whisking (Fanselow and Nicolelis, 1999; Castro-Alamancos, 2004; Crochet and Petersen, 2006; Ferezou et al., 2006, 2007; Hentschke et al., 2006; Poulet et al., 2012). This attenuation, combined with a shift to a more desynchronized cortical state (Poulet et al. 2012), could inherently reduce the probability of detecting a weak, passively applied stimulus. Additionally, we have previously demonstrated in the anesthetized animal that repetitively applied whisker movements place the cortex in an adapted state that proves detrimental for the detection of subsequent stimuli (Wang et al. 2010). Though the extent to which adaptation exists in the awake animal appears to be less than in the anesthetized animal (Castro-Alamancos 2004), attenuation due to adaptation would also likely serve to diminish detection performance. It has been shown that the pathway encodes information directly related to whisker motion, even when the whiskers are not in contact with an object (Yu et al., 2006; Leiser and Moxon, 2007; Khatri et al., 2009a). An alternative explanation for the reduced response probability, therefore, could be that the neural activity resulting from whisking could overwhelm that resulting from the stimulus itself, effectively decreasing the signal-to-noise ratio and degrading detection performance. Finally, the animals' attentional or motivational state could be different in the two cases, with trials in which the animals are whisking corresponding to epochs in which the animal is simply less attendant to the task. Though our dataset indicates that the response criterion is not significantly different in the two behavioral states, none of the above scenarios, or interactions thereof, can be ruled out without both a more complete measure of false-

alarm response probabilities and simultaneous recordings of cortical activity. While we cannot necessarily conclude that the suppression of whisking is an active strategy employed by the animals in our task, the results here indicate that in tasks where the animal must detect a weak, transient stimulus, the animal must balance incoming activity resulting from self-generated motion with that resulting from the stimulus itself.

VSD imaging of cortex in the anesthetized animal predicts performance in behaving animals

According to the 'sequential analysis framework' of decision making, sensory evidence about the presence of a stimulus is built up over time and compared to an internally determined threshold (Gold and Shadlen, 2007). This would allow the brain to respond quickly to a strong, unambiguous stimulus, but would require a longer integration period for weaker inputs. The VSD signal provides an excellent measure of the subthreshold population activity in layer 2/3 of the barrel cortex with good temporal resolution (Berger et al. 2007; Ferezou et al. 2006; Petersen et al. 2003a), thereby providing us with access to the signal that likely represents sensory evidence in the behaving animal, including the trial-to-trial variability (Petersen et al. 2003b), which might help to explain both the variability in the animals' response probabilities and in the timing of their responses. As in any sensory pathway, it is not currently known where the percept of a tactile input actually occurs in the vibrissa pathway, but lesion studies indicate that primary somatosensory cortex (S1) is necessary for simple sensory tasks such as the detection of a whisker contact (O'Connor et al. 2010a), and it is thus not mediated entirely in sub-cortical structures. Our observer was modeled as an exponentially leaky integrator with access to the averaged signal over a broad area of barrel cortex. The model contained two

important parameters that could be adjusted to provide a fit between the output of the integrator and the observed behavioral results: the time constant of integration and the threshold above which the neural signal must pass to trigger a response. For a particular time constant, choosing the proper threshold was especially critical to avoid either including too many false alarms if set too low, or missing too many low velocity stimuli if set too high. During task performance, the animals would likely dynamically adjust this threshold based on their motivation to correctly perform the task, and our model threshold would represent an average threshold used by the animals in the task.

We tested a range of time constants from 1ms up to 1000ms in our model, but found that the best fit between the predicted and behavioral response probabilities was achieved with a time constant of 20ms. This corresponds well with another recent study of temporal integration in the whisker system of rats engaged in a vibrotactile detection task, in which an integrator with a similarly short time constant provided a good match between the observed behavioral results and the recorded single unit activity (Stüttgen and Schwarz 2010).

The behavioral task was designed such that the animals had a short window in which to respond to the onset of the stimulus in order to receive a water reward on a given trial. This incentive to respond quickly was tempered with a relatively long timeout period in the event of a false-alarm. As shown in **Figure 2-4C**, this led to a decreasing reaction time with increasing stimulus velocity, with a 52 ms difference in mean reaction times between the threshold level deflection velocity and the maximum tested deflection velocity. This represents a 17% decrease in reaction times from the highest velocity

stimulus to the threshold level stimulus. If the output of the integrator was assumed to represent the final decision variable, it might be expected that the range of times at which the integrated signal crossed the detection threshold would display a similar 52 ms difference. Alternatively, if the output of the integrator is instead assumed to represent an early stage of the decision making process, it might be expected that the stronger, faster signals would continue to propagate more quickly. In this case, the percent difference in neural reaction times would be expected to match, as opposed to the raw difference. Indeed, as shown in the inset of **Figure 2-7D**, the measured reaction times match much more closely in percent change (16% change in the model reaction times), than in absolute terms. However, studies in the somatosensory (Luna et al., 2005) and visual system (Cook and Maunsell, 2002; Chen et al., 2006) of primates have estimated integration time constants in the hundreds of milliseconds using a similar exponentially leaking integrator of primary sensory information. The possibility remains that animals in our task could be integrating information over a similarly long timescale. Our simulations showed that doing so would both increase and spread out the neural reaction times, leading to a much closer match in the absolute latencies, but at the expense of accuracy in predicting the response probabilities.

Taken together, the results here show that the behavioral performance of the animal in simple tasks is well predicted by measurements of spatiotemporal cortical activation in parallel experiments in the anesthetized animal, despite the likely differences related to brain state. The approach further provides a potential framework for the evaluation of spatiotemporal cortical signaling in more complex tasks that require discriminability

between disparate sensory inputs, or for tasks that require more complex combinations of detection and discrimination.

Chapter 3 - The adaptive trade-off between detection and discrimination in cortical representations and behavior

---

A modified version of this chapter is currently in preparation for publication:

Ollerenshaw, DR, Zheng, HJV, Wang, Q, Stanley, GB, *The adaptive trade-off between detection and discrimination in cortical representations and behavior*, Under revision

Portions of this work were presented in poster form at the following:

Ollerenshaw, DR, Zheng HJV, Wang, Q, Stanley, GB, *The adaptive trade-off between detection and discrimination in the vibrissa system* Abstract for Poster Presentation, Computational and Systems Neuroscience (Cosyne) meeting, Salt Lake City, UT, February 2013

Ollerenshaw, DR, Bari, BA, Pace, CP, Millard, DC, Zheng, HV, Wang, Q, Stanley, GB, *Detection and classification performance in the whisker system of awake, behaving rats* Abstract for Poster Presentation, Society for Neuroscience, New Orleans, LA, October 2012

Ollerenshaw, DR, Bari, BA, Millard, DC, Orr, LE, Zheng, HV, Wang, Q, Stanley, GB, *Sensory adaptation increases discriminability at the expense of detectability in the whisker system of awake, behaving rats* Abstract for Poster Presentation, Society for Neuroscience, Washington DC, November 2011

The work presented in this chapter was completed jointly with He J.V. Zheng. Figures and text that represent work completed by HJVZ are attributed below.

3.1 Abstract

It has long been posited that detectability of sensory inputs can be sacrificed in favor of improved discriminability, and there is some recent electrophysiological evidence that this can be mediated through bottom-up sensory adaptation. The extent to which this trade-off exists behaviorally, and the complete picture of the underlying neural representations that likely subserve the phenomenon, remain unclear. An ideal observer analysis of cortical activity measured using voltage sensitive dye (VSD) imaging in the rodent vibrissa system showed that spatial discrimination performance was improved following adaptation, but at the expense of the ability to detect weak stimuli. Parallel behavioral experiments demonstrated adaptation enhanced performance in a two-whisker discrimination task, but degraded detection performance. Together, these results provide direct behavioral evidence for the trade-off between detectability and discriminability, that this tradeoff can be modulated through bottom-up sensory adaptation, and that these effects exist at the level of primary somatosensory cortex.

3.2 Introduction

Sensory adaptation has long been known to lead to changes in the nature of information flow in sensory pathways (Ahissar et al., 2000; Fairhall et al., 2001; Chung et al., 2002; Ego-Stengel et al., 2005; Higley and Contreras, 2006; Maravall et al., 2007; Khatri et al., 2009b). While adaptation has often been associated with an overall decrease in neural activity, a number of studies suggest important changes in coding properties in response to sensory adaptation that serve to improve information transmission in the face of complex inputs (Barlow, 1961; Moore et al., 1999; Fairhall et al., 2001; Moore, 2004; Clifford et al., 2007; Maravall et al., 2007; Wark et al., 2007). Consistent with this notion, perceptual studies in humans have demonstrated that sensory adaptation can lead to improved discriminability of tactile stimuli applied to the fingertip (Goble and Hollins, 1993, 1994; Tannan et al., 2006; Clifford et al., 2007). Combined, the evidence indicates that the effects of sensory adaptation represent an important sensory tradeoff in the natural world: detectability, or maximum sensitivity to unexpected inputs, can be sacrificed after adaptation to a stimulus in return for an improved ability to discriminate or categorize the stimulus (Moore et al., 1999; Wang et al., 2010). However, the link between the neurophysiological effects of adaptation and its perceptual consequences remains tenuous.

Although it has long been posited that detectability of sensory inputs can be sacrificed in favor of improved discriminability (Crick, 1984; Sherman, 2001; Moore, 2004), and indeed there is some experimental electrophysiological support (Sherman, 2001b; Lesica

and Stanley, 2004; Lesica et al., 2006; Wang et al., 2010; Adibi et al., 2013), there is no behavioral evidence for this assertion. The tension between providing detectable inputs from strong, robust neural representations versus providing discriminable inputs from more subtle representations is particularly salient in somatosensation, in the context of detectability and spatial discriminability of tactile inputs. Given its discrete and topographic nature, the rodent vibrissa pathway is particularly well suited to address this question (Woolsey and Van der Loos, 1970; Brecht et al., 1997; Petersen, 2007; Diamond et al., 2008b). Specifically, each of the facial vibrissae map directly to individual cortical columns, or 'barrels', in primary somatosensory cortex, that likely represent the fundamental computational sub-units of the pathway that lead to simple percepts. Thus, the question of the detectability versus discriminability of sensory inputs from neural representations can be addressed through analysis of the spatiotemporal activation of the cortical columns from the perspective of an ideal observer. Although the effects of sensory adaptation in the vibrissa pathway of the anesthetized rat have been demonstrated in a range of studies (Chung et al., 2002; Bruno et al., 2003; Khatri et al., 2004; Higley and Contreras, 2006; Katz et al., 2006; Webber and Stanley, 2006; Heiss et al., 2008; Temereanca et al., 2008; Ganmor et al., 2010; Wang et al., 2010), the relevance to behavior has not been established (Castro-Alamancos, 2004). Rodents are capable of performing complex behavioral tasks (Krupa et al., 2001; Uchida and Mainen, 2003; Mehta et al., 2007; Diamond et al., 2008a; O'Connor et al., 2010b; Stüttgen and Schwarz, 2010; Gerdjikov et al., 2010; Busse et al., 2011; Morita et al., 2011; Meier and Reinagel, 2011; Adibi et al., 2012; Ollerenshaw et al., 2012; Raposo et al., 2012; Histed et al., 2012; Lee et al., 2012; Mayrhofer et al., 2013), although spatial discriminability in the

vibrissa system has not been demonstrated. Behaviors trained explicitly to probe the detectability and discriminability of whisker inputs, together with the discrete, topographic neural representation that is experimentally accessible, set the stage for an experimental framework to elucidate the adaptive control of information flow in sensory pathways.

Here, using a combination of voltage sensitive dye (VSD) imaging and novel behavioral experiments in the rodent vibrissae system, we provide a more direct connection between the changes in cortical coding properties in response to sensory adaptation and their effects on behavioral performance in a detection and spatial discrimination task. VSD imaging provides a measure of the response of the cortex over a relatively large area with high spatial and temporal resolution (Kleinfeld and Delaney, 1996; Petersen et al., 2003a; Grinvald and Hildesheim, 2004; Berger et al., 2007), making it possible to measure the interactions of nearby stimuli in both space and time, as well as to resolve inputs across multiple cortical columns, or 'barrels'. We found that following sensory driven adaptation, the magnitude of the cortical response to a single whisker stimulus was reduced, along with a decrease in the spatial extent of activation, resulting in degraded ability to detect stimuli in exchange for enhanced spatial discriminability for an ideal observer of cortical activation. In a parallel set of behavioral experiments, head-fixed rats were trained in vibrissa-based detection and spatial discrimination tasks, both in the presence and absence of a preceding sensory adaptation stimulus. Consistent with the results from the anesthetized animal, behaving animals demonstrated an enhanced discriminability at the expense of a degraded detection performance. Using a variably

timed probe of the detectability and discriminability, we also determined that the timescale of the effects of the adaptation to be on the order of seconds. Together, these results provide direct behavioral evidence for the trade-off between detectability and discriminability, that this tradeoff is modulated through bottom-up sensory adaptation, and that these effects exist at the level of primary somatosensory cortex.

3.3 Methods

Voltage sensitive dye imaging in anesthetized animals

Acute voltage sensitive dye experiments were performed in an additional nine female Sprague-Dawley rats. Details of the surgical and imaging procedures can be found in Ollerenshaw et. al., (2012), and Chapter 2 of this document. Briefly, animals were initially anesthetized with 4-5% isoflurane in the home cage, followed by an injection of sodium pentobarbital (50 mg/kg i.p., initial dose). Supplemental doses were given as needed to maintain a surgical level of anesthesia. A small craniotomy (approximately 3x4 mm) was made on the left hemisphere over the barrel cortex (stereotaxic coordinates: 1.0-4.0 mm caudal to the bregma, and 3.0-7.0 mm lateral to the midline) (Paxinos and Watson, 2007). The dura layer was left intact and washed with Ringer's solution. Voltage sensitive dye (VSD RH1691, Optical Imaging) was allowed to diffuse into the brain during 2 hours of staining in which the dye solution was circulated with a micropipette every 5 minutes (Lippert et al., 2007). After staining, the surface was washed with saline. Saline or silicone oil was applied to the brain surface after washing.

Vibrissae were deflected in the rostral-caudal plane in a saw-tooth waveform of 17 ms in duration (τ = 2 ms). Each trial had 200 ms of pre-stimulus recording. In non-adapted trials, a single deflection (800-1200 °/s) was delivered to either one of the two adjacent vibrissae. In adapted trials, the same probe was preceded by 1 second of a 10 Hz pulsatile adapting stimuli. Each trial was 5 s, and there was at least 3.8 s of rest between the last deflection and the subsequent trial. Stimulation protocols were presented in a random order and repeated 50 times.

Description of behavioral methods

Behavioral studies were conducted using six female Sprague-Dawley rats (Charles Rivers Laboratories, Wilmington, MA; 7 weeks of age, ~250g at the beginning of the study), which were separate from those in the acute portion of the study. Animals were housed on a 12 hour reversed light/dark cycle with all experimental sessions occurring during the dark phase.

Procedure to implant head post

A stainless steel head post was implanted on each animal's skull in order to immobilize the animal during the behavioral tasks. All animals used in the behavioral task were habituated to human contact for a minimum of five days prior to the surgical procedure to implant the head post. The head post consisted of an M5 x 25 mm stainless steel machine screw implanted with the threaded end facing upward. All surgical procedures adhered to aseptic principles. Anesthesia was induced with isoflurane at 4-5%, followed by an injection of ketamine/xylazine/acemaprozine (48/10/1.6 mg/kg, IM). The depth of anesthesia was monitored through toe-pinch reflexes and a non-invasive continuous measurement of heart rate and blood oxygenation. Refer to Ollerenshaw et. al (2012) for details of surgical procedures and post-surgery monitoring.

Water restriction schedule.

Water restriction was implemented after 7-10 days of recovery from head post implantation. Training and data recording sessions took place Monday through Friday, daily, and animals did not have access to water in their home cages on those days.

Correct responses in the behavioral task were rewarded with 50-75μL aliquots of water, and animals were allowed to continue performing the task until sated. The weight of the animal was tracked daily and, when necessary, water supplements were provided after the daily experimental session in order to maintain the weight of the animal within 90% of its pre-implantation value. Water was provided *ad libitum* from Friday afternoon through Sunday afternoon of every week, and for a minimum of one full week every two months.

Behavioral apparatus and training procedures.

The behavioral apparatus and training procedures were similar to those previously reported (Ollerenshaw et al. 2012), and were based closely off of those described in Schwarz et al. (2010). Animals were placed in a custom built body restraint box, shown in **Figure 3-1A**, designed to limit body movement while allowing the animal to maintain a comfortable position. After the animal entered the restraint box from the rear, a vertical plate was slid into place behind the animal until its head protruded from the front of the restraint box. The head post was then rigidly held at the front of the box using a semi-circular aluminum clamp with two brass thumb screws, and a foot rest was positioned to limit motion of the animal's forepaws while allowing the animal to remain in a natural posture. After head fixation, the animals were transferred to a sound and light attenuating cubicle (Med Associates, ENV-014, St. Albans, VT), in which the behavioral tasks were performed. A water spout, which served both to deliver water rewards and record behavioral responses, was placed in front of the animal's mouth in a position that allowed it to be easily reached with the tongue. The water spout was instrumented to detect licks both electrically (Hayar et al., 2006) and mechanically using a piezo element mounted to

the lick spout clamp, as shown in **Figure 3-1B** and **Figure 3-3**. Stimuli were delivered using piezoelectric actuators (Part number PL140.11, Physik Instrumente, Auburn, MA) with a hollow glass capillary glued to the end, as described above. The actuators were positioned using a lockable articulating arm (Fisso Strato M-28, Baitella AG, Zurich), allowing for quick maneuvering of the capillary into position next to the face, after which an individual whisker was guided into the capillary using forceps. Images of the piezo actuators are shown in **Figure 3-1C** and **Figure 3-1D**. A white noise masking speaker in front of the animal served to limit the possibility of auditory confounds during the behavioral task. Task control and data logging was performed using a custom written user interface in Visual Basic 6, combined with a Sensoray S626 Data Acquisition card (Tigard, OR).

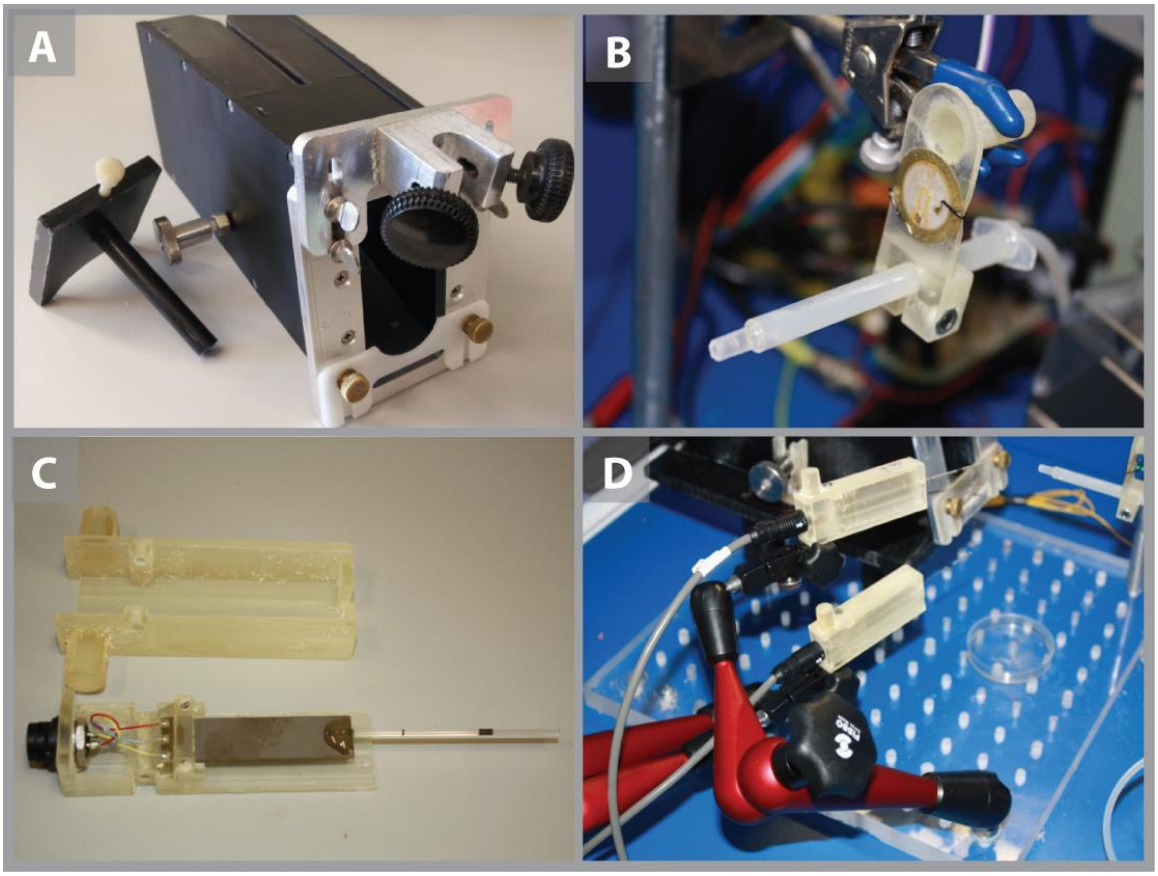

Figure 3-1 - *Components used in behavioral task.* **A.** The body and head restraint box, which were modeled off of designs used in the Schwarz Lab. Animals entered the box from the rear and the back door shown to the left of the image was placed behind the animal to prevent it from backing into the box. A 6cm aluminum rod was affixed to the implanted headpost, which was then clamped in place using the thumb screws at the top of the box. A foot plate was used to provide space for the animals to rest their paws, as well as to prevent animals from interfering with whisker stimulation. **B.** The lick detector and spout. Shown is a 1 mL syringe in a custom 3D printed clamp with a piezo element glued in place. Contacts of the animal's tongue were recorded as voltage transients. **C.** One of the piezoelectric actuators shown inside a custom 3D printed enclosure box. A hollow glass capillary was glued to the piezo element and was used to interface with individual whiskers on the animal's snout. **D.** Two piezoelectric actuators shown in the custom enclosures and attached to manipulator arms for easy adjustment at the beginning of each behavioral session.

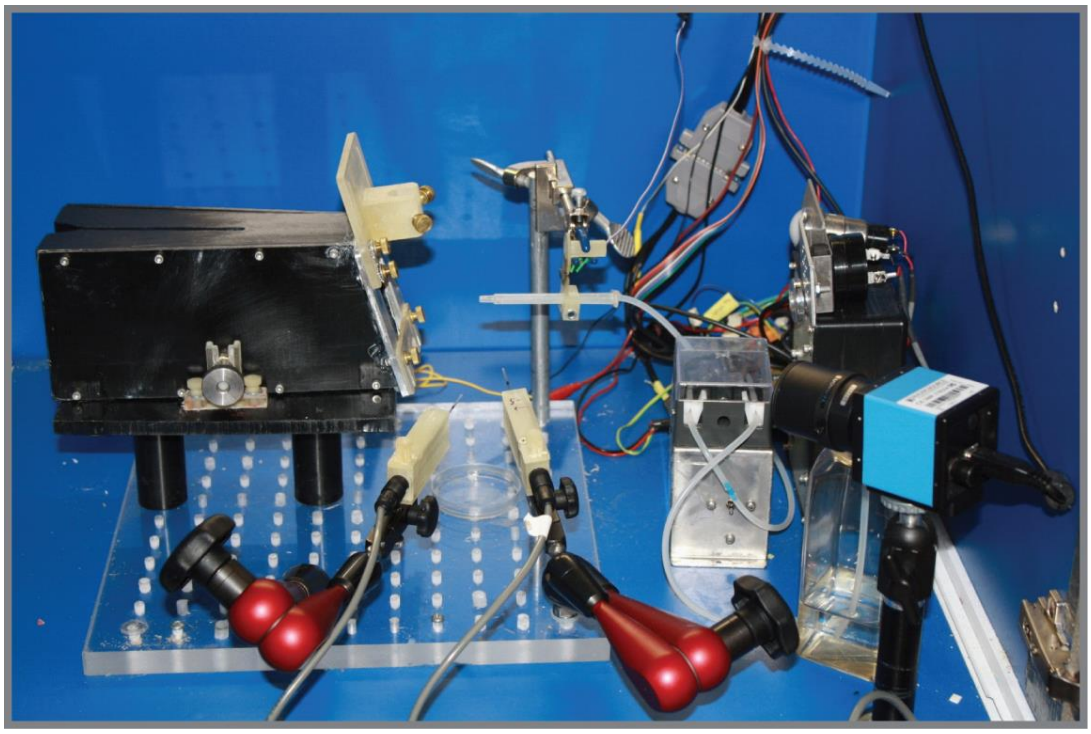

Figure 3-2 - *The interior of the behavioral chamber with all components in place*. The head-fixed animal would be secured in the restraint box to the left with the water spout positioned for easy access with the tongue. An infrared sensitive CCD camera is visible to the front left and was used to monitor the animals during the task.

After recovery from the implantation surgery, animals were slowly habituated to head fixation. In the initial phase of habituation, the period of fixation was kept very short to minimize stress to the animal, and the duration was gradually increased over the course of 1-2 weeks. The animals were then transferred to the behavioral apparatus, at which point training in the full behavioral task (detailed below) commenced. The interior of the behavioral chamber was illuminated with infrared lights (Lorex Technology Inc., model VQ2121, Markham Ontario) and the animal's behavioral state was monitored using a 30 fps CCD camera (The Imaging Source, LLC, model DMK 21BF04, Charlotte, NC). The interior of the behavioral chamber is shown in **Figure 3-2**. Behavioral sessions were

always terminated when the animal exhibited signs of stress or ceased performing the tasks. One to two behavioral sessions were generally performed per day with a given animal.

Stimulus design

A multi-layered piezoelectric bending actuator (range of motion: 1 mm, bandwidth: 200 Hz; Polytec PI, Auburn, MA) generated the vibrissa deflections. A 5 cm length of 20 µL glass pipette was glued to the end of the actuator and placed on an individual whisker 10 mm from the face. To ensure precise control of the stimuli, the voltage commands for the piezoelectric actuators were generated using a custom written Matlab routine deployed on a dedicated PC running the Matlab xPC real-time environment with 1 ms temporal resolution, with commands sent through a National Instruments PCI 6024e DAQ card. The actuators were calibrated using either a photo-diode circuit or high speed videography to determine the relationship between command voltage steps and the resulting deflection amplitudes and velocities, analogous to the method described by other studies (Andermann et al., 2004; Arabzadeh et al., 2005). Whisker deflections were ramp and hold stimuli similar to those used in previous studies (Stüttgen et al. 2006; Stüttgen and Schwarz 2008) and were always delivered in the rostral to caudal direction. The actuator tip followed a quarter sine wave trajectory from rest to its most caudal position. The amplitude of the stimuli remained fixed and the time to the maximum amplitude was varied to control the velocity of the deflection. After reaching its maximum amplitude, the whisker was held for 1 s, before slowly being returned to rest over 2 seconds. This slow return phase was designed to be below the animals' perceptual

threshold, thus ensuring that the behavioral response of the animals was triggered on the rising phase of the stimulus. On half of the trials (see description of behavioral task below), a 3 s, 12 Hz sine wave stimulus was applied prior to the detection stimulus to act as an adapting stimulus. Velocities in the detection task ranged from 25 º/s to 2,500 º/s. In the discrimination task, a single deflection velocity of 1,500 º/s was used.

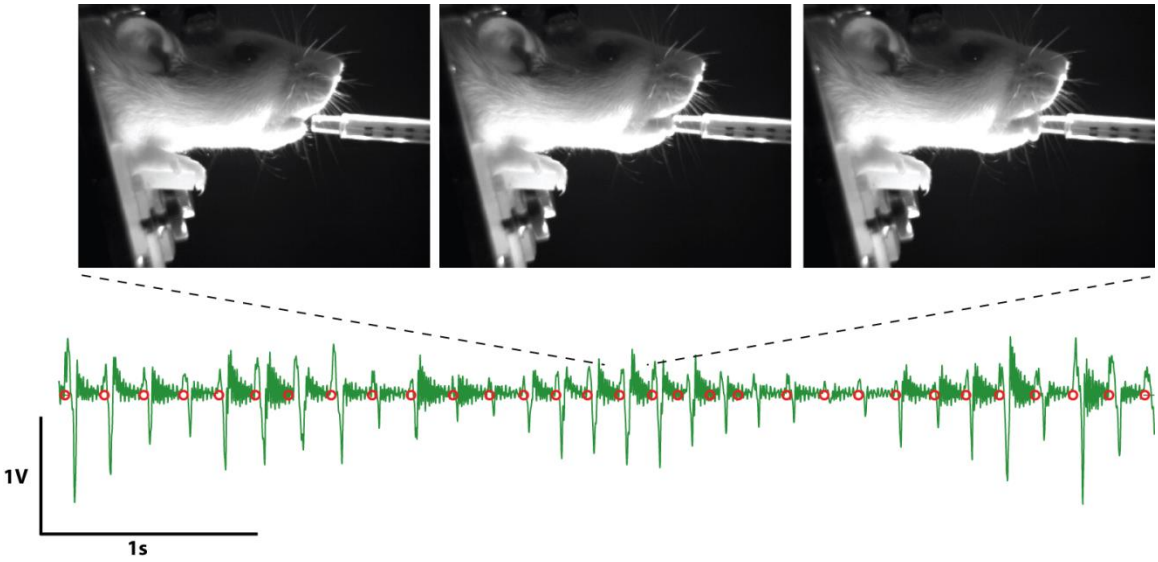

Figure 3-3 - *Sample of lick detection output trace.* Shown are three frames collected using a high speed camera at 500 frames per second while the animal freely licked the water spout. Below is a 5 second voltage trace from the lick detection circuit, with red circles showing the automatically detected lick times, which were verified from the high speed video.

Detection task design

The animals were initially trained in a go/no-go detection task similar to that described previously (Stüttgen et al. 2006; Stüttgen and Schwarz 2008; Ollerenshaw et al. 2012) and shown schematically in Figure 3-8. Data were collected from four animals in the

detection task and the piezoelectric actuator was placed on the C2 whisker for all animals but one, for which the D1 whisker was used. Two animals were moved directly to the discrimination task (see below) without collecting data in the detection task. The beginning of a new trial was signaled to the animal by the onset of a 3 s tone. On 50% of trials, a 12 Hz sinusoidal adapting stimulus was applied concurrently with the tone. Licking responses to the onset of the adapting stimulus were neither penalized nor rewarded. The offset of the tone was followed by a stimulus delay period that varied uniformly from 0.5-2.5 s, after which the detection stimulus (the S+ stimulus) was initiated. Animals then had a 1 s response window to initiate a licking response to the water spout. Licks detected during the response window were categorized as hits and resulted in a water reward. Failure to respond during the response window was categorized as a miss, but not penalized. To discourage impulsive licking of the water spout, a 1 s no-licking period was enforced before the delivery of a detection stimulus, with any licks during this period resulting in a further delay of the stimulus. Thus, if an animal initiated a licking response at the onset of the adapting stimulus, the detection stimulus would still be presented at the scheduled time so long as the animal ceased licking before the beginning of the no-licking period.

To further prevent potential auditory confounds, a second piezoelectric actuator was positioned near the animal but outside of the vibrissa array and was deflected randomly on a 0-5s uniform distribution. 15% of trials were designed as catch trials in which the second actuator (the S- stimulus) was triggered in place of the primary actuator. Responses to catch trials were labeled as false alarms and were penalized with a 5-10

second time-out during which a stimulus light directly in front of the animal was illuminated. Short sessions were periodically performed in which the primary actuator was removed from the whisker to further test for confounds. The animals responded to stimuli at approximately chance levels in these sessions, which were kept short to avoid frustrating the animal, indicating that only whisker-based tactile cues were being used in the task.

To exclude trials in which the animal failed to respond due to lack of motivation, every fifth trial was designed to be a suprathreshold (1,500 °/s) test stimulus, which was not included in constructing the animals' psychometric curves. The test stimulus was repeated if the animal failed to respond, and the session was terminated if the animal missed five consecutive test stimuli. Trials were excluded from the analysis if the animal failed to respond to the next test stimulus. Thus, every block of four randomized deflection velocities are bracketed by a set of successful responses to test stimuli.

Discrimination task design

After training in the detection task, animals were subsequently trained in a go/no-go spatial discrimination task, which is shown schematically in **Figure 3-8B**. Five of the six animals in the study were moved to this task. In the training phase of the discrimination task, the S- piezoelectric actuator was positioned on the furthest whisker that was practically accessible, generally the A2 or A3 whisker, while the S+ actuator remained on the same whisker that was used during the detection task. After the animals began demonstrating the ability to discriminate between distant whiskers, the S- stimulus was

moved closer to the S+ stimulus. The location of the S- stimulus was varied on each session between one of four possible locations: 1 whisker away in the same row, 2 whiskers away in the same row, 1 whisker away in the same arc, and 2 whiskers away in the same arc. The location of the S+ stimulus remained the same for each animal, and the location of the S- stimulus was chosen from a pseudo-randomized list of possible locations in advance of each session.

The discrimination task followed the same sequence as the detection task, with the exception that S+ and S- trials were provided with equal probability. The 3 s, 12 Hz adapting stimulus was applied to both whiskers on 50% of trials, followed by a 0.5-2.5 s stimulus delay. Thus, there were four types of trials presented to the animal, each with equal probability: S+ stimuli without adaptation, S+ stimuli following the adapting stimulus, S- stimuli without adaptation, and S- stimuli following adaptation. As in the detection task, the animals did not know *a priori* precisely when the stimulus would be delivered, requiring them to both detect the presence of a stimulus, and to subsequently classify the stimulus as being on the S+ or S- whisker. Animals were rewarded for responding to deflections of the S+ stimulus (hits) within the 1 s response window, and were penalized with a 5-10 s timeout paired with house lights for responding to S- stimuli (false alarms). Misses and correct rejections were not penalized or rewarded. As in the detection task, a 1 s no-licking period was enforced before the delivery of the stimulus in order to prevent impulsive licking. The velocity of the stimuli remained fixed at 1,500 °/s. Sessions were terminated when the animal failed to respond to 5 consecutive S+ stimuli. The actuators were visually inspected after each session to ensure that neither whisker

had slipped from the capillary, with the entire session discarded from analysis if so. Short sessions were performed with both piezoelectric actuators removed from the whiskers to ensure that animals were relying solely on tactile cues to perform the task. Animals failed to reliably respond to either the S+ or S- stimuli during these sessions.

Behavioral data analysis

Data from the detection task were pooled across four animals in order to construct the psychometric curves shown in **Figure 3-9B**. For each of the tested stimulus velocities, trials were categorized into three possible types: responses without adaptation (non-adapted), responses to stimuli within 0.5-1.5 s from the end of the adapting stimulus (adapted short recovery), and responses to stimuli within 1.5-2.5 s from the end of the adapting stimulus (adapted long recovery). Trials in which the adapting stimulus was present and the animal emitted an anticipatory lick during the no-lick period, thereby creating a delay between the adapting and probe stimulus of greater than 2.5 s, were omitted from the analysis. The first and last 10 trials from each session, in which the animals were likely either sated or not sufficiently engaged in the task, were excluded. Data points in the psychometric curve represent the probability of response to each stimulus velocity. Curves were fit using a polynomial of the form:

$$P(V) = \gamma + (1 - \gamma - \lambda)\left(1 - e^{-\left(\frac{V}{\alpha}\right)^{\beta}}\right) \quad (2)$$

in which V is the whisker deflection velocity, P is the response probability, γ and λ are the upper and lower asymptotes of the sigmoidal fit, and α and β are free parameters

governing the shape of the curve. The parameters of the fit were calculated using the Psignifit toolbox in Matlab (Fründ et al., 2011). Similar curve fits were calculated for each animal individually to determine the perceptual threshold for each animal, which was defined as the velocity at which the animal responded to 50% of stimuli.

Given the go/no-go behavioral paradigm, performance in the discrimination task can be measured as the difference in the probability of response to S+ stimuli (hits) vs. S- stimuli (false alarms). A simple metric for comparing the response probabilities is to measure their ratio. Applying the ratio test, an animal that was equally likely to respond to either stimulus type, and therefore failing to discriminate, would have a discrimination ratio of 1. Higher response rates to S+ stimuli would result in a discrimination ratio greater than 1. A similar metric known as the discrimination index (Gerdjikov et al., 2010), which is simply the difference in hit rate and false alarm rate, was also applied. The discrimination index will range from 0 for an animal responding with equal probability to both stimulus types, to 1 for an animal responding to all of the S+ stimuli and none of the S- stimuli. However, another commonly used metric for measurement of discriminability, d', is more difficult to apply due to the changes in detectability from the non-adapted to the adapted state (see results). In order to apply d', we must first account for this reduced detectability. **Figure 3-10** illustrates how changes in detectability will likely affect the measured hit and false alarm rates. In **Figure 3-10A** and **Figure 3-10B**, the box represents all stimuli presented to the animal, which is evenly divided between S+ and S- stimuli. The circle represents the proportion of all trials detected by the animal, which decreases from the non-adapted to the adapted state. Experimentally, we have

access to the fraction of all trials that the animal chooses to respond to, regardless of whether or not the stimulus was actually detected. Graphically, these measured response rates correspond to the fraction of each half of the square that is colored in dark green (for hits) or dark red (for false alarms). These values can be expressed mathematically as $P(R_{S+} \cap D)$ and $P(R_{S-} \cap D)$, in which $\cap$ represents the intersection. The fraction of the S+ and S- stimulus space contained by the detection circle can be written as $P(D)$. $P(D)$ is assumed to have remained constant from the detection task, allowing us to apply the experimentally measured values in the three states as listed above. Thus, using conditional probabilities, the probability that an animal responded to an S+ stimulus, a hit, given that it detected the stimulus can be written as:

$$P(R_{S+}|D) = \frac{P(R_{S+} \cap D)}{P(D)} \tag{3}$$

Similarly, the probability that an animal responded to an S- stimulus, a false alarm, given that it detected the stimulus can be written as:

$$P(R_{S-}|D) = \frac{P(R_{S-} \cap D)}{P(D)} \tag{4}$$

These values, which will hereafter be referred to as the "detection corrected" response probabilities, can then be substituted into the traditional equation for d' to calculate the detection corrected d', which becomes:

$$d' = z(P(R_{S+}|D)) - z(P(R_{S-}|D)) \quad (5)$$

in which z represents the inverse cumulative normal function (Macmillan and Creelman, 2004). Conveniently, taking the ratio of hit rate to false alarm rate causes the detection probability to cancel from the numerator and denominator, meaning that the ratio measurement is unaffected by changes in the overall level of detectability. It should be noted that, implicit in these calculations is the assumption that the animals were equally likely to detect stimuli applied to both the S+ and S- whisker. We were primarily concerned here with changes in discriminability from the non-adapted to the adapted states. Thus, if this assumption was not valid, the baseline level of discriminability in the non-adapted state using these measures would change, but observed changes from the non-adapted to the adapted states, which reflect changes in the relative response rates to S+ and S- stimuli, would remain valid. Further, evidence from anesthetized studies indicates that the spatiotemporal characteristics of the cortical response are consistent regardless of which macrovibrissa is deflected (Davis et al., 2011; Wang et al., 2012), suggesting that behavioral detectability levels would also remain consistent across macrovibrissae.

Data from the discrimination task were analyzed separately for each of the five animals that performed the task. Each of the three discrimination metrics discussed above was calculated for each animal. As in the detection task, responses on trials following adaptation were separated into those in which the stimulus was delivered within 0.5-1.5 s after the end of the adapting stimulus, referred to as “short recovery” trials, and those in

which the stimulus was delivered 1.5-2.5 s after the end of the adapting stimulus, referred to as "long recovery" trials. Trials on which the animal emitted an anticipatory response that resulted in the delay between the adapting stimulus and the probe stimulus being greater than 2.5 s were excluded from the analysis. Due to the fact that the location of the S- stimulus was moved on every session, the first 30 trials of each session were excluded from the analysis to allow the animal a period to re-learn the task on every session. The last 10 trials were also excluded to avoid including trials in which the animals' motivation had decreased. Data points in **Figure 3-12C-F** represent the means across five animals and error bars represent +/- one standard error of the mean.

3.4 Results

Adaptation spatially constrains the cortical response in the anesthetized animal

In work performed primarily by He JV Zheng in the Stanley laboratory, voltage sensitive dye (VSD) imaging of cortical activity was combined with controlled whisker deflections in a series of experiments on anesthetized rats to investigate the effects of sensory adaptation on the cortical response. The experimental setup is illustrated in **Figure 3-4**. Piezoelectric actuators were used to deflect individual whiskers, as depicted in the lower portion of the figure. The highly organized rows and arcs of facial whiskers map topographically to cortical columns (barrels) in the primary somatosensory cortex, such that deflection of a single whisker activates a homologous region of cortex (Brecht et al., 1997; Petersen, 2007; Diamond et al., 2008b). The VSD imaging equipment captures images of the resulting activation at 5 ms intervals, allowing the spatial and temporal evolution of the cortical signal to be tracked with relatively high temporal resolution over a large region of cortex. The recorded activity represents primarily subthreshold activity in layer 2/3 neurons, which receive their primary input from cortical layer 4 neurons (Kleinfeld and Delaney, 1996; Petersen et al., 2003b; Berger et al., 2007). An example of a recorded VSD signal is shown at the top of **Figure 3-4**. The images represent the average of 50 repeated presentations of the same 850 °/s rostral-caudal whisker deflection and the color scale of the images represent the percent change in the fluorescence relative to the background level ($\%\Delta F/F_0$). Typical of imaged responses, the VSD signal here initially appeared localized in the primary barrel at 10 ms after stimulus onset, quickly spread to neighboring barrels, peaked at about 20-25 ms, then gradually decayed back to

baseline at about 100 ms, consistent with previous findings (Petersen et al., 2003a; Wang et al., 2012). Subsequent analyses were based on the time-averaged response from the typical onset to peak time (10-25ms), as illustrated here.

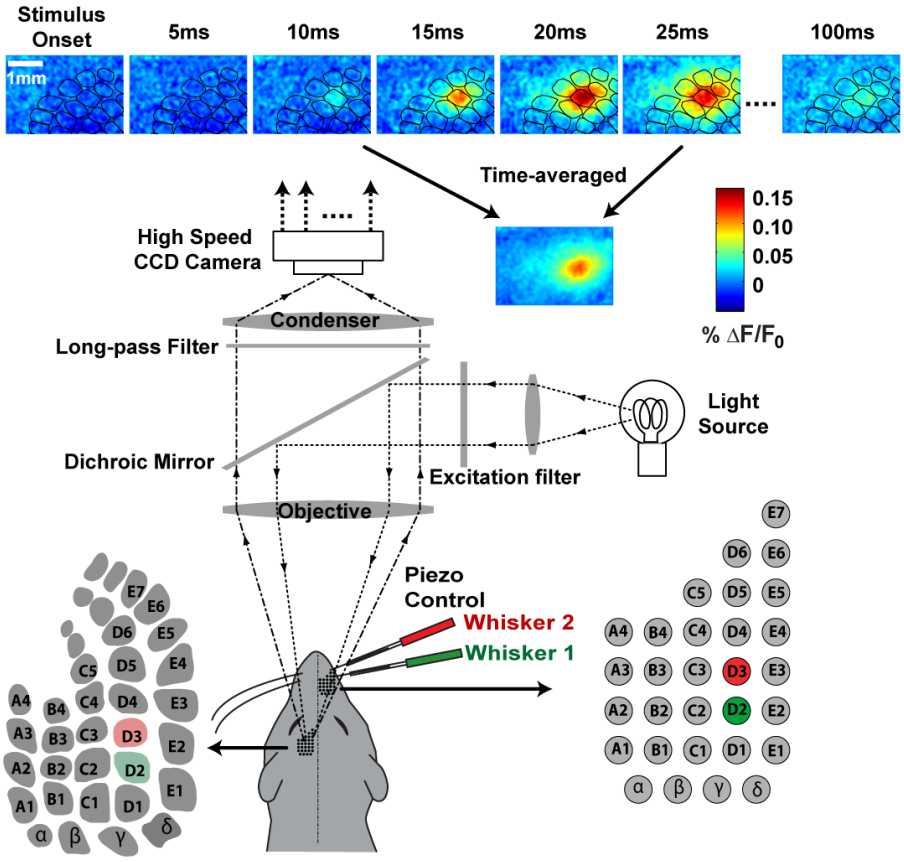

Figure 3-4 - Schematic of *In-vivo VSD imaging of the rat barrel cortex (courtesy of HJV Zheng).* In the rat vibrissa pathway, the cortical columns are topographically mapped to the whiskers on the snout. Each single whisker deflection evokes the strongest response in the corresponding barrel (primary barrel). A piezoelectric actuator delivers a probe deflection to either of the two adjacent whiskers while the VSD camera system simultaneously collects fluorescence signal from layer 2/3 of an anesthetized rat. The top panel shows an example response to a single whisker deflection averaged over 50 trials. The response initially appeared localized around the primary barrel at 10 ms after stimulus onset, quickly spread to neighboring columns, and peaked at about 20-25 ms. Overlaid on the VSD images is an outline of barrels functionally registered using the responses to different whisker deflections. A time-averaged frame from onset to peak (10-25 ms) was used for further analysis.

Under the assumption that the locus and the extent of neural activity is important in coding the location of a whisker contact (Sheth et al., 1998), we sought to measure both the amplitude of the cortical response as well as its initial spatial extent. An example of a typical response to two adjacent, separate whisker deflections is shown in **Figure 3-5A**. The images shown were averaged over 50 trials and time-averaged from signal onset to peak (10-25 ms, see Fig. 1). Each of these responses was fit with a 2D Gaussian function and an ellipse representing the half-height of the contour is superimposed on the figure. **Figure 3-5B** shows the superposition of these two contours to illustrate the amount of spatial overlap in the cortical activation when two adjacent whiskers are deflected separately and without a pre adapting stimulus. In contrast, **Figure 3-5C** shows the individual VSD responses to deflections of adjacent whiskers following the presentation of a 10 Hz, 1 second pulsatile adapting stimulus. The amount of cortical overlap in the adapted state is demonstrated by overlaying the 2D Gaussian fits, as shown in **Figure 3-5D**. It is evident from visual inspection that there is significantly more overlap of the responses in the non-adapted state (**Figure 3-5B**) than in the adapted state (**Figure 3-5D**).

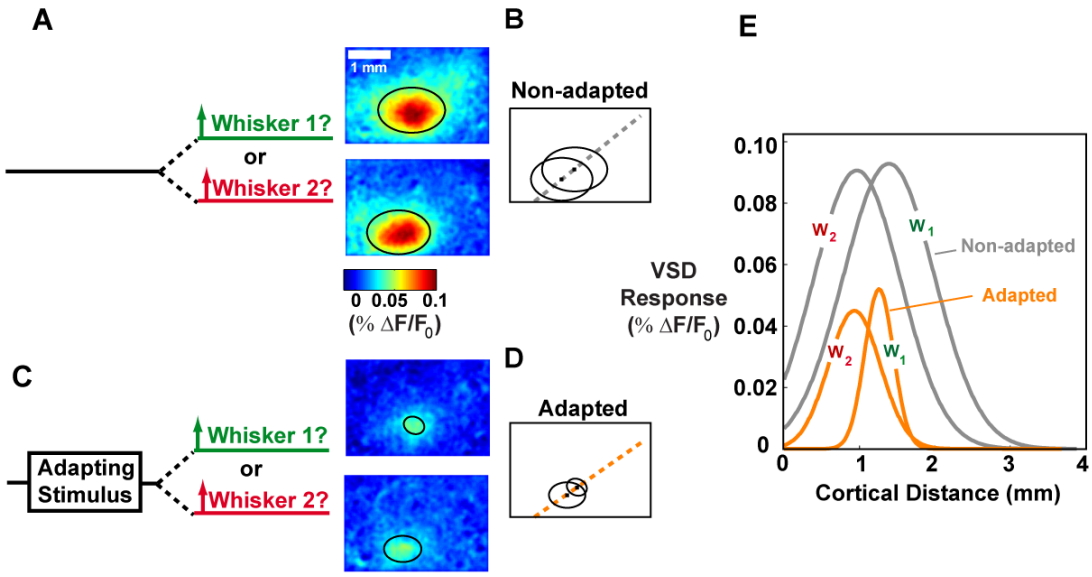

Figure 3-5 - *Cortical response decreases in magnitude and in area following adaptation (courtesy of HJV Zheng).* **A.** The cortical responses to a single whisker deflection in the absence of a preceding 10 Hz adapting stimulus. Whisker 1 (W1) and whisker 2 (W2) were adjacent to each other on the snout and stimulated separately. Images were averaged over 50 trials. The black ellipses on the images were half-height contours of the two-dimensional Gaussian fits to the images. **B**. Superposition of the Gaussian contours shown in **A**. **C.** In contrast, the same stimulus delivered in the presence of a preceding 10 Hz adapting stimulus evoked a cortical response that was significantly reduced in magnitude and in area. The black ellipses on the images were half-height contours of the two-dimensional Gaussian fits to the images. **D.** Superposition of the Gaussian contours shown in **C**. **E.** The one-dimensional view of the Gaussian fits through the two centers, indicated by the dashed lines in **B** and **D**. Note the reduced magnitude with adaptation, accompanied by a decrease in the overlap of the distributions.

The effects of the adaptation are more clearly visualized in **Figure 3-5E**. Here, cross sections were taken of the 2D Gaussian fits using the lines connecting the centers of activation for both fits in the non-adapted and adapted cases, shown as dashed lines in **Figure 3-5B** and **Figure 3-5D**. In general, adaptation reduced the magnitude of the cortical response magnitude, but also decreased the amount of overlap of the cortical responses to adjacent vibrissa deflections. This suggests that adaptation may have

differential effects on detectability and spatial discriminability of tactile inputs, which is explored using an ideal observer analysis below.

Adaptation degrades the detectability of the stimulus for the ideal observer

To quantitatively assess the impact of adaptation on detection, we measured the detectability of a stimulus against the pre-stimulus noise on a single trial basis in the non-adapted and adapted states using optimal detection theory (Duda et al., 1995; Macmillan and Creelman, 2004). The strength of the cortical response on each single trial was represented with a decision variable (DV), which was used by the ideal observer to classify each trial as signal or noise. This was done by pooling the neural activity, measured as the average fluorescence, within an approximately barrel-sized region of interest (ROI) in the 10-25 ms after stimulus onset, which generally includes the time from signal onset to peak. Note that the results were not dependent on the absolute size of the ROI, assuming that it remained within the range of an individual cortical column (less than 300-500 μm in diameter). The same ROI was applied to all single trials in all three cases: pre-stimulus noise, non-adapted response, and adapted response. For each case, the DVs over all 50 recorded trials were binned, and a Gaussian probability function was fit. **Figure 3-6A** shows a typical example of the noise (shown in black) and signal distributions in the non-adapted (grey) and adapted (orange) states. Corresponding examples of the trial-averaged VSD responses are shown for each of the three cases with the decision region overlaid in black.

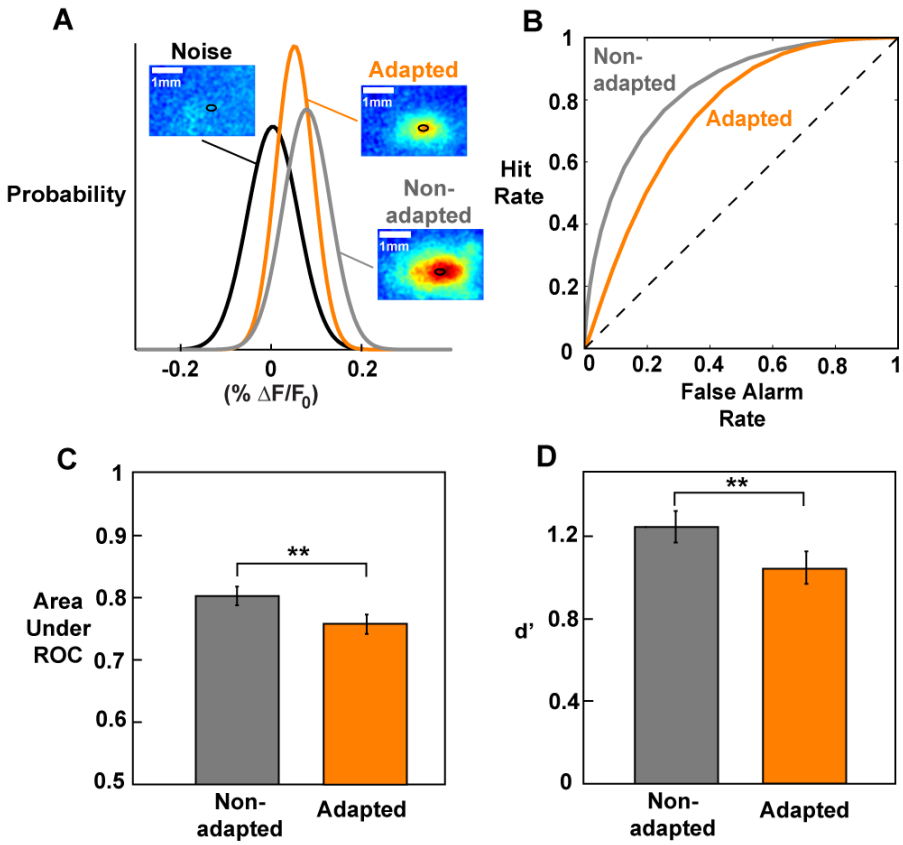

Figure 3-6- *Adaptation degrades detection for an ideal observer of population cortical activity.(courtesy of HJV Zheng)* **A.** The probability of decision variables from single-trial pre-stimulus noise, non-adapted, and adapted responses. A region of interest (ROI) approximately the size of a cortical column (300-500 µm in diameter) was defined as the 98% height contour of the two-dimensional Gaussian fit to the trial-averaged non-adapted response. The insets show the corresponding trial-averaged images for each case (noise, non-adapted, and adapted), with the ROI outlined in black. The same ROI was applied to all three cases. The average fluorescence within the ROI was extracted from each single trial as a decision variable (DV). **B.** Receiver operating characteristic (ROC) curves that represent the separation of non-adapted and adapted DVs from the noise DV distribution. A larger area under the non-adapted ROC curve (AUROC) signifies a larger separation of non-adapted signal from noise in comparison to the adapted case. **C.** The detection performance of the ideal observer (measured with AUROC) was degraded following adaptation, as the area under the ROC curve decreased ($p < 0.005$, $n = 18$, paired t-test). Error bars represent +/- 1 standard error of the mean. **D.** The d' value that measures the distance of signal distribution from the noise distribution decreased following adaptation ($p < 0.005$, $n = 18$, paired t-test). Error bars represent +/- 1 standard error of the mean.

Note that the adapted distribution in **Figure 3-6A** lies closer to the noise than does the non-adapted distribution, implying a reduction in detectability with adaptation. The separation of signal from noise was more objectively quantified using a receiver-operating characteristic (ROC) curve, which evaluates the performance over all threshold choices, where the threshold in this case is the average fluorescence level necessary for the observer to classify a signal as being present. For each threshold value, the false alarm rate (cumulative probability of the noise above threshold) versus the hit rate (cumulative probability of the signal above threshold) was plotted on the ROC curve. A larger separation between the signal and noise distributions yields a higher hit rate at a given false alarm rate, and consequently, a larger area under the ROC curve (AUROC). The corresponding ROC curves for the signal distributions in **Figure 3-6A** are shown in **Figure 3-6B**, where the non-adapted case has a larger AUROC. **Figure 3-6C** summarizes the AUROC across all datasets, demonstrating that the overall detection performance decreased after adaptation (non-adapted AUROC: 0.80 +/- 0.015; adapted AUROC: 0.76 +/- 0.016; $p < 0.005$, $n = 18$, paired t-test). Note that this measurement takes into account all possible choices of threshold, but that for intermediate ranges of threshold choice, there was as much as a 30% reduction in the hit rate for a given false alarm rate.

We also measured detectability using a standard detection theory variable d', which quantifies the separability between two distributions. A large separability (d') is a result of either a large distance between the means of the distributions and/or a small combined variance. **Figure 3-6D** summarizes d' across all datasets, again demonstrating a decrease

in detection performance after adaptation (non-adapted d': 1.24 +/- 0.076; adapted d': 1.05 +/- 0.078; $p < 0.005$, $n = 18$, paired t-test).

Adaptation enhances discriminability of the stimuli for the ideal observer

The ideal observer analysis was subsequently extended to measure changes in the spatial discriminability of the cortical response resulting from deflections of adjacent vibrissae in the non-adapted and adapted states. Based on the cortical response to a single whisker deflection, the observer was tasked with identifying which of two possible whiskers caused the subsequent cortical response. The ROIs for each of the two whiskers were defined as described above and were both applied to all single trials. The deflection of an individual whisker thus resulted in two variables of interest. For example, after a deflection of whisker 1, we measured the response in the corresponding ROI ($R_1|W_1$), as well as the response in the adjacent ROI ($R_2|W_1$). **Figure 3-7A** shows the response to each whisker deflection, with the two ROIs outlined in black. For a given whisker deflection, the corresponding ROI is shown in bold.

Figure 3-7B demonstrates the discriminability of stimuli for the ideal observer in the non-adapted state. The figure shows an example of all single-trial variables for a single experimental dataset. Each data point represents the variables from a single trial, with variables from deflections of whisker 1 shown in green and responses from deflections of whisker 2 shown in red. Trials were excluded from the analysis when the average fluorescence in the ROI fell below the 'detection threshold', which was chosen to correspond with a detection false alarm rate of 10%. This value was chosen based on the

reported false alarm rate from similar behavioral studies (Stüttgen et al., 2006; Stüttgen and Schwarz, 2008; Ollerenshaw et al., 2012). Given the topographic alignment of the vibrissa system, the cortical response to a whisker deflection is generally strongest in the primary barrel, leading to the clustering of responses evident in **Figure 3-7B**. The extent to which these two clusters can be discriminated between determines how well an observer would perform at correctly identifying the whisker which led to the particular cortical response. Linear Discriminant Analysis (LDA) was used to determine the line that maximally separates the two clusters, shown as the solid black line in **Figure 3-7B**. The projection of the raw variables onto the line orthogonal to the LDA line was defined as the decision variable, coming from two distinct, but overlapping probability distributions. The separability of the two probability distributions, measured using the standard detection theory variable d', was used as the metric for discrimination performance.

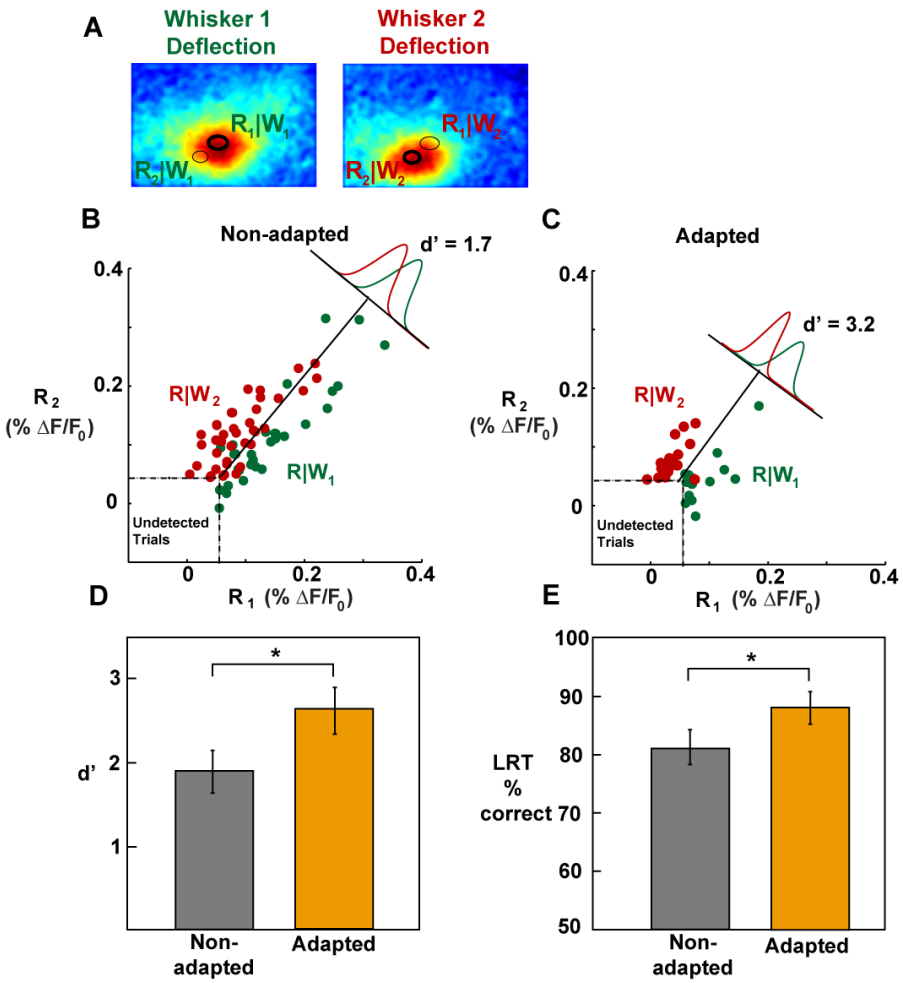

Figure 3-7 - *Adaptation improves discrimination performance for an ideal observer of population cortical activity. (courtesy of HJV Zheng)* **A.** The same method described in detection was used to derive the ROI for each of the two whisker stimulations (shown in bold ellipse). Both ROIs were applied to all single trials. Two responses were calculated for each single trial: the average fluorescence within the primary barrel area (bold ellipse), and that within the adjacent barrel area (thin ellipse). **B.** Responses above the detection threshold (see Methods) in the non-adapted case were grouped by whisker stimulation and separated using Linear Discriminant Analysis (LDA). The decision variable was defined as the projection of the response onto the axis orthogonal to the LDA line. The d' separation measure was then calculated for the two probability distributions of the decision variables. The d' in this example was 1.7. **C.** Same analysis as in **B** for the adapted case. The d' in this example was 3.2. **D.** Discrimination performance (d' of DV probability distributions) of the ideal observer significantly improved following adaptation ($p < 0.05$, $n = 9$, paired t-test). Error bars represent +/- 1 standard error of the mean. **E.** Discrimination performance using the likelihood ratio test also significantly improved following adaptation ($p < 0.05$, $n = 9$, paired t-test). Error bars represent +/- 1 standard error of the mean.

Figure 3-7C demonstrates improved discriminability for the ideal observer in the adapted case. With adaptation, the two variable clusters became more separated as compared to the non-adapted clusters, resulting in a larger separation of the projected probability distributions. However, due to the simultaneous reduction in signal amplitude that comes with adaptation, a higher percentage of the trials fell below the detection threshold and were subsequently eliminated from the analysis. The d' value for the shown adapted example was 3.2, whereas the corresponding non-adapted example had a d' value of 1.7. **Figure 3-7D** shows the average d' values for all of the datasets, demonstrating that discriminability was significantly improved for the ideal observer following adaptation (non-adapted d': 1.9 +/- 0.24; adapted d': 2.6 +/- 0.26; $p < 0.05$, $n = 9$, paired t-test).

As an alternative measure of discrimination performance, we also performed a likelihood ratio test (LRT), using Bayesian decision theory (Duda et al., 1995), with leave-one-out validation. For each single trial, we calculated the sufficient discriminant for the response variable **R** (the vector consisted of R_1 and R_2), and classified the trial into either one of the two known stimuli (whisker 1 or whisker 2) based on its discriminant value. The result of the classification was then checked against the actual stimulus, with the percentage of correct trials used as the final discrimination performance measure. **Figure 3-7E** shows the fraction of correct trials for all data sets. The performance in the non-adapted case was 80.6% +/- 3.1%. In the adapted case, the observer correctly classified 88.6 +/- 2.6%, again showing that discriminability was significantly improved for the ideal observer following adaptation ($p < 0.05$, $n= 9$, paired t-test).

Given that the primary cortical response is an essential step in the processing and eventual perception of a sensory stimulus (Houweling and Brecht, 2008; Huber et al., 2008; O'Connor et al., 2010a), the ideal observer analyses strongly suggests that sensory adaptation will lead to a corresponding perceptual decrease in detectability coupled with improved spatial discriminability in the awake animal.

The behavioral trade-off between detection and discrimination with adaptation

To directly test the perceptual effects of sensory adaptation, both a detection and a spatial discrimination task were designed and carried out using a separate set of head-fixed rats. The tasks were designed to allow the animals to be tested both in the presence and absence of a preceding sensory adaptation stimulus. The animals were trained first in a go/no-go detection task to determine the extent to which sensory adaptation affects the behavioral perceptual thresholds. These experiments were followed by a two-whisker go/no-go spatial discrimination task to determine if and to what extent discrimination performance was also affected by sensory adaptation.

The detection task was based on tasks published previously by our lab and others (Stüttgen et al., 2006; Stüttgen and Schwarz, 2008; Ollerenshaw et al., 2012), with the exception that the stimulus to which the animal was trained to respond was preceded by a 12 Hz sinusoidal adapting stimulus on a subset of trials. The task is shown schematically in **Figure 3-8A** and described in detail in the Methods section. Each trial in the task was initiated by a 3 s tone, during which a 12 Hz sinusoidal adapting stimulus was presented randomly on half of the trials. A variable velocity stimulus was subsequently presented on a uniformly varying time interval between 0.5 and 2.5 s after the end of the tone and

the animal had a 1 s window following the stimulus in which to emit a lick to receive a water reward. Thus, the probability of response as a function of stimulus velocity could be measured both in the presence and absence of sensory adaptation.

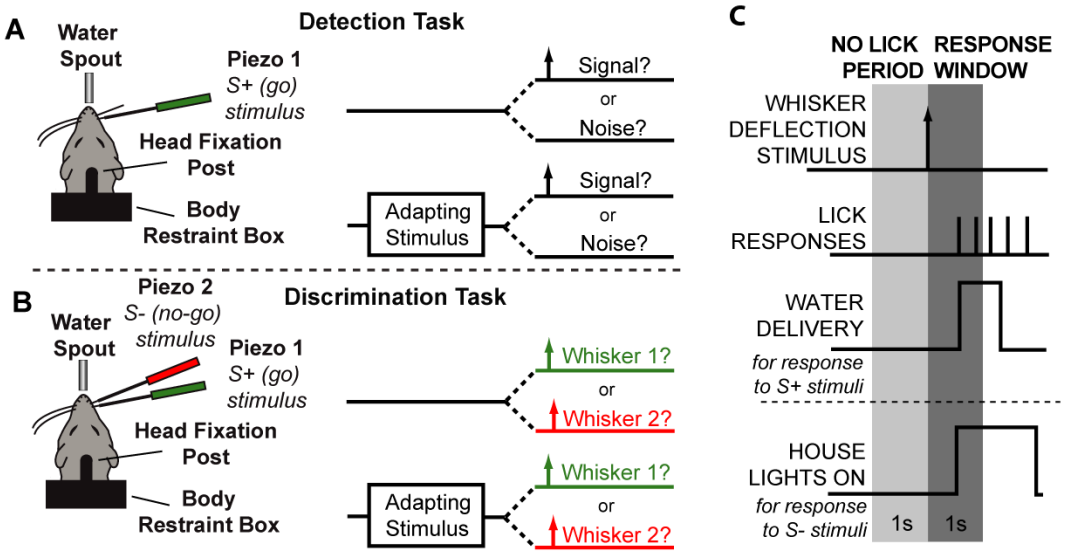

Figure 3-8 - *Schematic of the go/no-go behavioral detection and discrimination experiments*. **A.** Detection task. Rats were head fixed with their bodies in a restraint box. Animals performed the task for water rewards, which were delivered from a spout directly in front of their mouth. A probe stimulus was delivered through piezoelectric actuator at a randomized time and was preceded by an adapting stimulus on 50% of trials. The velocity of the probe stimulus was varied on each trial to measure the animal's perceptual threshold. Catch trials, in which no stimulus was presented, were randomly interleaved to measure chance performance. **B.** Discrimination task. Animals were subsequently trained on a go/no-go spatial discrimination task in which a second piezoelectric actuator was introduced on a nearby whisker. The task proceeded as in the detection task, with the exception that on a given trial either the S+ (go whisker) or the S- (no-go) whisker was deflected with equal probability. Animals were rewarded as before for responses to the S+ stimulus, but were penalized with a 5-10s timeout for responses to deflections of the S- (no-go) whisker. Deflection velocities remained at a constant suprathreshold value during the discrimination task. **C.** Detailed timeline of task. To prevent impulsive licking, the presentation of a probe stimulus was preceded by a 1 second no-licking period, during which licks to the water spout resulted in further delay of the stimulus. After the delivery of the stimulus the animals had a 1 second response window in which to lick the spout. Licks to the water spout on S+ trials (correct responses) resulted in a small water reward. Licks to the spout on S- trials (incorrect responses) resulted in the house lights coming on.

Adaptation degrades detectability of the stimulus for awake, behaving animals

Our results demonstrated that detectability was reduced following adaptation and that the time course of recovery from the effects of adaptation was on the order of a few seconds. Given the variable delay between the end of adaptation and the stimulus, we were able to examine the response probabilities for stimuli in two separate time bins in the adapted state: those that occurred 0.5 to 1.5 s after the end of adaptation, or "short recovery" trials; and those that occurred 1.5 to 2.5 s after adaptation, or "long recovery" trials. **Figure 3-9A** shows sample lick rasters in response to an intermediate strength (550 °/s) stimulus on 50 non-adapted trials and 50 trials each of the short and long recovery periods following adaptation. The lick rasters are aligned to the stimulus delivery time for each trial. Each black tick mark in the raster represents a contact of the animal's tongue with the response spout. The light gray vertical bar represents the enforced no-licking period and the green vertical bar represents the response window. If the first lick following the stimulus fell within the response window, water was dispensed from the response spout and the animals generally continued licking to consume the water. The dark gray horizontal bars in the right top panels represent the presence of the adapting stimulus, which occurred at a randomized time before the probe stimulus. Note that animals often emitted licking responses to the onset of the adapting stimulus, but that the licking tended to cease relatively quickly. It is apparent from the lick rasters that, for the whisker deflection velocity shown in this example, the response rate (percentage of trials on which a response occurred within the response window) was lower on trials following adaptation than on those trials without adaptation. In addition, the response rate was higher on trials with a longer period of recovery following adaptation.

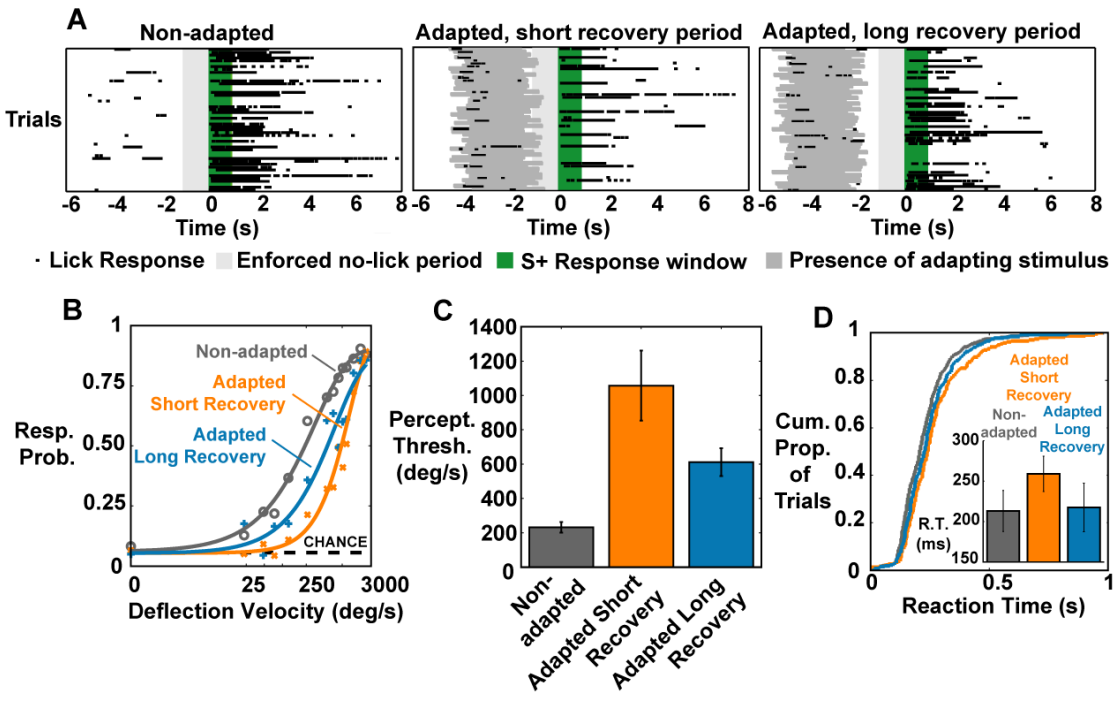

Figure 3-9 - *Behavioral perceptual thresholds and response times are increased with adaptation.* **A.** Example lick rasters in response to presentation of a 550 °/s stimulus under three conditions: non-adapted, adapted with a short (0.5-1.5 second) period of recovery between the end of adaptation and the probe stimulus, and adapted with a long (1.5-2.5 second) period of recovery. Each black tick mark indicates the time of contact between the animal's tongue and the water spout. The light gray vertical bar represents the enforced no-licking period and the green vertical bar represents the response window. Each dark gray horizontal bar indicates the presence of the adapting stimulus. **B.** Combined psychometric curve for all animals. The response probabilities are plotted as a function of whisker deflection velocity. The gray curve shows a sigmoidal fit to the responses in the non-adapted state, shown as circles. The orange curve shows a fit to the responses to stimuli occurring between 0.5 and 1.5 s after the end of the adapting stimulus, shown with Xs. The blue curve shows a fit to responses to stimuli occurring 1.5 to 2.5 s after the end of the adapting stimulus, shown with crosses. Error bars are omitted for clarity The black dashed line indicates the chance performance level, measured as the response probability to catch trials, or those in which no tactile stimulus was delivered. **C.** Quantification of perceptual thresholds. Each bar represents the perceptual threshold, measured as the point at which the sigmoidal fit crosses the 50% response probability level, with error bars representing +/- 1 standard error of the mean across animals. (non-adapted to adapted short recovery: $p < 0.05$; non-adapted to adapted long recovery: $p < 0.05$; paired t-test, $n = 4$). **D.** Reaction times in each condition. The cumulative distribution functions of the reaction times combined across animals are shown, with color conventions the same as in B and C. The inset shows the mean reaction times (R.T.) in each of the three conditions. Error bars represent +/- 1 standard error of the mean across animals (non-adapted to adapted short recovery: $p < 0.005$; non-adapted to adapted long recovery: $p = 0.63$; paired t-test, $n = 4$).

Reduced detectability manifests as a reduction in the probability of response for a given deflection velocity. **Figure 3-9B** shows the psychometric curves that resulted from the behavioral detection experiments for all animals across the range of tested velocities. The curves were constructed by fitting a Weibull function to the measured response probabilities with trials combined across animals (details in Methods). The gray circles and the solid gray curve fit represent the response probability for stimuli presented in the absence of adaptation. The black dashed line labeled as 'chance' indicates the response probability on catch trials, or those trials in which a deflection of the second piezoelectric actuator was substituted for the actuator attached to a whisker. The response probability on catch trials was 8.6%, which is consistent with the behavioral false alarm rate from similar studies (Stüttgen et al., 2006; Stüttgen and Schwarz, 2008; Ollerenshaw et al., 2012). Short sessions were performed with the piezoelectric actuator removed from the whisker to ensure that animals were only using tactile cues to perform the tasks. Animals performed near chance level during these control experiments.

After adaptation, a much stronger stimulus must be delivered in order to achieve the same response probability as seen in the non-adapted state, as shown by the orange curve in **Figure 3-9B,** which shows the combined psychometric curve in response to stimuli falling in the short recovery period. The curve is shifted dramatically to the right, indicating a reduction in detectability with adaptation. Importantly, the response probability for the strongest stimulus approached that seen in the non-adapted case, indicating that the change in performance is not due simply to changes in motivational level, or confusion on the part of the animals. The blue curve shows the psychometric

function for stimuli occurring in the long recovery period. This curve falls between the short recovery and the non-adapted curves, indicating that detectability is beginning to return to that seen in the non-adapted state.

The observed decrease in detectability can be quantified by measuring the perceptual threshold, which is defined here as the point at which the sigmoidal curve fit crosses the 50% response probability level. **Figure 3-9C** shows the average perceptual thresholds for each of the animals tested, which was 232 +/- 35 º/s in the non-adapted state. This threshold is very similar to that seen in a similar single whisker detection task (Stüttgen et al., 2006; Stüttgen and Schwarz, 2008). The average perceptual threshold increased to 1,057 +/- 204 º/s in the adapted short recovery state, then decreased to 611 +/- 81 º/s in the adapted long recovery state. Thus, detectability was reduced following adaptation to a sensory stimulus, with a fourfold increase in stimulus velocity required to achieve the same threshold performance level ($p < 0.05$, $n = 4$, paired t-test). Performance began to recover with timescales on the order of a few seconds, though it remained significantly above those in the non-adapted state ($p < 0.05$, $n = 4$, paired t-test), indicating that a time duration greater than 2.5 s was likely required for the animals to fully recover from the effects of the adaptation.

Reaction time was also increased with adaptation. **Figure 3-9D** shows the cumulative distribution functions (CDFs) for the reaction time distributions in response to the strongest five stimuli in each of the three states for all of the animals. Note that all three CDFs rise slowly and lie on top of one another for approximately the first 100ms

following stimulus onset. This extremely short reaction time likely represents trials in which the animal had already committed to emitting a response prior to the delivery of the stimulus. However, after approximately 100ms, the three curves begin to diverge with the curve representing the non-adapted reaction times (gray) rising most sharply, indicating faster responses on average. The curve representing responses to trials following adaptation with a short recovery time (orange) rises the least sharply, indicating slower reaction times. The inset to **Figure 3-9D** shows the average reaction times for each of the individual animals. As indicated by the CDFs, the average reaction times were lowest for non-adapted trials, with animals responding in 213 +/- 25 ms on average. The reaction time increased to 260 +/- 22 ms following adaptation with a short recovery period, then decreased to 217 +/- 30 ms with a longer recovery period. In general, there was a significant increase in reaction times from the non-adapted to the adapted short recovery state ($p < 0.005$, $n = 4$, paired t-test). However, unlike the perceptual thresholds, the reaction times in the long recovery state were not significantly different from those in the non-adapted state ($p > 0.05$, $n = 4$, paired t-test), indicating that reaction times had largely recovered to their non-adapted level after 2.5 seconds.

Spatial discrimination in the presence and absence of sensory adaptation

After performing the detection task, animals were then trained on a two whisker go/no-go spatial discrimination task, as shown in **Figure 3-8B**. In this task, the S+ or 'go' whisker remained the same as it had been in the detection task. However, the second piezoelectric actuator was attached to a second nearby whisker, which was deemed the S- or 'no-go' whisker. The task proceeded just as it had during the detection task, with the exception

that on a given trial, the stimulus was randomly chosen as either the S+ or S- whisker with equal probability. To avoid cueing the animal as to which whisker would be stimulated, both whiskers were deflected together during the adaptation phase of the trial. The velocity of the stimulus remained fixed at 1,500 °/s. Animals were rewarded for responding to the S+ stimulus as before, but were penalized with a 5-10 s timeout paired with the house lights when they responded to the S- stimulus.

Detection and discrimination are coupled in the go/no-go paradigm

While two alternative forced choice (2AFC) tasks are frequently used to measure discrimination performance, the go/no-go paradigm used here allowed for the delivery of stimuli at randomized times, forcing the animal to first detect the stimulus prior to making a classification choice. We were thus able to intertwine detectability and discriminability and to measure the animals' response probabilities at varying times after the offset of the adapting stimulus. Go/no-go tasks remain common in the literature, especially in tasks requiring head-fixation that make traditional two-alternative forced choice designs difficult due to the limited mobility of the animal (Stüttgen et al., 2006; Houweling and Brecht, 2008; Stüttgen and Schwarz, 2008; Voigt et al., 2008; Gerdjikov et al., 2010; O'Connor et al., 2010b; Lee et al., 2012). However, in all go/no-go tasks, when an animal fails to respond to a stimulus, it is often not clear whether this was due to a lack of motivation, to the animal not detecting the stimulus or because they categorized the stimulus as a 'no-go' stimulus. Despite the complexity in interpreting the data, the go/no-go task is arguably more representative of natural situations in which the timing of important sensory events is often not cued in advance.

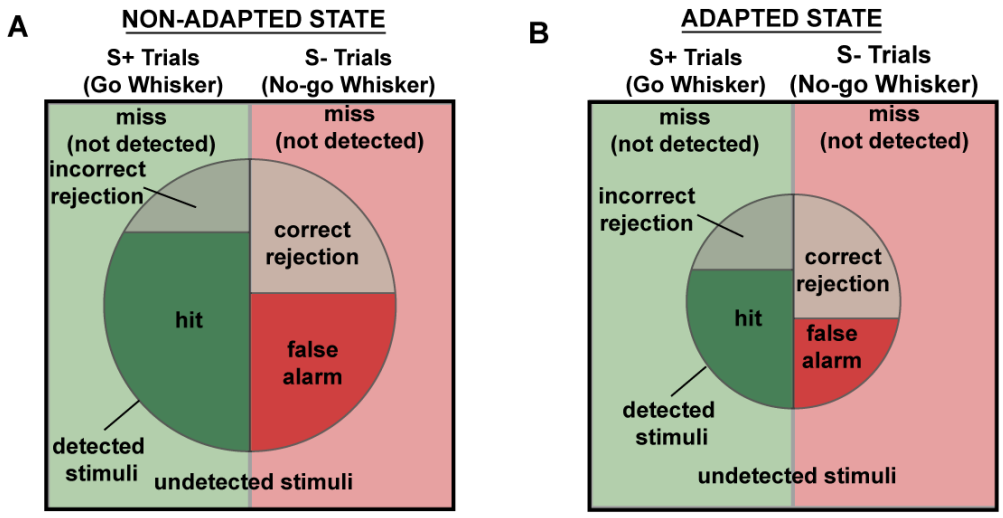

Figure 3-10 - *Changes in detectability affect the measurement of discriminability in a go/no-go task*. **A.** A diagram showing the theoretical interaction between detectability and discriminability in the non-adapted case. The square represents all stimuli delivered to the animal and is evenly divided between S+ and S- stimuli. The circle represents the subset of stimuli detected by the animal. Because the animal must first detect the stimulus before being able to classify it, all non-detected stimuli are categorized as misses and correct rejections for S+ and S- stimuli, respectively. Of those stimuli that the animal detects, those that it responds to are categorized as hits and false alarms for S+ and S- stimuli, respectively, while non-responses are categorized as misses (incorrect rejections) and correct rejections. **B.** Similar to **A**, but for the adapted state. Data from the detection task demonstrates that, at the velocity used in the discrimination task, the stimulus detectability was decreased with adaptation. This is shown with a smaller circle to indicate fewer detectable stimuli.

To demonstrate the interdependence of detectability and discriminability in the task used here, the two possible adaptation scenarios are shown schematically in **Figure 3-10A** and **Figure 3-10B**. The square in **Figure 3-10A** and **Figure 3-10B** indicates all possible stimuli delivered to the animal, which were evenly divided between S+ and S- stimuli. The circle represents the subset of stimuli that were detected by the animal. If we assume that detectability is constant across both the S+ and S- whiskers, the subset of detected

stimuli will also be evenly divided amongst S+ and S- stimuli. Stimuli falling outside the circle represent those that the animal missed, due either to a failure to detect the stimulus, or to a lack of motivation. The animal is thus left with only those stimuli falling within the circle to classify. In the ideal observer analysis of discriminability shown in **Figure 3-7B** and **Figure 3-7C**, this aspect of the behavioral task was taken into account by implementing a threshold below which responses were deemed as undetectable and removed from the analysis. Due to the fact that adaptation led to a decrease in the magnitude of the cortical response, a higher fraction of trials were excluded from analysis in the adapted state. This decrease in detectability is reflected in the smaller circle diameter in **Figure 3-10B** versus that in **Figure 3-10A**.

The results from the detection task (shown in **Figure 3-9A** and **Figure 3-9B**) indicate that the awake animals faced a similar challenge. During detection, the percentage of detectable trials decreased with adaptation, reducing the fraction of detected trials in which the animal was capable of making a discrimination response. The stimulus velocity used in the behavioral discrimination task resulted in response probabilities in the detection task of 86%, 73%, and 82% for the non-adapted, adapted short recovery, and adapted long recovery states, respectively. Experimentally, we have access to the overall hit and false alarm rates from the discrimination task, which are represented as the proportion of each half of the square in **Figure 3-10A** and **Figure 3-10B** that are shaded in dark green and dark red, respectively. Discriminability can then be measured as the ratio of the measured hit rate and false alarm rates, or simply their differences. The classical discrimination metric d' can also be applied after accounting for the observed

reduction in detectability (see Methods). Note that the assumption of equal detectability in both the go and no-go whiskers used here is only necessary when evaluating discriminability in a given state. When comparing discriminability across the non-adapted and adapted states, changes in the relative response rates to S+ and S- stimuli become the important measure. If adaptation accomplishes nothing other than an equal reduction in detectability for both the S+ and S- stimuli, this relative measure would not change. Further, though the assumption of equal detectability across whiskers was not directly tested in our behaving animals, evidence from anesthetized studies indicates that the spatiotemporal characteristics of the cortical response are consistent regardless of which macrovibrissa is deflected (Davis et al., 2011; Wang et al., 2012), suggesting that behavioral detectability levels would also remain consistent.

Simulated results emphasize the need to control for changes in detectability

The interdependence of detectability and discriminability, and the need to account for changes in detectability when calculating discriminability, can be clearly seen using simulated behavioral results. **Figure 3-11A-L** shows results from simulated data to demonstrate how the different measures of discriminability might look for three possible situations: one in which a subject employed a guessing strategy and responded to both stimuli with equal probability; one in which a subject was capable of discriminating between S+ and S- stimuli, but for which there was no change in discrimination performance with adaptation; and one in which the subject improves its detection performance with adaptation. In all three cases, the experimentally measured detection values of 86% and 73% were used.

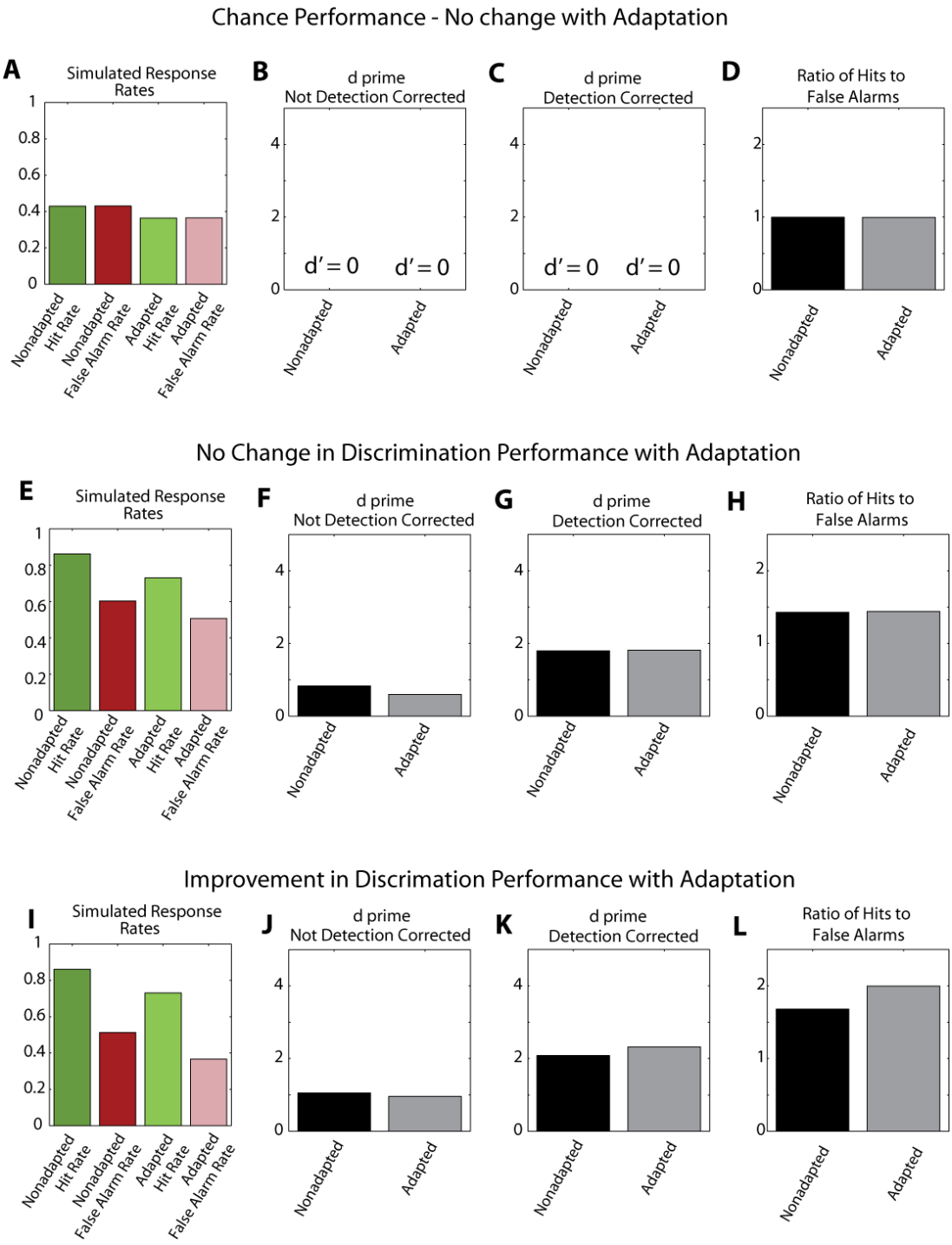

Figure 3-11 - *Simulated discrimination results under three possible scenarios.* **A-D**: an animal performing at chance, **E-H**: an animal capable of discriminating between two whiskers, but for which there is a reduction in detection performance with adaptation but no change in discrimination performance, and **I-L**: an animal that displays both a reduction in detection performance and an improvement in discrimination performance with adaptation.

In the first case, the subject responded to 50% of both the S+ and S- stimuli which were detected. This would represent a guessing strategy in which, once the animal detected a stimulus, it simply responded on half of the trials and withheld on the other half. **Figure 3-11A** shows how the measured response rates would appear in this case, after applying the reduced detectability with adaptation. The hit and false alarm rates are equal in both the non-adapted and adapted states, though the overall response rates are decreased with adaptation due to the decrease in detectability. **Figure 3-11B** and **Figure 3-11C** demonstrate that both the uncorrected and corrected d' values would be equal to zero in this case, given the equal hit and false alarm rates. The ratio of hit rate to false alarm rate, R, would equal 1 in both the adapted and non-adapted case, as shown in **Figure 3-11D**.

In the second case, the subject responded to 100% of detected S+ stimuli, but only 60% of detected S- stimuli. However, these response rates remained constant in both the non-adapted and adapted states. This is equivalent to a case in which the animal is capable of discriminating between two whiskers, but adaptation only affected detectability without leading to any change in discrimination performance. The decreased detectability is reflected in an overall decrease in the response probabilities in the adapted state in **Figure 3-11E**. However, **Figure 3-11F** shows that applying d' to the uncorrected response probabilities results in a measured decrease in performance, though the subject is performing equally well in both cases. Correcting for the decrease in detectability, on the other hand, allows d' to reflect the constant performance in both states, as shown in **Figure 3-11G**. The ratio, R, also reflects the constant performance across both the non-adapted and adapted states, as shown in **Figure 3-11H**.

Finally, in the third case the subject responded to 100% of detected S+ stimuli and 60% of detected S- stimuli in the non-adapted case, but improved its performance by reducing its false alarm rate to 50% of detected S- stimuli in the adapted case. The measured response probabilities that would result in such a case are shown in **Figure 3-11I**. However, despite the subject performing better in the adapted state, performance measured using d' applied to the uncorrected response probabilities shows a decrease in discrimination performance with adaptation, as shown in **Figure 3-11J**. If the decrease in detectability is instead controlled for, d' is shown to improve with adaptation, as shown in **Figure 3-11K**. The ratio, R, which is insensitive to changes in detectability, also reflects an improvement in performance with adaptation, as shown in **Figure 3-11L**. Thus, when measuring changes in discriminability that occur simultaneously with a decrease in detectability, either the hit to false alarm ratio or the detection corrected d' measure must be used to avoid obscuring improvements in discriminability.

Adaptation improves spatial discriminability in awake, behaving animals

In the two whisker discrimination task, results demonstrated that animals traded decreased detection performance for better spatial acuity. As in the detection task, inspection of the lick response rasters shown in **Figure 3-12A** and **Figure 3-12B** demonstrates that the response rate decreased with adaptation, but began to return to baseline levels with a longer period of recovery from adaptation. Note that on S- trials in which the animal did emit a licking response to the stimulus, licking quickly ceased due to the unavailability of water.

The overall hit and false alarm rates, shown in **Figure 3-12C** for all trials averaged across all animals, decreased from the non-adapted to adapted short recovery state, then increased somewhat with a longer recovery period. However, it is difficult to determine from these values alone whether any change in performance exists across the states.

When the ratio of hit rate to false alarm rate was calculated, as shown in **Figure 3-12D**, there was a significant increase in discrimination performance from the non-adapted state to the adapted short recovery state, with the ratio increasing from 1.44+/- 0.14 to 2.11 +/- 0.19 ($p < 0.005$, $n = 5$, paired t-test). With a longer recovery period, the discrimination performance decreased (hit to false alarm ratio of 1.72 +/- 0.17), though it remained significantly above the non-adapted value ($p < 0.05$, $n = 5$, paired t-test), indicating that recovery was not complete by 2.5 seconds after the end of adaptation. Similarly, **Figure 3-12E** shows that the detection corrected d' measurement displays a similar trend, with the discrimination performance increasing from 2.09 +/- 0.26 to 2.72 +/- 0.29 with adaptation ($p < 0.05$, $n = 5$, paired t-test), but beginning to recover to 2.53 +/- 0.20 with greater time between the probe and adapting stimulus. A third metric of discrimination known as the 'discrimination index' (DI), which is simply the difference in hit and false alarm rates (Gerdjikov et al. 2010), was also calculated. Using this metric, the animals also showed an increase from the non-adapted (DI = 0.255 +/- 0.054) to the adapted short recovery (DI = 0.395 +/- 0.048) states ($p < 0.05$, paired t-test), then a decrease (DI = 0.335 +/- 0.046) in the adapted long recovery state (non-adapted to adapted long recovery: $p < 0.05$, $n = 5$, paired t-test).

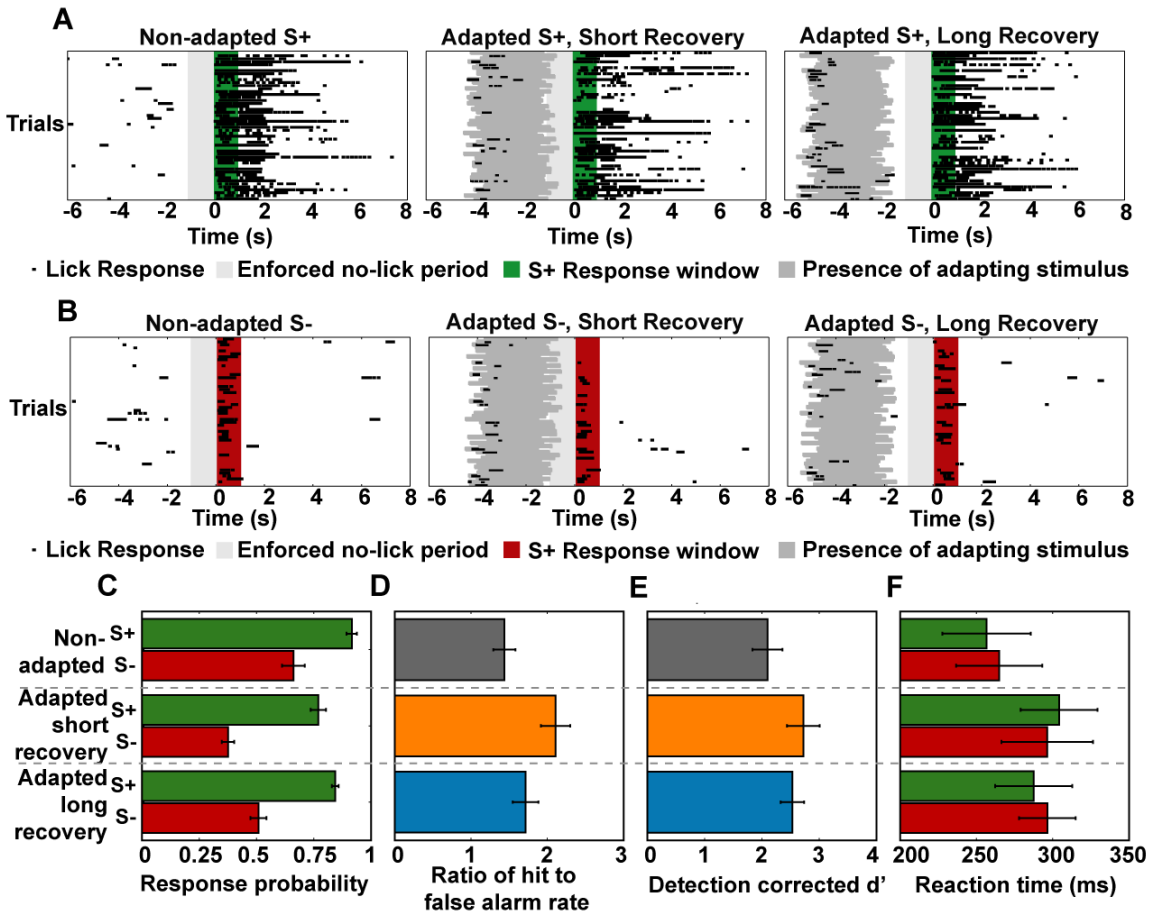

Figure 3-12 *-The spatial discrimination performance of the animals is improved with adaptation.* **A.** Sample lick response rasters for S+ stimuli in the non-adapted, adapted short recovery, and adapted long recovery conditions. All conventions are the same as in Fig. 6A. **B.** Sample lick rasters for S- stimuli in all three conditions. The vertical red bar represents the response window, during which a response results in a timeout paired with house lights turning on for 5-10s. **C.** Response probabilities to S+ and S- stimuli are shown in green and red. From top to bottom, each pair of bars represent the non-adapted state, the adapted short recovery state and the adapted long recovery state. **D.** Discriminability quantified as the ratio of the hit rate to the false alarm rate. Discriminability is measured using the data in A for the non-adapted (grey), adapted short recovery (orange) and adapted long recovery (blue) states. (non-adapted to adapted short recovery: $p < 0.005$; non-adapted to adapted long recovery: $p < 0.05$; paired t-test, $n = 5$). **E.** After correcting for the decrease in detectability as measured during the earlier detection task, d' was calculated in each of the three conditions. The color conventions are the same as in **C** and **D** (non-adapted to adapted short recovery: $p < 0.05$; non-adapted to adapted long recovery: $p = 0.21$; paired t-test, $n = 5$). **F.** The mean response latency across animals is shown for both S+ and S- stimuli in each of the three possible states. Color and shading convention is the same as in **C**. All Error bars represent +/- 1 standard error of the mean.

In all three states, there is no difference in reaction time for hits versus false alarms ($p > 0.05$ in all cases, paired t-test), indicating that the animals reaction time was not affected by the stimulus type. The average reaction times in the discrimination task are plotted in **Figure 3-12F**. However, as in the detection task, the reaction time does increase significantly with adaptation from 260 +/- 28 ms to 302 +/- 26 ms ($p < 0.05$, $n = 5$, paired t-test) followed by a decrease with a longer recovery period to 290 +/- 22 ms ($p < 0.05$, non-adapted to adapted long recovery, paired t-test). The animals also displayed longer reaction times in each of the three states in the discrimination task compared to the detection task, possibly as a result of the greater cognitive demand required of the discrimination task.

While the identity of the S+ whisker was held fixed over the course of all of the behavioral sessions, the identity of the S- whisker was varied. However, all of the discrimination results plotted in **Figure 3-12** were calculated with all S- whisker locations combined for each animal. Although in total there was not enough data to draw strong conclusions about whether the animals performed better when the S+ and S- whiskers were in the same row vs. the same arc, or whether they were immediately adjacent or separated by one whisker, some trends were observed, as shown in **Figure 3-13**. In the non-adapted state, when the data was parsed by S- location, the animals performed slightly better when the S- whisker was immediately adjacent in the same arc (Hit to false alarm ratio = 1.34 +/- 0.13) vs. immediately adjacent in the same row (Hit to false alarm ratio = 1.29 +/- 0.06). Similarly, animals performed better for non-adjacent whiskers in the same arc (Hit to false alarm ratio = 2.00 +/- 0.52) vs. nonadjacent

whiskers in the same row (Hit to false alarm ratio = 1.37 +/- 0.04). Similar trends exist in the adapted short recovery state, with performance being better when S+ and S- whiskers are separated by a larger distance, and when they are in the same arc vs. the same row (adjacent whisker, same row: Hit to false alarm ratio = 1.86 +/- 0.17; adjacent whisker, same arc: Hit to false alarm ratio = 1.95 +/- 0.27; non-adjacent whisker, same row: Hit to false alarm ratio = 2.56 +/- 0.57; non-adjacent whisker, same arc: Hit to false alarm ratio = 3.44 +/- 1.07). While these trends indicate increases in performance with larger distance between stimuli, and with stimuli separated by arc instead of row, the differences were relatively small and did not reach the level of statistical significance ($p > 0.05$ for all non-adapted to adapted results, paired t-test) due to the relatively small number of examples at each separation. While the true nature of the topographically specific aspects of the observed phenomena thus remain unclear, we are left to speculate that any such relationships would likely relate to the way in which the animal actively engages surfaces and objects and the resultant statistical properties of the tactile signals entering the pathway.

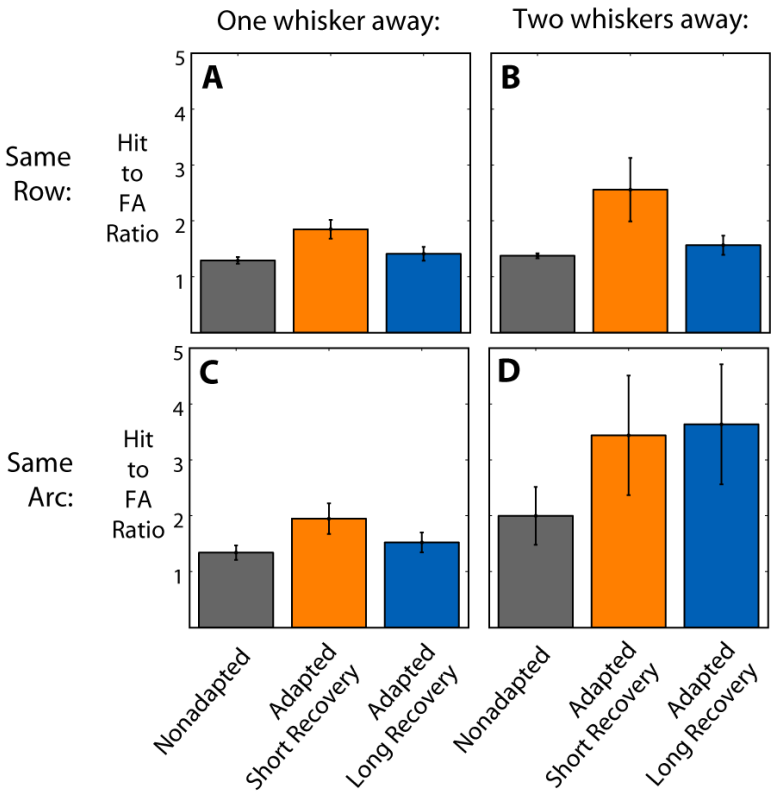

Figure 3-13 - *Discrimination results separated by whiskers used in the task.* **A.** One whisker away, same row. **B.** Two whiskers away, same row. **C.** One whisker away, same arc. **D.** Two whiskers away, same arc. Note that all combinations of whiskers show improved discriminability with adaptation, and that all but one show the effect of decreasing performance with more recovery time. Also note that performance in all states is slightly better with increased separation, and when whiskers are separated arc-wise vs. row-wise.

3.5 Discussion

In the presence of persistent stimulation, sensory systems have long been shown to exhibit various forms of rapid and reversible adaptation (Barlow, 1961; Ahissar et al., 2000; Fairhall et al., 2001; Chung et al., 2002; Higley and Contreras, 2006). It has been posited that these forms of adaptation do not just represent deleterious reductions in firing rates, but instead represent fundamental changes in coding properties that likely possess ethological relevance. Stimuli arriving when the pathway is in the non-adapted state are more likely to generate a large cortical response, alerting an otherwise quiescent or inattentive animal to the presence of an unexpected stimulus (Fanselow and Nicolelis, 1999; Moore et al., 1999; Sherman, 2001b; Chung et al., 2002; Khatri et al., 2009b; Diamond and Arabzadeh, 2012), presumably at the expense of specificity. However, with active exploration of an object, the system is placed into an adapted state, subsequently reducing the magnitude of the cortical response, but improving the ability of the system to discern the finer features of sensory stimuli (Fanselow et al., 2001; Kohn and Whitsel, 2002; Moore, 2004; Maravall et al., 2007). Such a change would improve the ability of the system to discriminate between disparate stimuli. Studies with freely behaving animals have demonstrated that the cortical response to peripheral inputs is reduced when the animal is whisking (Fanselow and Nicolelis, 1999; Castro-Alamancos, 2004; Crochet and Petersen, 2006; Ferezou et al., 2006, 2007; Hentschke et al., 2006; Poulet et al., 2012) potentially implying that the animal's own self-motion serves to place it into an adapted state similar to that described here. Indeed, detectability is significantly improved in the absence of whisking (Ollerenshaw et al., 2012), potentially part of an active

strategy by the animal to facilitate information flow in this very specific context. Sensory adaptation thus leads to a tradeoff between detectability and discriminability, regulated through the dynamics of the thalamocortical circuit and shown to be a hallmark of sensory processing in the natural sensory world (Lesica and Stanley, 2004).

The evidence presented here strongly suggests that the improved discriminability with adaptation results from a sharpening of the spatial response at the level of S1. Intrinsic optical imaging results in the anesthetized monkey have pointed to such a sharpening effect with adaptation (Tommerdahl et al., 2002; Simons et al., 2005, 2007). In a previous study of the vibrissa pathway using VSD imaging, Kleinfeld and Delaney (1996) revealed a spatial sharpening in cortical activation when whiskers were stimulated with high frequency trains of deflections. Sheth et al. (1998) used a combination of single electrode recordings and intrinsic optical imaging to demonstrate that, with frequencies of adaptation above 5 Hz, the cortical response to a whisker deflection in an anesthetized rat became more focused, and speculated that this could lead to enhanced discriminability (Moore et al., 1999; Moore, 2004). Similarly, using micro-electrode recordings of single-units in S1, Brumberg et al. (1996) demonstrated that when a whisker was continuously stimulated with a white noise deflection pattern, the deflection of an adjacent whisker led to a more constrained cortical response than when the whisker was deflected alone. Adaptation has long been known to modulate receptive field structure and corresponding tuning properties, an example of which is the sharpening of the whisker deflection directional specificity of individual cortical and thalamic cells (Khatri et al., 2009b). However, the precise effects the adaptive changes of these tuning properties have on the

detectability and discriminability of different sensory inputs has only more recently been investigated (Wang et al. 2010). From a purely perceptual perspective, previous studies using tactile stimuli applied to fingertip in human subjects have shown that adaptation to a sensory stimulus leads to an increase in the subjects' ability to discriminate amplitude (Goble and Hollins 1993), frequency (Goble and Hollins 1994), and the spatial location (Tannan et al. 2006) of the stimuli. These studies were largely psychophysical in nature, and the underlying electrophysiological mechanisms were not fully investigated. The present results help to bridge the gap between characterizations of adaptation from a coding perspective, afforded by precisely controlled experiments conducted under anesthesia, and the corresponding psychophysical observations during behavior.

Relevant to the findings here, a previous study suggested that sensory adaptation at the level of the thalamocortical circuit was largely absent in rodents during active behavioral states (Castro-Alamancos 2004). This was attributed to the fact that when animals were in novel environments and engaged in exploratory behavior, the cortical response to the first stimulus in a train of adapting stimuli was already reduced, limiting the ability to further reduce the cortical response with adaptation. It was asserted that, in effect, the cortex was already in an adapted state during active states. However, it should be noted this lack of adaptation in the awake state was limited to periods during which the animal was involved in exploratory behavior or engaged in a novel task. When animals were trained in a task that required them to detect whisker stimuli, the adaptation effect returned after the animals became familiar with the task. Given that the animals trained in our detection and discrimination tasks were exposed to the tasks over the course of many weeks, they

were likely operating in this regime of familiarity with the task, and thus would be expected to show the effects of adaptation. A central finding here suggests a dynamic trade-off between detectability and discriminability that exists at both the neural and perceptual level: adaptation enhances discriminability at the expense of detectability. Consistent with previous acute studies conducted under anesthesia (Maddess et al., 1988; Greenlee et al., 1991; Chung et al., 2002), here the effects of the rapid sensory adaptation observed in the behaving animals decayed on the order of a few seconds, providing an estimate of the timescale for the behaviorally relevant effects of sensory adaptation, and setting the stage for a dynamically adapting coding framework in the fluidly changing natural environment.

The voltage sensitive dye imaging method applied here provides measurement of the activity of a large population of cortical neurons at a relatively high resolution, both spatially and temporally. It is able to accurately follow the time course of adaptation (10 Hz) and simultaneously report the spatial spread of neural activity. This spatiotemporal characterization is relevant to both the detection task, where even a single whisker deflection can activate a strong widespread cortical response that could subserve the relevant perceptual cue, and the spatial discrimination task that presumably relies on the spatial extent of the activation of the topographic representation at some level of processing. Although the activity recorded is sub-threshold, the VSD signal follows linearly with sub-threshold membrane voltage recorded with whole cell recording and likely reflects the probability of action potential firing (Petersen et al., 2003a; Berger et al., 2007). The VSD imaging technique applied here primarily reports the activity in

L2/3, which likely reflects spiking activity one synapse earlier in the cortical input layer 4 (Petersen et al., 2003b; Grinvald and Hildesheim, 2004). Although as with linking any behavioral percept to the underlying neural activity, it cannot be directly asserted that the percepts utilized by the animal to perform the detection and discrimination tasks in this study exist at the level of cortical layer 4, the ideal observer analysis shows us that the necessary information is present at this level of processing and that the adaptive modulation of the detectability/discriminability is also reflected at this stage. The neural activity in the primary sensory cortex has long been considered the fundamental neural basis for downstream sensory percepts and behavior. Studies have shown that a lesion in S1 abolishes the animal's ability to detect a stimulus (O'Connor et al., 2010a) while micro-stimulation of S1 influences the animal's stimulus detection and discrimination performance (Romo et al., 1998, 2000; Houweling and Brecht, 2008; Huber et al., 2008). The VSD signal from layer 2/3 in S1 can therefore be considered as the initial sensory evidence upon which the animal ultimately builds a decision about the features of simple stimuli. It is generally presumed that sensory evidence in the form of activity in primary sensory areas is constantly monitored by higher cortical areas to form a so-called decision variable (Gold and Shadlen, 2007). The decision variable is then compared to a threshold, based on which a behaving animal may make a decision and classify the stimulus as signal or noise, or discriminate between different possible stimulus types. As we did in this study, the comparison between the ideal observer analysis and the output of a behaving animal allows us to speculate what information the animal has access to, what candidate codes can be ruled out (Jacobs et al., 2009; Stanley, 2013), and how the animal might perform calculations that lead its decision (Macmillan and Creelman, 2004).

In the natural world, animals do not necessarily know precisely when, or even if, important stimuli will arrive. Sensory systems are therefore required to initially detect a stimulus before it can subsequently be classified as behaviorally relevant or not. In this scenario, after the initial detection of the stimulus, detection performance can be sacrificed in favor of improved discriminability, a framework that has long been posited (Crick, 1984; Sherman, 2001b; Lesica and Stanley, 2004; Lesica et al., 2006). The go/no-go behavioral paradigm used here, which included both timing uncertainty and trials in which no stimulus was present (catch trials), partially simulated these natural conditions in a way that would likely not be captured in a classical two alternative forced choice (2AFC) task. By associating one whisker with a reward and the other with a penalty, the animals were required to first detect *whether* a whisker was deflected, then subsequently decide if that particular stimulus would result in reward. Moreover, a 2AFC task requires the existence of two distinct response indicators, which could include two lick ports or two response levers (Mayrhofer et al. 2013), both of which add significantly to the complexity of the task, especially in the head-fixed condition required by the precise stimulus delivery in this experimental paradigm. Despite the additional complexity in interpreting the results from our task, which reflect both a decrease in detectability and an increase in discriminability, they provide more insight into the interactions between detectability and discriminability than a simple 2AFC task might.

The complementary results in both the anesthetized and awake animals demonstrated here would seem to indicate that the improved discriminability with adaptation cannot be

fully explained by top-down mechanisms such as changes in attentional state or expectation of the stimulus (Kok et al., 2012), which are of course absent in the anesthetized animal. Sensory adaptation has been shown to lead to a decrease in firing rate as early as the trigeminal ganglion (Fraser et al., 2006), as well a decrease in firing synchrony of thalamic neurons (Temereanca et al., 2008). This phenomenon has been shown to lead to decreased stimulus detectability and improved velocity discriminability at the cortex (Wang et al., 2010) due to the extreme sensitivity of the layer 4 cortical neurons to the timing of the thalamic inputs (Alonso et al., 1996; Usrey et al., 2000; Roy and Alloway, 2001; Bruno, 2011; Stanley et al., 2012) and its importance in determining cortical feature selectivity (Stanley et al., 2012; Stanley, 2013). Though changes in thalamic synchrony were not directly tested in this study, the reduced spread of cortical activity seen in the VSD imaging experiments could reflect a less synchronous drive from the thalamus, leading to a reduced activation of non-aligned regions of cortex. In addition, adaptation has been shown to alter the excitatory and inhibitory drive in cortex, which subsequently affects the "window of opportunity" that determines the sensitivity of layer 4 neurons to the timing of thalamic inputs (Gabernet et al., 2005; Higley and Contreras, 2006; Heiss et al., 2008). Indeed, recent evidence from the behaving mouse demonstrated that optogenetic activation of cortical inhibitory neurons in V1 led to improved visual discrimination performance (Lee et al. 2012). Some studies have also suggested that short-term depression of thalamocortical synapses is a likely mechanism for the observed effects of adaptation (Gil et al., 1999; Beierlein et al., 2002; Castro-Alamancos, 2002; Chung et al., 2002; Heiss et al., 2008). Taken together, our results indicate that sensory adaption at or below the level of the primary sensory cortex does

lead to important coding changes with profound perceptual effects, which when combined with top-down mechanisms, provides a precise means by which to gate information flow to cortex.

The frequencies of the adapting stimuli used in the present study were chosen to fall within the natural 5-15 Hz range at which rats rhythmically palpate their vibrissae, or "whisk", during exploratory behavior (Gustafson and Felbain-Keramidas, 1977; Carvell and Simons, 1990; Brecht et al., 1997; Bermejo et al., 2002; Berg and Kleinfeld, 2003). Exploratory whisking in air drives activity along the pathway (Leiser and Moxon, 2007; Curtis and Kleinfeld, 2009), and thus presumably serves to adapt the cortical response. Therefore, the passively applied adaptation used here may place the cortex into an adapted state that is similar to that achieved naturally by whisking, priming the system for improved discriminability (Moore 2004). Lower frequencies of adaptation may leave the system in the non-adapted state in which it is best suited for detecting weak and transient stimuli (Fanselow and Nicolelis 1999; Ferezou et al. 2006). A more complete characterization of the effects of adaptation across a broader range of frequencies would therefore be important in understanding how natural behaviors modulate the observed detectability/discriminability tradeoff. Further, while the parallel findings in the anesthetized animal point to a reduction in the spatial spread of the cortical response as the primary cause of the improved discriminability, the full extent to which this generalizes to the awake animal, as well as the subcortical processes leading to these changes and the corresponding top-down mechanisms that further gate information flow, must be more fully examined during behavior in the awake animal.

Chapter 4 - The effect of adaptation on the thalamic input to cortex in the awake animal

---

Portions of this work were presented in poster form at the following:

Ollerenshaw, DR, Zheng HJV, Wang, Q, Stanley, GB, *The adaptive trade-off between detection and discrimination in the vibrissa system* Abstract for Poster Presentation, Computational and Systems Neuroscience (Cosyne) meeting, Salt Lake City, UT, February 2013

Ollerenshaw, DR, Bari, BA, Pace, CP, Millard, DC, Zheng, HV, Wang, Q, Stanley, GB, *Detection and classification performance in the whisker system of awake, behaving rats* Abstract for Poster Presentation, Society for Neuroscience, New Orleans, LA, October 2012

4.1 Abstract

To gain insights into the neural mechanisms underlying the behavioral tradeoff in discriminability and detectability described in Chapter 3, animals were implanted with arrays of chronic recording electrodes in the ventral posterior medial (VPm) nucleus of the thalamus and subsequently trained to perform the detection with adaptation task previously described. Previous studies in the anesthetized animal have shown that important changes in coding properties occur in the thalamocortical circuit in response to sensory adaptation. The predicted consequences of these thalamocortical coding changes have been predicted to impact detection and discrimination performance in a way that closely mirrored the results seen in the anesthetized cortical imaging results and the behaving animals of Chapter 3, making it a natural target for neural recordings in the awake behaving animal. The results described here demonstrate that thalamic relay neurons in the awake animal respond to a passively applied adapting stimulus by firing both fewer and less temporally precise spikes in response to each successive pulse in the train, closely mirroring previous findings in the anesthetized animal. In addition, both the reduced firing rate and timing precision were shown to recover with a similar timescale as was seen in the previous behavioral results, and detection task performance declined as both quantities were reduced. Finally, a network model of the thalamocortical system was employed to demonstrate that the measured changes in thalamic coding properties are sufficient to lead to a sharpened cortical response and improved spatial discriminability. Together, these results further indicate that changes in thalamic coding properties contribute to important perceptual consequences, including a tradeoff in detectability and discriminability during behavior.

4.2 Introduction

Nearly all incoming sensory information passes through the thalamus en route to the primary sensory areas of cortex and beyond. Due to its strategic position in the pathway, combined with the large convergence of both feedback and feedforward connections, the thalamus has long been thought to possess important processing functions for the neural signal on its way to the cortex (Crick, 1984). Indeed, a large body of relatively recent work indicates that the thalamus serves as a gateway to cortex, modulating both how much and what type of information is ultimately relayed to higher processing areas (Guido and Weyand, 1995; Sherman, 2001a, 2007; Swadlow and Gusev, 2001; Beierlein et al., 2002; Lesica and Stanley, 2004; Lesica et al., 2006; Marsat and Pollack, 2006). There is evidence that these changes in thalamic processing are modulated both by top down processes such as attention, which act on thalamic processing via feedback from L6 of the cortex through the thalamic reticular nucleus (Crick, 1984; Bourassa and Deschênes, 1995; Guillery et al., 1998; Shipp, 2004; McAlonan et al., 2008; Thomson, 2010; Olsen et al., 2012), and also by bottom up processes such as sensory adaptation (Khatri et al., 2004; Lesica et al., 2007; Temereanca et al., 2008; Wang et al., 2010). Measuring transformations in information processing characteristics of the thalamus in response to sensory adaptation in the awake, behaving animal can thus provide a critical link between the behavioral and cortical changes described in Chapter 3, as well as the underlying changes in neural coding that lead to these changes.

In the whisker system of rats, the primary information processing stream for whisker inputs is known as the lemniscal pathway and passes through the ventral posterior medial (VPm) nucleus of the thalamus before leading to the barrel cortex in the primary sensory cortex (Brecht et al., 1997; Pierret et al., 2000; Petersen, 2007; Diamond et al., 2008b). The lemniscal pathway is thought to carry spatially encoded information due to the restricted receptive fields found in the VPm, while the parallel paralemniscal pathway, which passes through the adjacent posterior medial (POm) nucleus of the thalamus, primarily carries temporal information related to whisking phase and active touch (Sosnik et al., 2001). Thus, due to its critical location in the pathway as well as its known role in dynamically gating sensory information prior to its arrival at the cortex, the VPm provides an ideal recording site for measuring the information used in the detection and spatial discrimination tasks used here, which rely on passively applied stimuli to one or multiple whiskers.

A previous study from our laboratory described a series of important changes in thalamic processing that led to improved discriminability of whisker inputs at the expense of detectability (Wang et al., 2010). By simultaneously measuring single unit activity in both the thalamus and the cortex, this study showed that improved velocity discriminability could be measured after adaptation through ideal observer analysis of the cortex, and that this improvement came at the expense of detectability. However, an equivalent improvement in discrimination performance did not exist at the thalamus. Thus, it was the changes in the nature of the thalamic input to the cortex that mediated these information processing changes in the cortex. The two major changes measured in

the thalamus were a reduction in the overall firing rate and a reduction in the timing synchrony across thalamic neurons. Importantly, modeling studies demonstrated that the reduction in thalamic firing rate alone was not sufficient to drive the observed effects at the cortex, and that changes in synchrony of the firing of thalamic neurons on their downstream targets led to the improved cortical discriminability. Thalamic synchrony itself is thus an important part of the neural code (Bruno, 2011; Stanley, 2013).

As with most studies on the changes in thalamocortical processing, the study mentioned above relied on an ideal observer analysis of neural activity in anesthetized animals to make predictions about the perceptual consequences of adaptation. However, there are profound differences in the processing state of the anesthetized brain when compared to the awake state (Steriade et al., 1993; Greenberg et al., 2008; Constantinople and Bruno, 2011). Importantly, a study by Castro-Alamancos (2004) suggested that the effects of adaptation on the thalamocortical circuit could be confined largely to anesthetized or inattentive animals, and that the thalamocortical circuit in the awake and attentive animal was already in the adapted state. Therefore, recordings in the thalamus of awake behaving animals during our sensory adaptation task provides an important missing link between studies in the anesthetized animal and the perceptual consequences of sensory adaptation.

Here, we implanted an array of chronic recording electrodes into the VPm nucleus of the thalamus in three animals, which were subsequently trained in the detection with adaptation task described in Chapter 3. The results closely paralleled those in the

anesthetized study of Wang et al. (2010), showing an approximately 20% reduction in elicited spikes in response to adaptation along with an approximately 35% reduction in timing precision of recorded multiunit activity, which was used as a proxy for the synchronous firing across multiple neurons. In addition, both a reduction in thalamic spiking activity and timing precision were correlated with reduced detection performance. Finally, the measured changes in thalamic firing rate and timing precision applied to the input of a model of spatial and temporal processing in the rodent thalamocortical system. This model predicted a sharpened cortical response following adaptation which would lead to improved spatial discriminability. Together, these results confirm that adaptation has a profound effect on thalamocortical processing which may help to explain the cortical and behavioral results demonstrated in Chapter 3.

4.3 Methods

Description of behavioral methods

The combined behavioral and electrophysiological studies described in this chapter were conducted using three female Sprague-Dawley rats (Charles Rivers Laboratories, Wilmington, MA; 7 weeks of age, ~250g at the beginning of the study). Animals were housed on a 12 hour reversed light/dark cycle with all experimental sessions occurring during the dark phase. The animals were trained to perform a detection task identical to that described in Chapter 3, with the exception that the stimulus was modified to provide more clearly defined epochs in which to characterize the neural response. The 12 Hz sinusoid used in Chapter 3 was replaced with a 10 Hz series of 1,500 deg/s, 10 ms pulsatile stimuli similar to that used in Wang et al. (2010). The ramp-and-hold probe stimulus from Chapter 3 was replaced with single 10 ms stimulus of varying amplitude (and thus velocity). These brief, pulsatile stimuli provided much better defined events against which to measure the neural response. A single suprathreshold velocity of 1,500 deg/s was used during training and served as a test pulse (presented on at least every fifth trial to probe animal motivation) during the behavioral task.

All details relating to training, habituation, and water restriction are identical to those described in Chapter 3. However, it should be noted that of the three animals for which data is presented in this chapter, only two successfully learned the behavioral task. The head cap became destabilized for the third animal, requiring premature euthanasia.

Surgical Procedures

Surgical procedures adhered to methods described in Chapter 3 and in Ollerenshaw et al., 2012, with the addition of procedures to implant chronic recording electrodes into the ventroposterior medial (VPm) nucleus of the thalamus. After inserting the skull screws to anchor the headcap, a craniotomy ~2.5mm square and centered at 3mm caudal to bregma and 3mm lateral to midline (Paxinos and Watson, 2007) was marked on the surface of the skull. The perimeter of the craniotomy was cut with a dental drill and care was taken to avoid damaging the underlying cortical surface. After removing the bone fragment, the dura was removed to allow insertion of the electrode array with minimal dimpling.

Prior to inserting the chronic recording array, a single platinum/tungsten microwire electrode (Thomas Recording GmbH, Giessen Germany) was used to locate the VPm. The electrode was slowly lowered to 4.5 mm below the cortical surface using a hydraulic microdrive (David Kopf Instruments, Tujunga California), after which the whiskers were manually deflected with a wooden rod while amplifying the recorded signal through a loudspeaker as the electrode was further advanced. Multiple penetrations were made to allow visual alignment of the cortical vasculature with the underlying regions that provided whisker locked activity.

The chronic recording array was then clamped into the hydraulic drive using a custom built jig (visible in **Figure 4-3C**). The arrays were designed to provide approximately 1.5 mm of travel and were positioned near the top of their range of travel prior to

implantation, thus allowing the electrodes to be advanced further into the neural tissue only after the animals had been trained in the behavioral task. Due to the long interval required for habituation and training of the animals after the initial implantation of the electrodes, the drive was required to avoid the signal loss often associated with fixed recording electrodes (Polikov et al., 2005). The chronic recording array (4x2 array for one animal, 2x2 array for others, in addition to a reference electrode, see below for details) was then positioned over the identified location of the VPm and slowly advanced to a depth of 4.5 mm below the cortical surface. Care was taken in locating the recording array to avoid damaging any of the large vessels on the cortical surface. The cortical surface was then covered in sterile agarose, after which the craniotomy was sealed and the microdrive cemented in place with light curing dental cement (Henry Schein, Melville NY). The ground wires for the recording array were connected to two of the skull screws over the cerebellum which had wires pre-soldered to the screw heads. The headstage connector was positioned over the skull contralateral to the microdrive and cemented in place. The headpost was positioned over the rearmost skull screws, and the headcap was built up as described in Chapter 3 using light curing dental cement. The animals were given a minimum of 1 week of recovery prior to commencing behavioral training.

Construction of the microdrive and electrode array

In the days prior to each implantation surgery, an array of electrodes for chronic recording was installed on a custom built microdrive adapted from the design described in Haiss et al. (2010). The recording electrodes were constructed from quartz insulated

platinum/tungsten wire from Thomas Recording (80µm outer diameter, 25µm core diameter). The wires were pulled inside of a sealed nitrogen chamber on a vertical electrode puller (Thomas Recording GmbH, Giessen Germany) to reduce the tip diameter. The tip was then sharpened on an electrode grinding wheel (Thomas Recording GmbH, Giessen Germany) while being visually inspected under a microscope to achieve the desired tip geometry. Impedances of 1-3 MΩ measured at 1 kHz were targeted for the recording electrodes. A representative example of a pulled and ground electrode with a measured impedance of 2.6 MΩ is shown in **Figure 4-1**. Each recording array also contained 1-2 reference electrodes which were not pulled prior to grinding, leaving a larger region of exposed recording surface at the electrode tip that resulted in an impedance of 300-500 kΩ. Each recording electrode was cut to a length of 1.5 cm and had a 3.5 cm length of copper wire (Cooner Wire, Chatsworth CA) soldered to the non-sharpened end. Nail polish was painted onto the solder junction to help prevent shorting of electrode channels after the solder junctions were placed in close proximity on the microdrive.

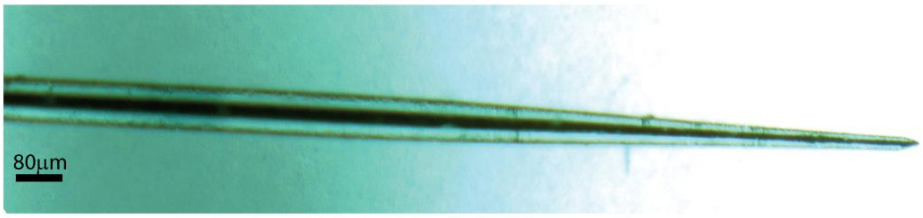

Figure 4-1 - *Close view of a quartz insulated platinum/tungsten Thomas Recording electrode used for extracellular electrophysiological recordings*. The electrode was manufactured from 80MICROm diameter electrode stock material and was first pulled to reduce the tip diameter, then ground to expose the tip for recording. The electrode impedance measured 2.6MΩ prior to implantation.

A CAD rendering of the microdrive upon which the electrodes were installed is shown in **Figure 4-2**. The components labeled as the 'base' and the 'rider' were printed on an Object Eden 250 3D printer by the Georgia Tech Invention Studio. Threads were manually tapped into the central hole on the rider after printing. The screw used to operate the drive was an M1.6 x 10 mm stainless steel screw with a slotted head and 0.35 mm pitch (Mcmaster-Carr, Part number 91613A025, Atlanta, GA). The lower 3-4 mm of the threads were removed with a hand file while turning the screw in a lathe, after which two concentric notches were cut into the end using a rotary drill with a cutting tool installed. The removal of the threads and the notches were necessary to allow the screw to turn freely in the base without moving in the axial direction. Guide tubes, shown in green in **Figure 4-2**, were made from either 1 mm diameter glass capillary tubing or 1 mm diameter stainless steel hypodermic tubing, with the stainless steel tubing found to be preferable for longevity. After assembling the individual components, the drive was completed by filling the diamond-shaped opening shown in **Figure 4-2B** with light curing dental cement, then turning the drive to its upper and lower extremes to ensure that it functioned properly.

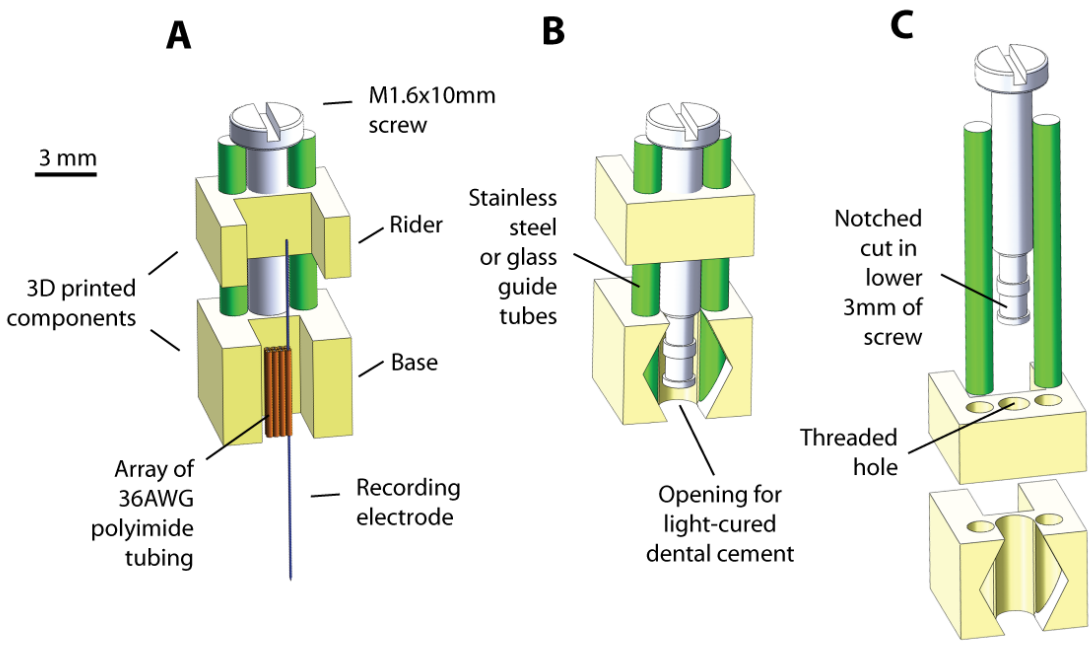

Figure 4-2 - *CAD rendering of the microdrive used for thalamic recordings*. The design is adapted from Haiss et al. (2010) **A.** View from the front of the drive showing the two 3D printed parts (shown in yellow), the base and the rider. An array of polyimide tubes are glued to the base to act as guides for the recording electrodes. A single electrode is shown in the rendering and would be cemented to the rider. A flexible wire would be soldered to the top of the electrode to connect to the headstage connector. **B.** Rear view of the microdrive assembly. The cutout in the rear was designed to be filled with light-cured dental cement to hold the screw in place. The guide tubes, shown in green, were built from either glass pipettes or stainless steel rods. **C.** An exploded view of the microdrive assembly. Note the notches cut into the lower 3mm of the screw, which were designed to be surrounded by dental cement to allow the screw to rotate without moving axially.

After the drive was complete, an array of 36AWG polyimide tubes (Amazon Supply, part number B0013HOX2A) were cemented to the base to act as guides for the recording electrodes. The tubes had an inner diameter of 127 um (0.005”), allowing the electrodes to pass through with little resistance, and an outer diameter of 241 um (0.0095”), which acted as the limit on inter-electrode spacing. The electrodes were passed through the polyimide tubing, taking care not to damage the sharpened tips, and the tops of the

electrodes were then cemented in place on the rider, with the flexible copper wires protruding upward, as shown in **Figure 4-3A**. The electrodes were positioned with approximately 6mm of free shank extending beyond the drive base, as shown in **Figure 4-3B**. To protect the drive and the electrode shanks after implantation, the drive was enclosed in a 1.5 cm length of 0.25 inch x 0.25 inch square brass tubing, which was cut from 12 inch piece of stock (Amazon Supply, part number B000FN6966). A hole was drilled approximately 5 mm from the top of the brass tubing to allow the wires to pass through and the hole was subsequently sealed with dental cement. The wires were soldered to the male ends of 6x2 male-to-female header (Digikey, part number S9009E-06-ND), which served as the connector for the headstage during recordings. **Figure 4-3C** shows an image of a completed drive inside of the protective brass tubing. The drive is held in a custom 3D printed jig that clamps the drive using a thumb screw. This allowed the drive to be cemented in place after implantation, after which the thumb screw was loosened and the jig removed. **Figure 4-4** shows an image of an experimental rat with the drive installed over the animal's left hemisphere. The connector and the head post are both indicated in the image.

Figure 4-3 - *Images of the electrode microdrive used for thalamic electrophysiology*. **A.** A completed 4x2 electrode microdrive array prior to insertion in the protective brass tubing. Electrodes extend approximately 5mm beyond the base, which will be cemented to the skull just above the craniotomy. The upper portion of the drive is threaded and will move downward on the outer guide tubes as the screw is turned counter-clockwise. The wires to the upper right continue to a male-to-female connector. **B.** A closer view of a single row of the electrodes during the construction process. Note the polyimide guide tubes from which the electrodes emerge. **C.** An image showing the completed microdrive prior to surgical implantation. The drive as shown in A is cemented inside the square brass tubing to prevent damage after implantation, while still providing access to the head of the screw in order to advance the electrodes. The tubing is held in a custom built jig to facilitate quick removal during the surgical implantation.

Thalamic recordings in the awake animal

All neural recordings were obtained using a 16 channel Neuralynx Cheetah recording system running the Cheetah 5 data acquisition system (Neuralynx, Bozeman MT). Copper cladding was added to the exterior of the behavioral chamber to act as a Faraday cage and limit recording noise. Spikes were obtained by applying a 600-9000 Hz bandpass filter to the 30 KHz recorded signal, then applying a manually chosen threshold to limit the inclusion of ongoing noise. Spike files were manually post-processed using the SpikeSort3D (Neuralynx, Bozeman MT) to remove motion and licking artifacts. All further analysis on the neural data was performed using custom written Matlab scripts. A recording session was excluded from further analysis if the mean latency to the first recorded post-stimulus spike exceeded 7 ms, which would indicate that the recording

electrode was not located in a topographically aligned VPm barreloid with a stimulated whisker.

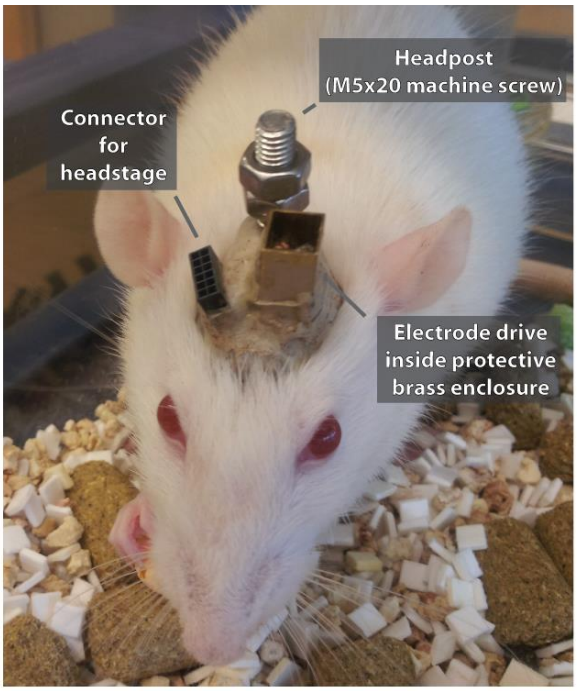

Figure 4-4 - *An image of an experimental rat approximately 3 months after the headpost and electrode drive were surgically implanted.* The brass tubing and headcap were painted with conductive silver paint to act as a Faraday cage for the electrodes and minimize noise. The microdrive screw can be accessed through the top of the brass tubing. Both the headpost and the electrical connector are indicated in the photo.

After recovery from surgery and a period of 3-6 weeks to train the animal to tolerate head fixation, the animals were re-anesthetized with isoflurane and the electrodes were slowly advanced until manual deflections of the vibrissae resulted in noticeable stimulus locked activity when the amplified activity was played through a loudspeaker. A piezoelectric actuator was then attached systematically to a number of individual whiskers and a 1 Hz punctate deflection was applied for a minimum of 60 trials per whisker. This allowed identification of the principal whisker for each of the recording electrodes by comparing

the strength of the elicited responses to each whisker deflection. However, because there was often ambiguity in identifying the principal whisker, along with the fact that the ~250 um inter-electrode spacing made it very likely that the electrode array spanned the representation of multiple vibrissae, we elected to perform all awake recordings with approximately five vibrissae simultaneously placed in the actuator. The electrodes were systematically advanced in steps of approximately 30 μm (0.1 turns) every 2-4 days. The electrodes were generally advanced prior to a given recording and behavioral session. Animals performed 1-2 behavioral sessions per day. Sessions were terminated when the animals failed to respond to at least 5 consecutive test pulses or when animals showed signs of discomfort or stress with head fixation.

Neural data analysis

All data was analyzed using custom scripts written in Matlab (Mathworks, Natick MA). The number of spikes elicited per stimulus was measured in a 30 ms post-stimulus window. First spike latency and timing precision were measured as the mean and standard deviation of the time of the first spike in the 30 ms post stimulus window, respectively. An alternative measure of timing precision was the TC40 metric (Pinto et al., 2000), defined as the number of spikes representing 40% of the total, divided by the time required to produce 40% of the total spikes. To avoid including recording sessions in which the principal whisker was not deflected, sessions in which the non-adapted mean first spike latency exceeded 7 ms were excluded. All adaptation measures were calculated by pooling the response to the final three pulses in the adapting train. For analyses of responses to probe stimuli (those following the end of adaptation by a gap of 0.5-2.5 s),

sessions were excluded from the analysis if fewer than three trials of a particular type (short or long recovery) were obtained.

Histological verification of electrode location

The electrode location was histologically verified in one of the three animals included in this dataset. The animal was deeply anesthetized using a ketamine/xylazine/azemaprozine cocktail (48/10/1.6 mg/kg, respectively), after which 50 μA of DC current was applied to for two periods of 10 s each, separated by a 10 s gap, to two of the eight recording electrodes to generate lesions for locating the electrode tips. The electrodes were not retracted prior to lesioning, meaning they were in the deepest portion of tissue that they encountered during any recording session. After lesioning, the animal was anesthetized with an overdose of sodium pentobarbital and perfused intracardially with sterile 0.1 M phosphate-buffered saline (PBS; pH 7.4) followed by 4% paraformaldehyde. The brain was then removed and post-fixed for 24 hours. The brain was sectioned at 70μm and stained for cytochrome oxidase activity following the protocol outlined in Wong-Riley (1979). The sections were imaged using Neurolucida software (MBF Biosciences) at 5X magnification.

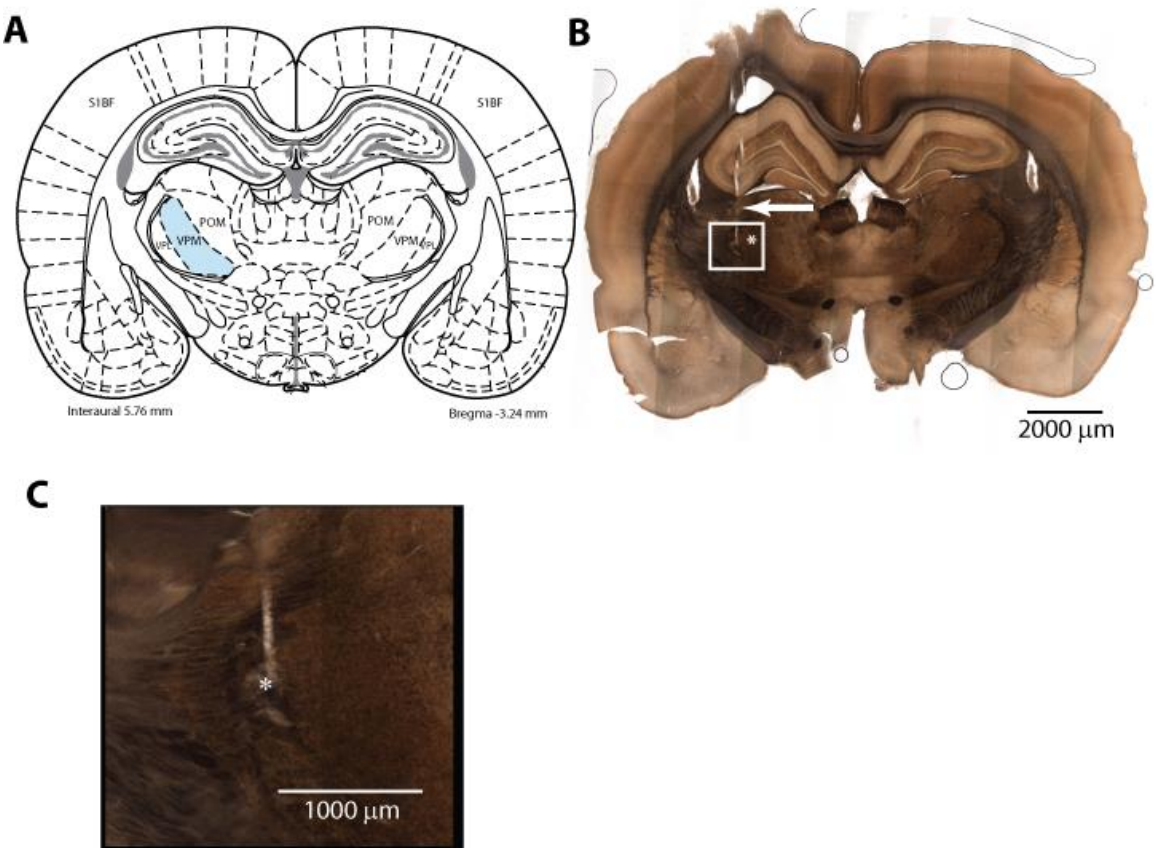

Figure 4-5 - *Histological verification of electrode placement.* **A.** An atlas image from Paxinos and Watson (2007) was used to verify the location of the electrode tip in the ventral posterior medial (VPm) nucleus of the thalamus. Note the damage to the cortex directly above the VPm, which may have been caused by tissue sticking to the electrode shanks during the postmortem removal of the brain. **B.** Cytochrome oxidase stained sections allows for the identification and localization of the electrode tracks (arrow) and the lesion created at the electrode tip (asterisk). **C.** An enlarged image of the area bounded by the white box in B showing a close view of the lesion site. (Thanks to Clare Gollnick for performing the staining, sectioning and image processing, and Radhika Patkar for assistance with the perfusion).

Thalamocortical modeling

A network model built in collaboration with Daniel Millard was used to investigate the relative importance of the magnitude and synchrony of the thalamic input population activity in driving the response of downstream cortical barrels. The network architecture

was based on a published model by Kyriazi and Simons (1993), where each independent cortical column included 100 thalamic neurons that projected to a downstream cortical population comprised of 700 excitatory neurons and 300 inhibitory neurons. The relative size of excitatory and inhibitory cortical populations was based off of previous anatomical studies (Woolsey, 1975; Simons and Woolsey, 1984).

Each cortical neuron was modeled as a quadratic integrate and fire neuron (Izhikevich, 2003, 2007), which accounts for the neuronal dynamics that would result from a full Hodgkin–Huxley-type model, but allows the computational efficiency of integrate-and-fire models. Each neuron in the model was modeled according to the following set of equations:

$$\dot{v} = 0.04v^2 + 5v + 140 - u + I \tag{6}$$

$$\dot{u} = a(bv - u) \tag{7}$$

where v is the membrane potential and u is a recovery variable instituting the nonlinear dynamics of the neuron. Spiking was determined by the membrane potential passing a fixed threshold of 30mV, at which point $v \rightarrow c$ and $u \rightarrow u + d$. The parameters were set according to Izhikevich (2007). While u and v described the membrane dynamics of the individual neurons, the input, I, delivered to the cells was responsible for generating the network dynamics. The input delivered to each cell was composed of a membrane noise term, I_m, and summed post-synaptic potentials from the thalamocortical and intracortical activity, I_S, according to the following set of equations:

$$I = I_m + I_S \tag{8}$$

$$I_S = \sum_{i=1}^{N} w_i \cdot s_i \tag{9}$$

where N is the total number of thalamic and cortical input neurons, w_i represents the synaptic weight of i^{th} neuron on the given cell, and s_i is one if the i^{th} thalamic or cortical cell has just spiked and zero otherwise. I_m was correlated Gaussian noise and produced membrane potential fluctuations across the cortical population. The connectivity and synaptic weights were extrapolated from Kyriazi, et al., (1993) and updated according to more recent in-vivo work (Bruno and Sakmann, 2006). This type of network has previously been shown to exhibit many of the common response features and rhythms of in-vivo cortical circuits (Izhikevich, 2007).

The input spikes were drawn from an inhomogeneous Poisson process, where the parameters of the process were used to systematically vary the magnitude and synchrony of the input population activity, according to the following equation:

$$A(t) = t \cdot \exp\left(-t/\tau_{sync}\right) \text{ with } \int A(t)dt = N_{spikes} \tag{10}$$

where τ_{sync} modified the synchrony of the spikes and N_{spikes} gave the average number of spikes per neuron per trial above the background activity. The output of the model was taken as the average number of spikes generated by the excitatory cortical units in a 30 ms window following the onset of the stimulus.

4.4 Results

Neural recordings were obtained from the ventroposterior medial (VPm) nucleus of the thalamus in awake, behaving rats using arrays of chronic recording electrodes attached to adjustable microdrives. The electrodes were implanted just above the VPm, after which the rats were subsequently trained to tolerate head fixation. The electrodes were then advanced into the VPm and animals were trained on the detection task described in Chapter 2. The electrodes were systematically advanced through the VPm as the animals performed 1-2 behavioral sessions per day. Neurons in the thalamus were found to adapt to repetitive stimulation by firing both fewer and less temporally precise spikes. The neurons showed recovery from adaptation on a similar timescale as was seen in the behavioral detection and discrimination tasks and the reduced spike count and precision were correlated with reductions in behavioral detectability. Finally, the recorded changes in thalamic firing with adaptation were used to drive a spatiotemporal model of cortical activation, pointing to an important role of thalamic spike timing in driving the sharpened cortical response and the resulting improved spatial discriminability.

Single and multi-unit recordings are consistent with VPm recordings

The recordings obtained from the chronically implanted electrodes consisted almost entirely of multiunit recordings. **Figure 4-6** shows sample recordings from the electrodes in an awake animal, with **Figure 4-6A-C** representing a rare single-unit recording and **Figure 4-6D-F** representing a much more typical multi-unit recording. **Figure 4-6A** and

Figure 4-6D represent the raw voltage traces from which spikes were extracted. **Figure 4-6B** and **Figure 4-6E** show a representative sampling of the units collected in a 30 ms post-stimulus window, along with the average overlaid in red. **Figure 4-6C** and **Figure 4-6F** show rasters and peristimulus time histograms (PSTHs) for two each recording session. Trials are aligned to the time of delivery of a 1,500 deg/s rostral-caudal stimulus delivered to the whiskers. Recordings with unit isolation comparable to that seen in **Figure 4-6A-C** were only obtained on small subset of recording sessions and they are shown here to demonstrate some of the typical features that are indicative of VPm recordings. Of particular note are the short spike latencies (4-6 ms) and the characteristic depression following the initial stimulus driven activity (Lee et al., 1992; Kyriazi et al., 1993; Fanselow and Nicolelis, 1999; Webber and Stanley, 2004). The multi-unit recording shown in **Figure 4-6D-F** shares many of these characteristics, but it should be noted that the baseline rate is higher and more spikes are elicited per stimulus, both of which indicate that the activity of multiple neurons is being recorded.

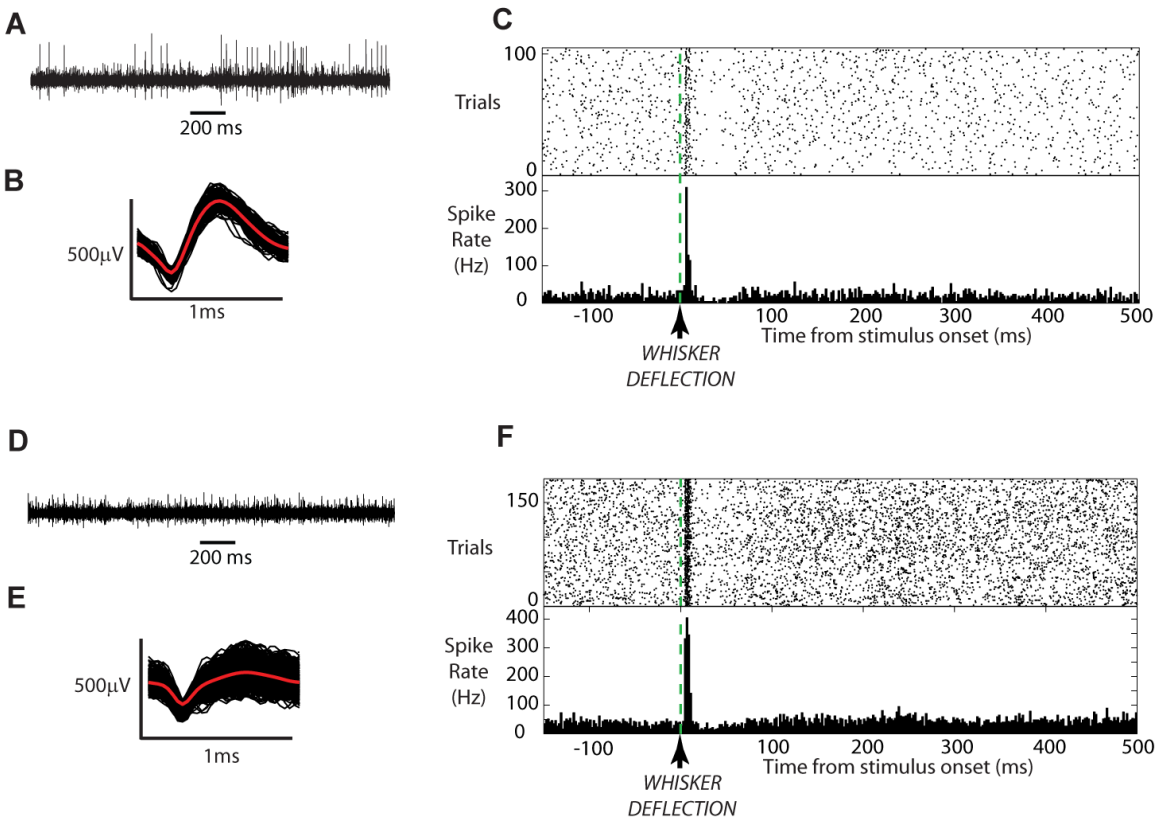

Figure 4-6 - *Examples of recordings from chronically implanted electrodes 2+ months after implantation.* **A.** 2 seconds of a raw voltage trace from a session with an identifiable single unit. **B.** An overlay of approximately 200 individual traces of an identified unit from the voltage trace shown in A, with the average shown in red. **C.** A raster plot and a peristimulus time histogram (PSTH) for the unit shown in B in response to a 1,500 deg/s whisker deflection at time 0. **D.** Same as A for a typical multi-unit recording session. **E.** Same as B for the multi-unit waveforms identified from the voltage trace shown in D. **F.** Same as C for the units shown in E.

VPm neurons adapt to persistent stimuli by firing fewer and less temporally precise spikes

As in the detection task described in Chapter 3, the probe stimulus to which the animal was trained to respond was preceded by a 3 second train of adapting stimuli on approximately 50% of trials. The sinusoidal adapting stimulus from Chapter 2 was replaced with a 10 Hz train of 1,500 deg/s pulsatile stimuli (Wang et al., 2010) to provide

more clearly defined epochs for characterizing the neural response to each successive pulse in the adapting train. **Figure 4-7** shows a raster and PSTH from a typical recording session in which 51 presentations of the adapting stimulus were presented to the animal. The response to each successive pulse can be clearly distinguished and qualitative inspection of the PSTH points to a successive decrease in responsiveness of the recorded units over the course of adaptation.

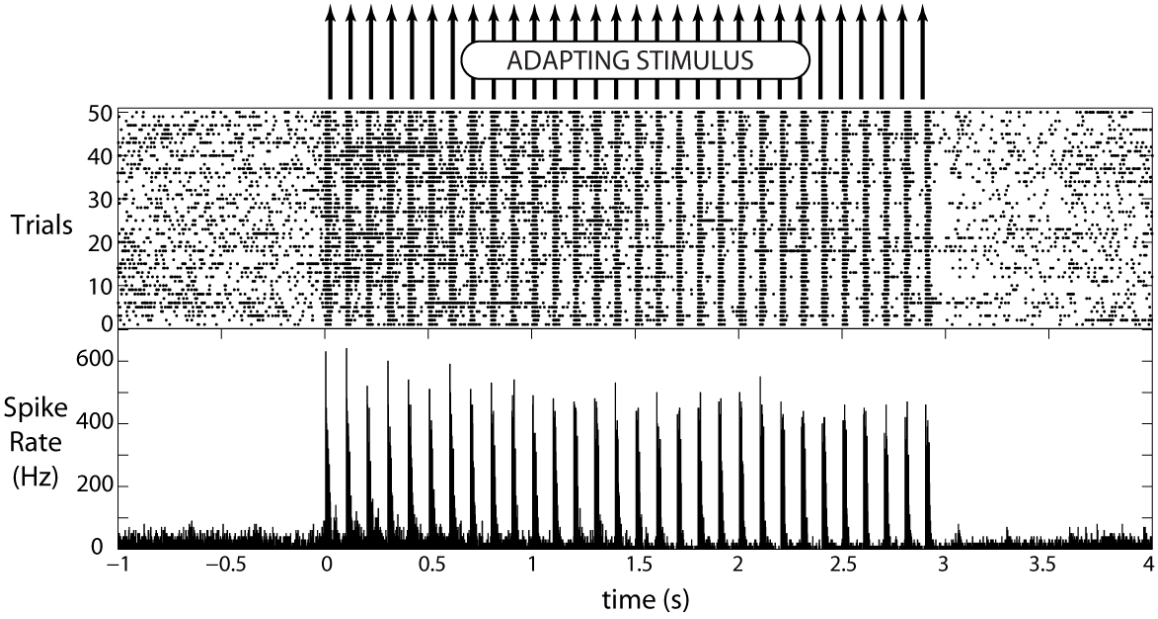

Figure 4-7 - *Example of a recording from the VPm of an awake animal during presentation of an adapting stimulus.* At top is a schematic demonstrating the presentation of a 3 second, 10 Hz, 1,500 deg/s adapting stimulus. The spike raster shows the response of a multi-unit recording over 51 presentations of the adapting stimulus. The PSTH below demonstrates a reduction in the firing rate with successive presentations of the adapting stimulus.

When averaged over all recording sessions in all three animals in the study, the effect of adaptation can clearly be seen, as shown in **Figure 4-8**. The combined PSTH is shown in **Figure 4-8A**. **Figure 4-8B** shows the mean normalized spike count across all sessions. The firing rate took a dramatic drop from the first to the second pulse in the adapting

train, recovered slightly, then approached a steady-state level of adaptation of 79.2% of the non-adapted firing rate. Both the characteristic dip in the second pulse and the steady-state thalamic adaptation ratio match closely with recordings from the VPm of anesthetized animals in a very similar paradigm by Wang et al. (2010), in which an adaptation ratio of 80% was measured. These results were also very similar to another study in the anesthetized thalamus of rats by Khatri et al. (2004), which reported a 30% reduction in the evoked response with adaptation. However, is it should be pointed out that the study of Khatri et al. reported this adaptation value in response to a much higher frequency (40 Hz) stimulus. A more directly comparable adaptation paradigm was performed by Ganmor et al. (2010), which also showed a very similar adaptation ratio of approximately 80% in the VPm in response to a high intensity 18 Hz stimulus. However, they noted much stronger adaptation to low intensity stimuli. Though all of the findings reported here were for thalamic recordings, these previous studies also showed that adaptation is more robust at the cortex. Similarly, Castro-Alamancos et al. (2004) measured a cortical adaptation ratio of as low as 35% for quiescent or well-trained animals, though there was a less robust cortical adaptation ratio of approximately 80% for animals in an engaged, or 'activated,' state.

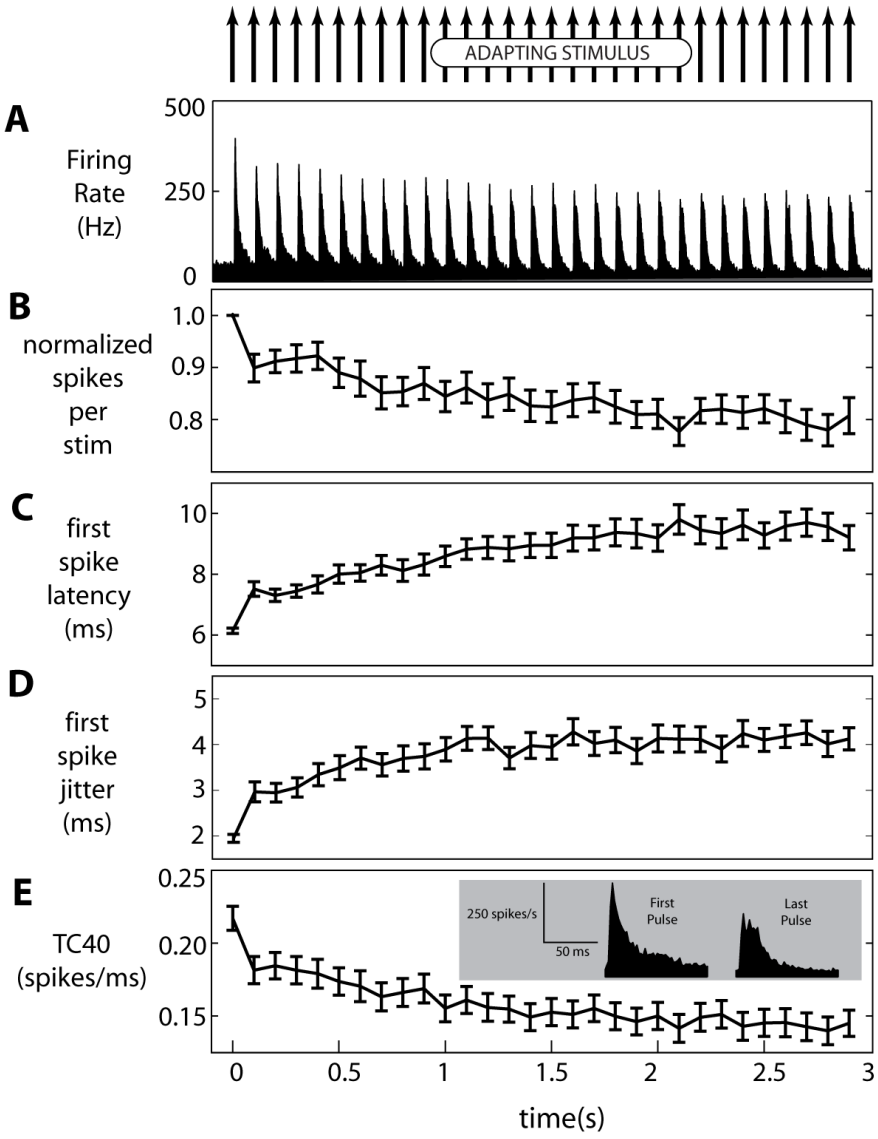

Figure 4-8 - *Adaptation as a function of time for all animals combined.* **A.** The combined PSTH for all animals and recording sessions. **B.** The number of spikes per stimulus for each pulse in the 3 second, 10 Hz train of adapting stimuli, normalized to the spike count in response to the first pulse. After adaptation, the firing rate was 79.2% of its non-adapted value. **C.** The mean latency to the first spike following the stimulus increased from 6.1 +/- 0.09 ms in the non-adapted state to 9.2 +/- 0.4 ms in the adapted state. This relatively small increase in first spike latency indicates that the electrodes were in the VPm, as opposed to the nearby POM nucleus of the thalamus, which displays a more dramatic shift in the first spike latency with adaptation. **D.** The first spike jitter, measured as the standard deviation, also increased with adaptation, going from 1.9 +/- 0.09 ms to 4.1 +/- 0.24 ms with adaptation. **E.** Timing precision, as measured using TC40, decreased from 0.217 +/- 0.008 spikes/ms in the non-adapted state to 0.145 +/- 0.008 spikes/ms after adaptation. The inset shows the first and last PSTH combined across all animals and recording sessions (all values $p < 0.005$, $n = 56$, two sided t-test).

Figure 4-8C shows the effect of adaptation on first spike latency in the thalamus. This relatively small shift in latency, from 6.1 ms in the non-adapted state to 9.2 ms in the adapted state, provides further evidence that recordings were obtained from the VPm nucleus of the thalamus, as opposed to the nearby POM nucleus . The POM, which is part of the 'paralemniscal' pathway also carrying vibrissa related information, displays a much more profound shift in first spike latency with adaptation (Ahissar et al., 2000). In addition to a reduction in firing rate, adaptation has been shown to lead to decrease in the timing synchrony of the thalamic inputs to cortex (Wang et al., 2010). While multiple simultaneous single unit recordings are required to accurately measure synchrony, a proxy for synchrony across multiple neurons can be the timing precision of a multi-unit cluster across trials. The simplest measure of timing precision is likely the first spike standard deviation, or jitter, which increased from 1.9 +/- 0.09 ms to 4.1 +/- 0.24 ms with adaptation. An alternate measure of timing precision is the TC40 metric, in with 'TC' stands for 'temporal contrast' (Pinto et al., 2000). TC40 is defined as the number of spikes representing 40% of the total response magnitude in 30 ms post stimulus window, divided by the time required to generate the first 40% of the total response magnitude. **Figure 4-8E** demonstrates that timing precision decreases by approximately 33% by this measure, from 0.217 in the non-adapted state to 0.145 in the adapted state. This is also very similar to the percentage reduction in synchrony measured in the anesthetized animal (Wang et al., 2010). The inset of **Figure 4-8E** demonstrates the difference in temporal contrast between the responses to the first and last stimuli in the adaptation train. Together, these results indicate that sensory adaptation exists as early in the sensory pathway as the thalamus in the awake animal and that, at least for the conditions

described here, the percent reduction in both elicited spikes and timing precision closely matches values in the anesthetized animal in a similar paradigm.

While **Figure 4-8** represents the adaptation data pooled over all three animals, **Figure 4-9** represents the data for each individual animal, demonstrating that the effect is relatively consistent and robust. **Figure 4-9A** shows the normalized spike rate, for which the adapted value was 75.9%, 94.4%, and 81.1% of the non-adapted value for animals 1-3, respectively. **Figure 4-9B** shows the mean first spike latency, which was 6.1 ms, 5.5 ms and 6.2 ms in the non-adapted state and 8.1 ms, 9.5 ms, and 11.0 ms in the adapted state for animals 1-3 respectively. **Figure 4-9C** shows the timing precision measured as TC40, which was 0.22 spikes/ms, 0.14 spikes/ms, and 0.22 spikes/ms in the non-adapted state and 0.15 spikes/ms, 0.10 spikes/ms, and 0.14 spikes/ms in the adapted state for animals 1-3 respectively. The pooled adaptation results shown in **Figure 4-8** represents data acquired over 56 recording sessions, leading to strong statistical significance of the results. However, it should be noted that when the data is averaged by animal as in **Figure 4-9**, the sample size is reduced to three and the p-values increase ($p = 0.09$, $p = 0.05$, $p = 0.05$ for the spike count, latency, and precision changes, respectively, using a paired t-test).

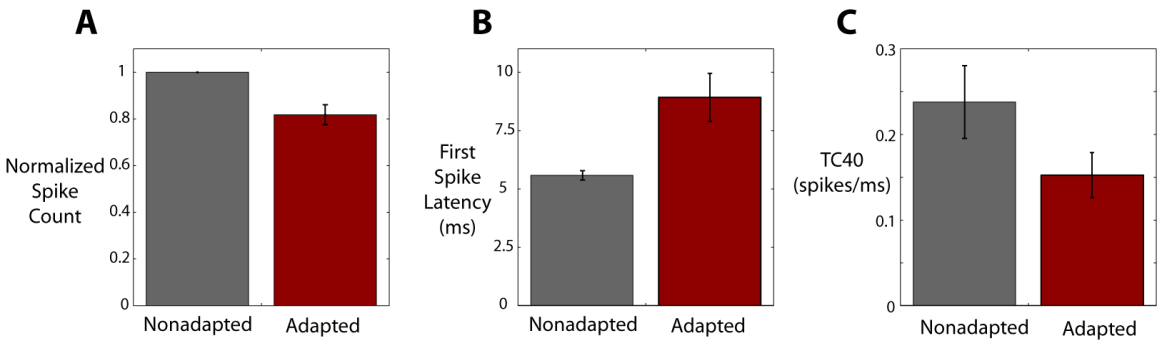

Figure 4-9 - *Summary of adaptation results for each animal individually.* **A.** Normalized spike count. **B.** First spike latency. **C.** Timing precision as measured through TC40.

Recovery from adaptation in the VPm mirrors the behavioral time course of recovery

The behavioral detection results from Chapter 3 indicated that the animals displayed a markedly reduced ability to detect stimuli in a short window (0.5-1.5 s) following the end of adaptation, but that their detection performance began to improve with a longer (1.5-2.5 s) period of recovery from the effects of adaptation (see **Figure 3-9**). To test the extent to which this was also true in the thalamus of awake animals, the responses to probe stimuli in both the short and long recovery epochs were calculated and are shown in **Figure 4-10**. Scatter plots of both the number of elicited spikes and the timing precision are shown in **Figure 4-10A** and **Figure 4-10C**, respectively. In both cases, the short recovery (shown as orange Xs) and long recovery (shown as blue Os) values were plotted against the non-adapted values. Data points below the unity line indicate a lower spike count or timing precision. Visual inspection of **Figure 4-10A** and **Figure 4-10C** indicates that most data points lie below the unity line, indicating that both the spike count and the timing precision of thalamic firing in response to a probe are decreased from their non-adapted levels. However, in general, the short recovery values lie further below the unity line (orange Xs tend to lie below the blue Os), indicating the effects of

adaptation are more profound with short periods of recovery from adaptation, which mirrors the results from the behavioral tasks described in Chapter 3.

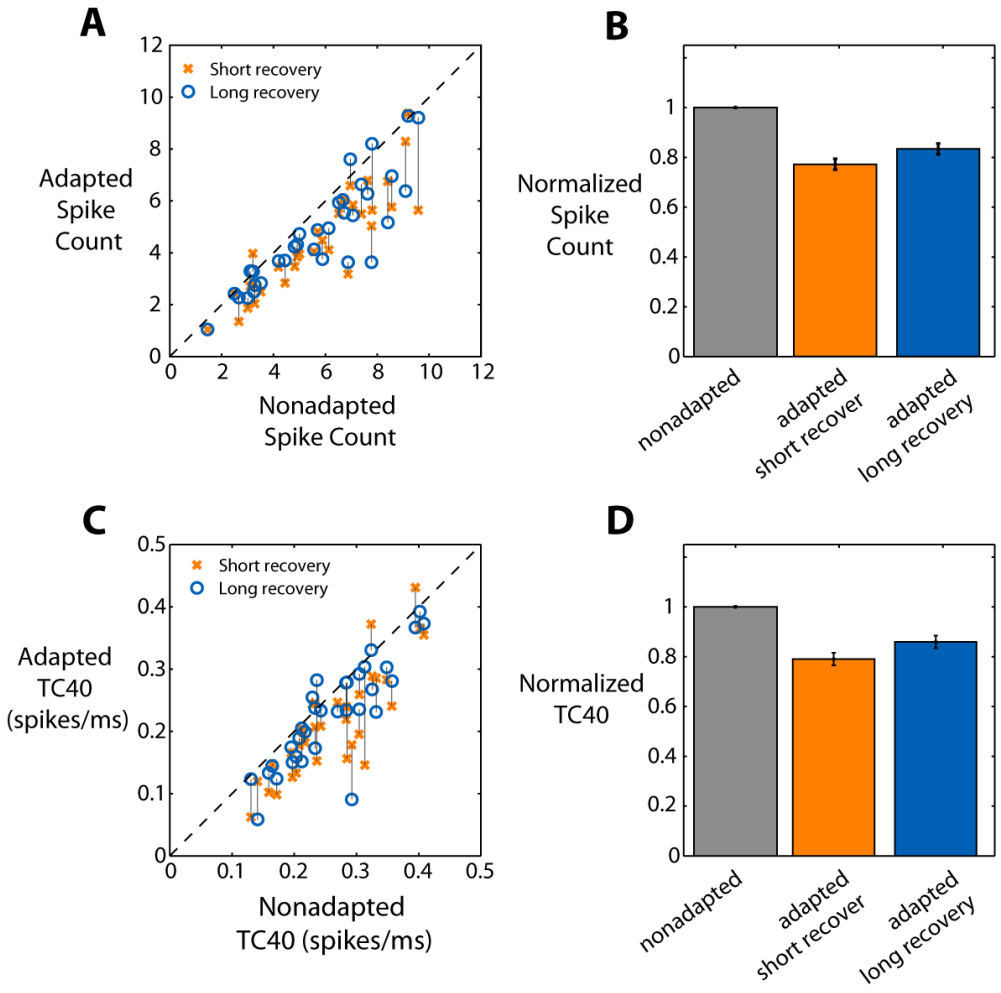

Figure 4-10 - *Firing rate and timing precision in response to the probe stimulus.* **A.** Scatter plot of spikes in a 30 ms window following the probe stimulus. On a given session, both the mean spike count in response to short recovery stimuli (those falling in the 0.5-1.5 s post-adaptation window, shown as orange Xs) and long recovery stimuli (those falling in the 1.5-2.5 s post adaptation window, shown as blue Os) are plotted against the mean number of spikes elicited by non-adapted probe stimuli. Gray lines connect data points from a given session. **B.** Same data as A, but each data point is normalized against the non-adapted value. **C.** Scatter plot of firing precision measured as TC40. Same conventions as A. **D.** Same data as C, but each data point is normalized against the non-adapted value.

The timescale of recovery of the thalamic neurons to their baseline firing characteristics closely matches the recovery of the behavioral detection and discrimination performance, as shown in **Figure 4-10B** and **Figure 4-10D.** Here, the recovery effect was demonstrated by normalizing the spike count and timing precision, respectively, against the non-adapted value for each recording session. **Figure 4-10B** shows that the firing rate was reduced on average to 78 +/- 2.7 percent of the non-adapted value for short recovery periods ($p < 0.005$, $n = 43$, paired t-test), then began to recover to 84 +/- 2.6 percent the non-adapted value ($p < 0.005$, $n = 43$, paired t-test) with additional time for recovery. Similarly, timing precision as measured using TC40 was reduced to 81 +/- 3.0 percent of the non-adapted value with a short period of recovery ($p < 0.005$, $n = 43$, paired t-test) and increased to 87 +/- 3.0 percent of its non-adapted value ($p < 0.05$, $n = 43$, paired t-test) with additional recovery time.

Reduced spike count and timing precision corresponds to a reduction in detection performance

The previous analyses have all considered the effect of adaptation on the thalamic response without considering the behavioral response of the animals. **Figure 4-11** shows the firing rate and timing precision for data from the two animals that successfully learned the detection task when trials were separated by behavioral response. **Figure 4-11A** and **Figure 4-11B** show rasters and PSTHs from a single behavioral session for hit and miss trials, respectively. Qualitatively, there is a slight shortening and widening of the PSTH in the miss trials, indicating fewer and less temporally precise thalamic spikes as a result of stimuli that the animal failed to correctly detect. This effect becomes clearer

when examining all behavioral sessions on a scatter plot, as shown in **Figure 4-11C** and **Figure 4-11D**. Both the number of spikes per stimulus and the timing precision show a significant decrease ($p < 0.05$ for both quantities, paired t-test, $n = 53$) for miss trials vs. hit trials, indicating that a decrease in both quantities could make stimuli less detectable for the animal. Though the decrease in both quantities was small, relatively small differences may be magnified when passing from the VPm to the cortex, especially given the known sensitivity of the cortex to variations in thalamic coding properties (Bruno and Sakmann, 2006; Wang et al., 2010; Bruno, 2011).

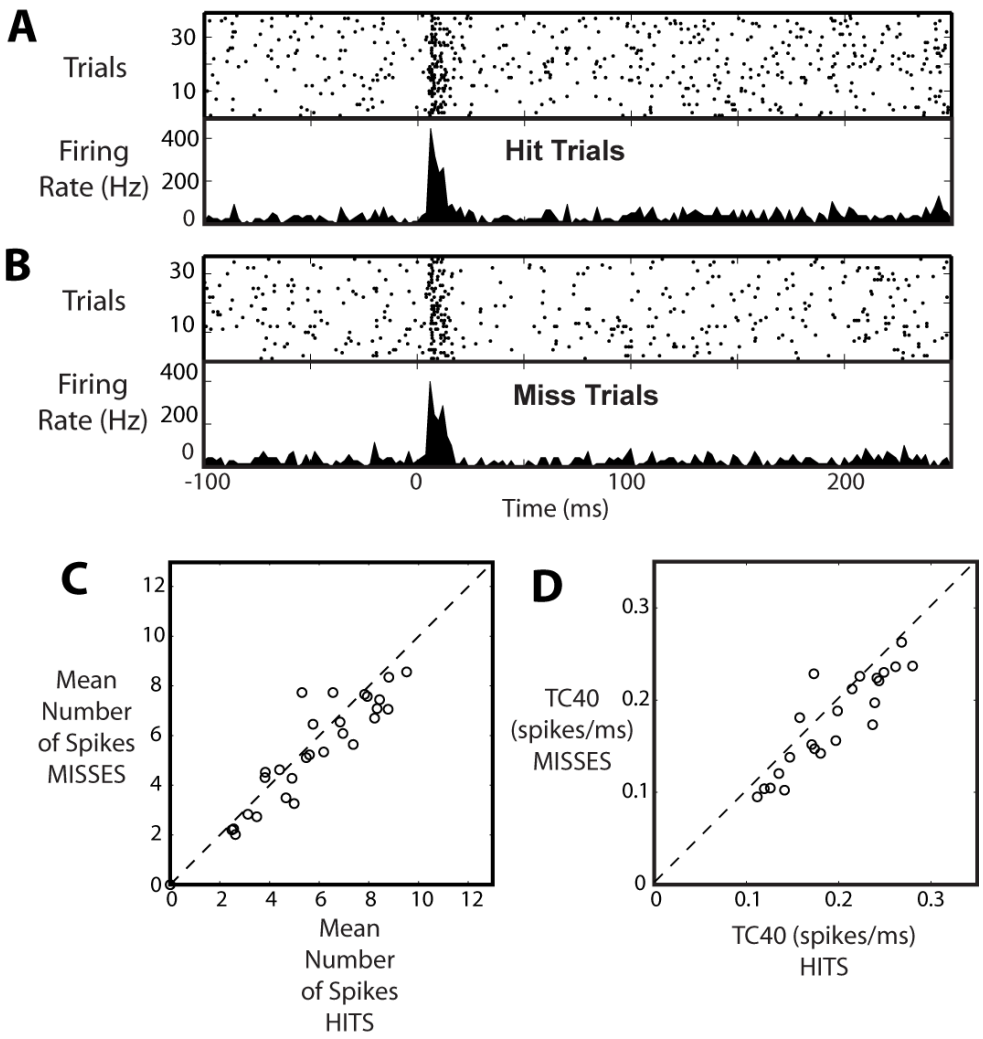

Figure 4-11 - *Firing rate and timing precision for trials separated by behavioral outcome.* **A.** An example PSTH from a single behavioral session showing the thalamic response on only the trials on which the animal correctly responded to the stimulus (hits). **B.** An example PSTH from the same behavioral session as A showing the behavioral response on only the trials in which the animal failed to respond to the stimulus (misses). **C.** A scatter plot from all recorded behavioral sessions showing the average firing rate for hit trials vs. miss trials. Note that most points lie below the unity line, indicating a lower mean firing rate on miss trials. ($p < 0.05$, paired t-test, $n = 53$) **D.** Same convention as C for timing precision. ($p < 0.001$, paired t-test, $n = 53$).

A model of the thalamocortical circuit provides a link between the cortical and behavioral results of adaptation and the measured changes in VPm coding properties

To link the measured effects of adaptation in the thalamus with the previously described improvements in spatial discriminability and the corresponding changes in cortical processing, a model was used to simulate the cortical response to thalamic inputs in both the non-adapted and adapted states. The model was based on a published model of a single thalamic barreloid in VPm and a cortical (layer 4) barrel by Kyriazi and Simons (Kyriazi et al., 1993) with dynamics modeled on more recent work by Izhikevich (2007). The Izhikevich model retains the computational simplicity of an integrate and fire simulation, but captures some of the more biophysically realistic elements of spiking of more complex models. The inputs to the model were based on the thalamic data recorded from the awake animal that was reported above. In the model, each cortical layer 4 barrel was treated as an independent unit (Goldreich et al., 1999), and there was assumed to be no connectivity between a given thalamic barreloid and an adjacent cortical barrel, an assumption that is based on results from anatomical studies (Bruno and Simons, 2002; Bruno and Sakmann, 2006; Oberlaender et al., 2012). Each barreloid was modeled as a homogeneous population of excitatory relay cells that synapse onto both excitatory and inhibitory units in layer 4 of the cortex. The excitatory and inhibitory units in the cortex also synapse onto one another, allowing the model to account for feed-forward inhibition (Swadlow, 2003; Gabernet et al., 2005). A schematic of the model is shown in **Figure 4-12A**. However, despite the known segregation of cortical barrels, both cortical barrels and thalamic barreloids do not have perfectly selective receptive fields and they do demonstrate responses to adjacent whiskers (Simons, 1978; Armstrong-James and Fox,

1987). This was included in the model by assuming that an adjacent thalamic barreloid responds with 50% fewer spikes and a 50% increase in first spike standard deviation relative to its neighbor, values which were estimated from Wang et al. (2012) and Minnery et al. (2003), respectively. These parameters allow the spatial spread of the cortical activation in response to a single whisker to be simulated, which is shown in **Figure 4-12B**. To account for the effect of adaptation, the measured reductions in firing rate and timing precision discussed above (a 21.3% and 36.2% reduction in firing rate and timing precision, respectively) were applied to the simulated inputs to both the primary and adjacent thalamic barreloids. This led to the normalized firing rate in the principal and adjacent whiskers that is shown in **Figure 4-12B**, which shows a much sharper response after sensory adaptation. It should be noted that the VSD recording captures sub-threshold activity in layer 2/3 of cortex, while the model here captured the VPm projections to spiking in cortical layer 4. However, the early onset frames of cortical activation as measured by layer 2/3 VSD imaging (as carried throughout our analyses) have been shown to be reflective of the suprathreshold activation of layer 4 cortical neurons (Petersen et al., 2003a).

To assess discriminability in both the non-adapted and adapted states, the difference in activation between the principal and adjacent barrels was calculated. The model demonstrated an increase in this discriminability quantity from 0.27 +/- 0.14 in the non-adapted state to 0.57 +/- 0.24 in the adapted state, as shown in Fig. 11C. Given that we had complete control over the input to the model, it was also possible to measure the individual effects of changing just the firing rate while leaving the timing precision fixed.

This led to a much smaller increase in discriminability to just 0.39 +/- 0.21, which is shown as the bar labeled 'synchrony control' in **Figure 4-12C** and as the black line in **Figure 4-12B**. This further confirms the importance not just of the absolute reductions in firing rate in driving improved discriminability, but also of the corresponding changes in timing precision (Wang et al., 2010). Taken together, the results here suggest that the adapting stimulus paradigm utilized in the behavior had a significant effect on the thalamic firing properties in the awake animal, that thalamic firing correlated with detection performance, and that the adaptive modulations in both thalamic firing rate and synchrony likely play some role in the sharpening of the spatial activation in cortex that we showed to result in an enhanced discriminability at the expense of detectability.

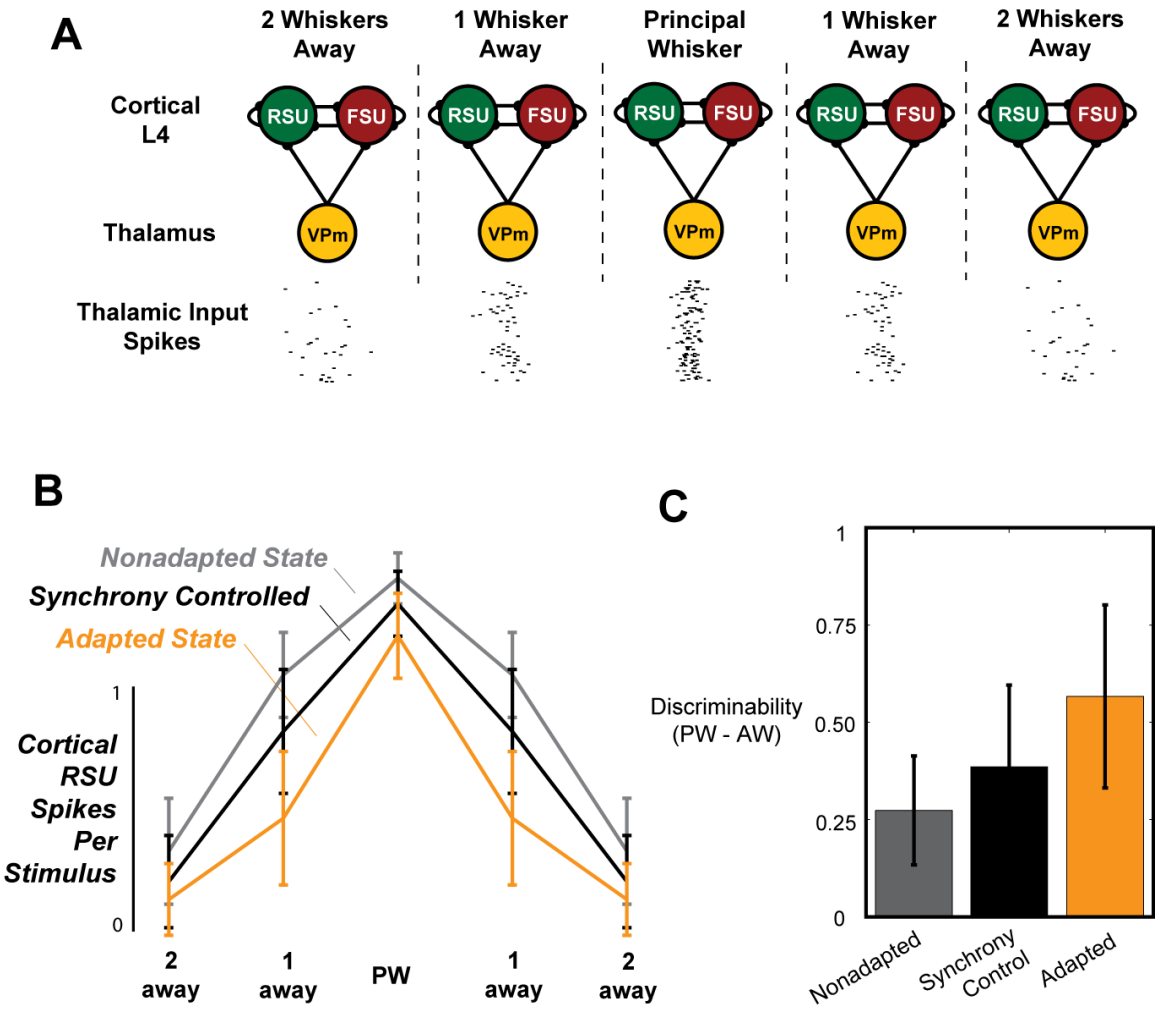

Figure 4-12 - *Output of a simulated thalamocortical circuit demonstrating the effects of adaptation on spatial discriminability at the cortex*. **A.** A schematic of the model configuration. Each barreloid-to-barrel connection is treated as an isolated circuit. Each thalamic barreloid in VPm nucleus of the thalamus contains only excitatory relay cells. The input neurons in layer 4 of the cortex consist of both excitatory regular spiking units (RSUs) and inhibitory fast spiking units (FSUs). These cells receive both thalamocortical and intracortical inputs. Sample thalamic input spike trains are shown below each column, demonstrating the reduction in precision and spike count with distance from the PW that is built into the model. **B.** The output of the model, which is the number of spikes generated by the regular spiking units in each barrel, in response to a deflection of the principal whisker (PW). The black line represents trials in which only the spike count was allowed to adapt but the timing precision was held constant. **C.** Discrimination performance of an observer of the simulated cortical activity, here measured as the difference in activity in the principal and adjacent whiskers. Discriminability was greatly improved after adaptation. However, when allowing only the firing rate to change with adaptation, but holding firing synchrony constant before and after adaptation (labeled as synchrony control), the discrimination performance is less dramatically improved.

4.5 Discussion

The results here indicate that adaptation to a sensory stimulus, which in this case was a train of pulsatile stimuli applied to multiple vibrissae simultaneously at 10 Hz, leads to relatively strong changes in the response properties of the recorded thalamic neurons, with potentially important perceptual consequences. Specifically, neurons were found to respond with fewer elicited spikes per stimulus and with reduced timing precision after adaptation. These changes closely tracked those seen previously in the anesthetized animal in a similar paradigm (Wang et al., 2010). Further, the effects of adaptation began to recover with a similar time course as was seen in the behavioral tasks described in Chapter 3, which was on the order of just a few seconds. When the neural data was parsed based on the behavioral responses of the animals in the detection task, both a lower spike count and a reduced timing precision were found to be correlated with trials in which the animal failed to detect the stimulus, indicating that both variables were likely important in making stimuli detectable for the animal. Finally, modeling results indicate that the observed shifts in the thalamic response are capable of leading to the reduced magnitude and sharpened cortical response seen in Chapter 3, which could largely explain the reduced detection performance and improved spatial discrimination performance seen with adaptation.

While recordings of single unit activity was possible in rare cases, as shown in **Figure 4-6**, all of the data included in the analyses detailed here displayed the lower signal to noise and less repeatable waveform shapes characteristic of multiunit responses (Super

and Roelfsema, 2005). However, given that thalamic barreloids consist of a homogeneous population of glutamatergic relay cells (Barbaresi et al., 1986; Harris, 1986; Ohara and Havton, 1994; Lavallée and Deschênes, 2004), the recorded multiunit clusters are likely to consist entirely of excitatory thalamocortical projection neurons. Thus, while the inability to isolate the timing of the responses of single neurons makes measurement of firing synchrony impossible, measurements of the overall timing precision of the recorded multiunit activity across trials likely tracks very closely with the synchrony of multiple individual neurons. We thus chose to use the 'temporal contrast,' or TC40, measure first described by Pinto et al. (2000), which describes the time required for the sampled population to generate 40% of the total response magnitude, as a proxy measurement for the overall measure of population synchrony. To avoid confusion with other more direct measures of synchrony, we have used the term 'precision' to describe this measure.

Despite the different metric used, it is worth noting that the multiunit timing precision measured here, as well as the overall decrease in evoked firing activity, showed a very similar magnitude of decrease with sensory adaptation as was measured in the study of Wang et al. (2010). In that study, modeling work demonstrated that the changes in synchrony were critical in driving the decreased detectability and improved velocity discriminability seen at the cortex, pointing to the level of thalamic synchrony as an important part of the neural code (Bruno, 2011). The reduced behavioral detectability shown in Chapter 3 can thus likely be explained by the weaker and less temporally precise input to the cortex after adaptation, which would in turn lead to a less robust and

detectable downstream cortical response to a whisker deflection following sensory adaptation.

Further indication of the behavioral importance of both the decreased firing rate and precision with adaptation comes from the correlation of both factors with reduced behavioral detection performance, as shown in **Figure 4-11**. Combined, these results provide further proof not only of the existence of sensory adaptation effects in the thalamocortical circuit of the awake animal, but also of the behavioral importance of the resulting changes. These results could be seen as contradicting the often repeated finding from Castro-Alamancos (2004), indicating a lack of sensory adaptation in the thalamocortical circuit of the awake animal. However, as in Chapter 3, it should be emphasized that the animals used in this study were quite familiar with the behavioral paradigm prior to the beginning of the neural recordings reported here, and that the lack of thalamocortical sensory adaptation predicted by Castro-Alamancos applied largely to animals involved in novel tasks. Thus, our results contradict the widespread conclusion drawn from Castro-Alamancos's work, that sensory adaptation does not exist in the awake animal, but they do not contradict the results as actually reported in that study.

However, despite the correlation between reduced detectability and the presence of sensory adaptation, the improved discriminability in a two whisker spatial discrimination task following adaptation, as demonstrated in Chapter 3, does not follow trivially from the observed changes in thalamic coding. Given this, we opted to use a spatial model of the thalamocortical system with inputs based off of those recorded from the thalamus of

the awake animal in both the non-adapted and adapted states to better understand the mechanisms that could control this phenomenon. The model was based off of a well-accepted thalamocortical model first published by Kyriazi and Simons (Kyriazi et al., 1993) with dynamics based on more recent work by Izhikevich (2007). While the Kyriazi model simulated only a single cortical barrel, the model was extended here to include multiple adjacent barrels to simulate the spatial response to a whisker deflection in both the non-adapted and adapted states. Assuming that changes in synchrony or timing precision scale linearly in both the primary and adjacent barreloid with adaptation, the model indicates that the drive from an adjacent barreloid drops below the threshold for reliably driving activity in its aligned cortical barrel sooner than does the principal barreloid. This effectively sharpens the cortical response and thereby improves the ability of the model to correctly identify which whisker was deflected. These simulated responses correspond well with the sharpened cortical responses measured through VSD imaging by He Zheng (shown in Chapter 3), as well as those seen previously through intrinsic optical imaging (Sheth et al., 1998). It should also be emphasized again that the model was designed to simulate the layer 4 cortical response, while both VSD imaging and intrinsic optical imaging capture activity from the more superficial cortical layers, which possess more lateral connectivity.

While the results shown here provide an important link between the behavioral effects resulting from sensory adaptation shown in Chapter 3 and the underlying shifts in neural coding, work remains to fully describe the methods by which changes in information processing is affected by adaptation and how that leads to the observed

detectability/discriminability tradeoff. For instance, significant progress would be made by recording single thalamic relay neurons simultaneously both within and across individual barreloids to better characterize changes in firing synchrony. In addition, all recordings performed here were obtained while the animal was performing only the detection with adaptation task, while making the assumption that the underlying changes in neural coding are largely comparable during the spatial discrimination task. However, it is possible that the animals adopt a somewhat different strategy in these two tasks, leading to fundamentally different effects in thalamocortical processing as a result of sensory adaptation. Finally, the adapting stimulus used here was chosen to closely match the frequencies at which the animal palpates its own whiskers during active touch under the assumption that the resulting changes in coding properties might be similar to those seen during whisking. However, a more direct link between the behavioral consequences of adaptation to a passively applied stimulus as opposed to processing changes occurring as a result of active touch should be explored using more complex and ethologically relevant behavioral tasks.

Conclusions

As sensory systems are faced with a constantly changing environment, the ability to modify the operating characteristics of the system to meet the current task demands is extremely important in maximizing neural coding efficiency. I specifically investigated the ability for sensory systems to switch between a state optimized for the detection of weak, transient stimuli to one optimized for encoding details of the stimulus to maximize discriminability. My work is unique in that it used a combination of carefully controlled behavioral tasks and neural recordings in both anesthetized and awake animals to explore how sensory processing was affected by both the active sensing strategy employed by the animal and by passively applied sensory adaptation. This work provides the most complete connection to date between the large body of research into the effects of sensory adaptation using anesthetized animal models and both the behavioral and neural consequences of adaptation in the awake animal.

The work presented in this dissertation firmly establishes the importance of sensory adaptation on shaping the way information is processed in the thalamocortical circuit of an awake, behaving animal. Specifically, this work establishes the role of sensory adaptation in improving the ability of animals to discriminate between nearby tactile inputs, but at the expense of their ability to detect weaker inputs. Importantly, the recordings I obtained from the thalamus of awake, behaving rats demonstrate that the effects of adaptation exist sub-cortically and were of a similar magnitude as earlier results found in the anesthetized animal. Further, the modeling results demonstrated here, combined with the results from earlier anesthetized studies, point to changes in thalamic

coding properties as the important driver in modulating the changes in cortical processing the resulting behavioral and perceptual consequences. While arguments have been made in the past for a detection/discrimination (or sensitivity/specificity) tradeoff as a result of sensory adaptation in the awake animal (Moore et al., 1999; Moore, 2004), the present results provide the first behavioral demonstration of this tradeoff, combined with corresponding neural recordings to help explain the underlying mechanism driving the behavioral changes. In addition, clear measurements were made of the extent of thalamic adaptation, as well as the time course of recovery, both at the neural and behavioral levels.

The behavioral paradigm used here - the single whisker detection task and the two-whisker discrimination task, both either in the presence or absence of adaptation – also represent an important point of novelty and a potentially important contribution to the field. The paradigm developed as part of this project should provide a powerful experimental setup for future studies of sensory adaptation or behavioral modulation on detection and discrimination performance.

The importance of behavioral tasks in studying sensory processing

While many important insights into the nature of neural coding can be gained through studies of the anesthetized animal, the importance of studying sensory systems in awake, behaving animals has been increasingly recognized in recent years. While studies in the anesthetized animal provide obvious advantages for experimental control, some important problems result. First, obviously, is the fact that by their very design, anesthetic

drugs fundamentally alter the function of the neural circuitry that is under study. However, more subtly, animals under anesthesia are in a different information processing state, one which more closely resembles sleep. But beyond these differences in information processing, it is only during the performance of a sensory mediated task in an awake, behaving animal that we can truly begin to link predictions based on neural coding to actual changes in perception. Thus, the results of the behavioral tasks from Chapters 2 and 3 provide a particularly powerful demonstration of the detection/discrimination tradeoff. By training the animals to perform these psychophysical tasks, we were able to effectively 'ask' them what they were feeling through their behavioral response. Returning to the framework of **Figure 1-1**, this gave us direct access to the output of the decision process, *D*, which could be used to draw inferences on the animal's stimulus representation, *R*.

It should be noted that the head-fixation techniques used here represent a compromise between a precisely controlled study in an anesthetized animal and a more naturalistic behavioral task in an awake and unconstrained animal. Though some aspects of the animal's natural behavior are lost through head-fixation, in many ways the technique maintains the most important characteristics of both types of studies: the stimulus control and repeatability of an anesthetized study combined with active, awake information processing modes in the circuitry and the ability to measure the animals' behavioral outputs.

Combined with head-fixation, the rodent vibrissae system proved to be an especially powerful model system for the studies used here. Rodents, and especially rats, are capable of learning relatively demanding behavioral tasks. This turned out to be an important point given the complexity of the behavioral tasks used here. Further, the system has been studied in detail for over a century, dating to Vincent's pioneering work (Vincent, 1912), leading to a very thorough understanding of the pathway. As such, the vibrissae system has become one of the most widely used model systems not just for somatosensation, but for sensory processing and in general. Though the vibrissa system is a highly specialized sensory system unique to rodents, the insights gained here should help to provide a better understanding of how sensory systems process information in the face of changing environmental demands.in many species, including the human.

The role of primary sensory information in decision making

The VSD imaging results from the anesthetized animal presented in Chapters 2 and 3 also proved useful in better understanding the potential coding strategies used by the animal, as well as how changes in the cortical population response could lead to changes in detection and discrimination performance. Importantly, given that these recordings were obtained in the anesthetized animal, they served to further demonstrate that the effects of adaptation exist at the level of S1 even in the absence of attention or other top-down processes. Again, returning to the framework of **Figure 1-1**, these recordings, combined with the modeling work of Chapters 2 and 4, allowed us to approximate the animal's stimulus representation, *R*, based on recorded neural activity, *N*. The resulting predictions of the animal's decisions, *D*, closely matched those seen in the behavioral tasks,

increasing our confidence that the recorded neural activity closely matched that used by the awake animals in the tasks.

The thalamic recordings from Chapter 4 pointed to the underlying coding changes that help explain both the changes in the cortical response seen in the anesthetized animal as well as the behavioral changes in detection and discrimination measured in the awake animal. This directly represents the 'transmission/transformation' stage in **Figure 1-1** from neural activity, *N*, to the final stimulus representation, *R*. The results here show that adaptation is not only present in the thalamocortical circuit of the awake animal but that it also carries important perceptual consequences. Both the reduction in the overall firing rate and the reduction in timing precision across thalamic neurons were shown to be important drivers in the reduced detection and improved spatial discrimination performance with sensory adaptation.

Detection and discrimination as different types of tasks

While the discussion here has treated detection and discrimination as two distinct types of tasks, they are in no way mutually exclusive. On the contrary, during natural behavior, dynamically shifting task demands would likely force the system to perform both functions interchangeably. For instance, an animal at rest would benefit from being especially sensitive to unexpected stimuli to alert it to potential threats or opportunities, and this could be achieved by the system generating a large but nonspecific response to all inputs. However, as the animal becomes actively engaged in exploring their

environment, placing its systems into a state that is more biased toward discrimination, the need for detecting stimuli is obviously not removed.

While it is useful from an experimental standpoint to treat these two types of tasks as distinct, it is perhaps more useful to the consider information processing states as encompassing a continuum, with detectability and discriminability lying on either extreme. The system is capable of moving along this continuum dynamically as task demands require, and it is unlikely to ever reach either extreme in which only type of task is possible. Indeed, in the behavioral discrimination task from Chapter 3, due to the uncertainty in stimulus timing, animals were still required to first detect the stimulus prior to indicating their decision on the stimulus type. As the results demonstrated, animals detected the stimulus with lower probability after sensory adaptation, but their detection performance was not eliminated entirely.

Further, it should be emphasized that there are likely many possible ways in which the system can be moved along the detection/discrimination continuum. For instance, there is a rich literature demonstrating that changes in attention or behavioral state lead to profound effects on sensory processing, including some high profile recent work (Niell and Stryker, 2010; Briggs et al., 2013; Polack et al., 2013). Such top-down processes could alone be responsible for putting the sensory system into a processing state that is more suited to the current task demands, such as detection or discrimination.

More directly related to the vibrissa system, Castro-Alamancos (2002) showed that stimulating the reticular formation (RF) of anesthetized rats resulted in a focusing of the cortical response to a whisker deflection, very much in line with the adaptation results presented by Sheth et al (1998). Castro-Alamancos makes the argument that RF stimulation results in neuromodulator release in the thalamus that places the thalamocortical circuit of the anesthetized animal into a state that more closely resembles the awake, active state. Thus, the extent of cortical activation resulting from a whisker deflection, and presumably the resulting spatial discriminability, can be modulated both by top-down attentional processes, which RF stimulation is meant to mimic, as well as by bottom up, sensory driven processes, such as the sensory adaptation studied here.

The role of sensory adaptation in shaping information processing

The adapting stimulus used in this study is a general periodic adapting stimulus that is designed solely to move the system between two operating modes: the detection mode or the discrimination mode. The important parameter of the adapting stimulus used here is likely that it falls within the natural range of whisking frequencies, and so puts the system into a related state to that which would be achieved if the animal were actively whisking. In addition, the adapting stimulus leads to important changes in the spatial processing of the pathway, leading the reduced cortical overlap that presumably allows the animals to perform better at the spatial discrimination task.

The term “adaptation” has a number of different meanings and interpretations and some care is necessary in discussing sensory adaptation to ensure that definitions are not

confused. For instance, "stimulus specific adaptation" refers to the system responding to specific parameters of the stimulus (Wark et al., 2007). This both allows the system to encode information more efficiently and causes novel stimuli to be easier to identify (novelty detection).

The idea of efficient coding was first stated by Barlow (1961). Briefly, efficient coding predicts that a system would be match its range of outputs (minimum to maximum firing rates, for instance) to the relevant range of sensory inputs. The work of Gardner et al. (2005) cited in the introduction of this dissertation is an example of this. That study demonstrated that the range of responses in the human primary visual cortex changed depending on the contrast of the visual adapting stimulus, with the contrast response function centering on the contrast of the adapting stimulus.

Separately, adaptation can lead to the system reducing responsiveness to a particular type of stimulus, thereby allowing stimuli with different characteristics to stand out. This is fundamentally what's occurring with the waterfall illusion, which was also cited in the introduction to this dissertation. The cells encoding motion in a certain direction are likely adapting out, leaving cells that encode the opposing direction to dominate, which becomes especially apparent after the moving stimulus is removed.

It should be emphasized that we are not asking the rats to perform a task that is directly related to the parameters of adaptation, though such a study would certainly be useful. An obvious example of such a task would be a direction discrimination task. Perhaps the

animals would be better at identifying the direction of deflection if they were previously adapted to a single direction. For instance, after a rostral-caudal adapting stimulus, perhaps a deflection that is only slightly off-horizontal is easier to identify than in the non-adapted state. This would apply that the rostral-caudal specific neurons have adapted out, helping to facilitate the response of the off-axis sensitive neurons.

Information processing modes and top down versus bottom up modulation

It is possible that many of the processing changes resulting from sensory adaptation are related to the processing changes resulting from behavioral and/or attentional modulation. One tantalizing link between these concepts shown here is the improved detectability in the non-adapted state, shown in Chapter 3, and in the non-whisking state, as demonstrated in Chapter 2. In both cases, a lack of whisker motion, whether self-imposed or passively applied, appeared to put the system into a state that was better for detecting weak inputs. However, there are some important differences between passively applied stimuli and stimuli resulting from an animal's own active exploration of the environment that must be acknowledged.

First, the biggest difference is likely the lack of the efferent copy during passively applied stimuli (Blakemore et al., 1998; Cullen, 2004). When an animal is whisking, the system has access to the motor commands that are driving that behavior (Curtis and Kleinfeld, 2009), so resulting activity in the pathway is certainly different when and animal whisks at 12 Hz versus when the whiskers are passively stimulated at 12 Hz.

Further, there are obviously some fundamental differences in the way the whiskers are moved during active whisking versus passively applied sinusoidal deflections. For instance, during whisking, all whiskers move basically together (Berg and Kleinfeld, 2003; Mitchinson et al., 2007), versus just one or two whiskers during our task. Further, the whiskers are being moved during whisking as a result of activity from muscles surrounding the follicles. This undoubtedly leads to different patterns of activation of the nerve endings in the follicle than does moving a whisker back-and-forth while the facial muscles are not actively engaged in the motion.

But if we accept whisking as an external indication of the internal state, then perhaps it is reasonable to link the resulting state to that which is achieved through sensory adaptation. In other words, it must first be assumed that there's a quiescent state in which the animals are primed for unexpected inputs versus an actively engaged state in which the animals are prepared to discriminate between stimuli (see the detection vs. discrimination discussion above, as well as Fanselow and Nicolelis (1999) and Ferezou et al. (2007)), and that whisker motion is but one manifestation of these two states. It is also necessary to accept that passively applied repetitive inputs to the system have the effect of pushing the system toward the discrimination state.

It is also likely that whisker motion may not be necessary for the animal to move between these two states and that top down control of attention would be sufficient to achieve the same end result. For instance, when animals begin running, the way that V1 processes visual information fundamentally changes (Neill and Stryker 2010; Polack 2013), and

changes in attention alone, without any overt behavioral indication, have been shown to lead to potentially important coding changes in the thalamocortical circuit (Wurtz et al., 1982; Briggs et al., 2013; Gilbert and Li, 2013). There is also extensive evidence from the whisker system that information is processed differently based on behavioral state (Ferezou 2007; Fanselow 1999; Poulet 2008 and 2012).

Thus, if passively applied stimuli have the effect of changing the information processing state of the system, and if these changes are similar to the changes resulting from whisking or other forms of active exploration, and if different behavioral states make either detection or discrimination easier, then it seems reasonable to link the results presented here from passively applied stimuli to those resulting from either active touch or top-down changes in processing.

Broader implications

The results presented here were obtained from simplified and somewhat artificial laboratory experiments. However, the broader goal is to better understand sensory processing in general, not just in the context of the tasks presented here in the rodent vibrissa system. From the moment we are born, every bit of information we obtain about the world around us is collected through our sensory systems. Most of what we know about how the brain collects and processes this information comes from highly artificial laboratory experiments. In particular, in behavioral experiments, very specific kinds of tasks are defined and tested, whether in animals or in humans, such as the relatively constrained detection and discrimination tasks used here. However, the real world

involves more complicated stimuli and overlapping task demands. The goal of the work presented here is to take a step toward uncovering the potential trade-offs between demands placed on the brain by different kinds of tasks.

The work presented here could lead to better understanding of diseases or disorders resulting from potential abnormalities of the thalamocortical system, one example of which is autism spectrum disorder. Autism has been connected to an increased ratio of excitation to inhibition in thalamocortical circuitry (Rubenstein and Merzenich, 2003; Dorrn et al., 2010), as well as a different ratio of the size of the thalamus to the rest of the brain (Hardan et al., 2006). Beyond the traditionally recognized symptoms of autism, these anatomical differences have also been connected with increased tactile sensitivity (Blakemore et al., 2006; Cascio et al., 2008). More directly related to the research presented here, it has been shown that sensory adaptation does not lead to improved spatial discriminability in autistic subjects (Tommerdahl 2007). This appeared to result from the fact that autistic subjects performed the discrimination task in the non-adapted state with equivalent acuity to normal subjects in the adapted state, thus leaving little room for improvement. The results presented in this dissertation could point to potential mechanistic explanations for these findings. For instance, the increased excitation/inhibition ratio in the cortex could leave the system less susceptible to changes in thalamic precision and firing rates that result from adaptation. It is also possible that, through corticothalamic feedback, the increased excitation in cortex leaves the thalamus in a perpetually adapted state, thus preventing further state changes with presentation of an adapting stimulus. Regardless of mechanism, if somewhat subjective and difficult to

diagnose diseases like autism manifest as differences in sensory processing, which can be directly tested using simply psychophysical tasks, this could lead to more objective means of diagnosing these diseases. But perhaps more importantly, diseases resulting from aberrant neural function cannot truly be understood without first having a better understanding of how the system performs in a non-diseased state, as was the goal of the work presented here.

Future work

The work presented in this dissertation provides a number of opportunities for continued investigation. In Chapter 2, it was shown that the animals performed better in a detection task on trials in which they limited their own self-motion, and whisking only occurred on a minority of trials. However, we were not able to determine whether this limited self-motion represented a strategy that the animals were adopting to improve their performance in the detection task. Future work could track whisking over larger time intervals to determine whether whisking tends to cease after a cue indicating that a stimulus is imminent. Further, if whisking has the effect of placing the animal into a state similar to that caused by the passively applied adapting stimulus used in Chapters 3 and 4, then it should follow that discrimination performance would be improved when animals are engaged in active whisking. Designing a task that allows this to be tested directly would be challenging, but would further help to connect the results in Chapter 2 with those that follow. Such experiments would also lead to a better understanding of the coupling of motor behavior with sensory inputs in general.

Similarly, though the tasks used in Chapters 3 and 4 were convenient from an experimental design setup and extremely powerful in allowing the questions of interest to be addressed, the fact remains that they were somewhat artificial. It would useful to know to what extent the findings would generalize to more natural stimuli. For instance, during contacts with surfaces, the whiskers undergo high velocity stick/slip events that can be used as a signature of a particular surface texture (Ritt et al., 2008; Jadhav and Feldman, 2010). Are stick/slip events differentially encoded with multiple passes of the whiskers as the system begins to adapt and does this allow the animal to better discriminate between textures? More generally, it would be useful to design tasks that allow the animals to adjust their operating properties based on the immediate task demands, as opposed to pushing the system between states using purely bottom-up, passively applied stimuli.

In addition, future studies should attempt to apply methods for measuring the cortical population response in the awake animal as it is engaged in a task. Voltage sensitive dye imaging in the awake animal, which is one possible method for obtaining this data, presents many challenges, but it would allow direct measurement of how changes in behavioral state (quiescent, active but with still whiskers, actively whisking, etc.) affects the spatial spread of cortical activity, and how these changes affect the animal's ability to discriminate stimuli on a trial-by-trial basis.

Though it should be emphasized that the multiunit recordings from Chapter 4 were extremely useful for measuring coding changes in response to sensory adaptation, denser thalamic recordings with better single unit isolation would allow for a more thorough

exploration of the relationship between changes in firing synchrony and behavioral performance. For instance, it would become possible to apply stimuli to single or multiple whiskers while simultaneously measuring activity both across barreloids to measure extent of spatial spread before and after adaptation, as well as within barreloids to measure simultaneous single unit activity in a barreloid and explore changes in relative timing, or synchrony, both with and without adaptation. The ability to more reliably isolate single thalamic units would also make it possible to measure thalamic bursts, which are thought to play a role in feature detection (Swadlow and Gusev, 2001; Lesica and Stanley, 2004; Marsat and Pollack, 2006).

However, even with improved behavioral tasks and recording techniques in either the thalamus or the cortex, we would still not have access to the underlying mechanism that drives the observed thalamic coding changes with adaptation. We would likely need simultaneous recordings from multiple brain areas, likely including the layer 6 corticothalamic feedback (Lam and Sherman, 2010; Olsen et al., 2012) as well as the thalamic reticular nucleus, to gain a more complete understanding of how these coding changes arise. In addition, to accurately measure causation as opposed to simple correlation, we would need to be able to directly control the activity in specific nodes of the circuit, likely through optogenetic means, to prove that both the neural and behavioral effects of adaptation could be manipulated in a predictable manner. Such experiments would require both large scale recordings and optogenetic techniques (Fenno et al., 2011) to control specific cell types, cortical layers, or thalamic nuclei during behavior. The

technology for doing so is just now becoming available, and future experiments will undoubtedly address these questions more thoroughly.

Bibliography

Adibi M, Arabzadeh E. A comparison of neuronal and behavioral detection and discrimination performances in rat whisker system. *Journal of neurophysiology* 105: 356–65, 2011.

Adibi M, Diamond ME, Arabzadeh E. Behavioral study of whisker-mediated vibration sensation in rats. *Proceedings of the National Academy of Sciences of the United States of America* 109: 971–6, 2012.

Adibi M, McDonald JS, Clifford CWG, Arabzadeh E. Adaptation improves neural coding efficiency despite increasing correlations in variability. *The Journal of neuroscience : the official journal of the Society for Neuroscience* 33: 2108–20, 2013.

Ahissar E, Sosnik R, Haidarliu S. Transformation from temporal to rate coding in a somatosensory thalamocortical pathway. *Nature* 406: 302–6, 2000.

Alonso JM, Usrey WM, Reid RC. Precisely correlated firing in cells of the lateral geniculate nucleus. *Nature* 383: 815–9, 1996.

Andermann ML, Ritt J, Neimark MA, Moore CI. Neural correlates of vibrissa resonance; band-pass and somatotopic representation of high-frequency stimuli. *Neuron* 42: 451–63, 2004.

Arabzadeh E, Zorzin E, Diamond ME. Neuronal encoding of texture in the whisker sensory pathway. *PLoS biology* 3: e17, 2005.

Barbaresi P, Spreafico C, Frassoni C, Rustioni A. GABAergic Neurons are Present in the Dorsal Column Nuclei but Not in the Ventroposterior Complex of Rats Retrograde transport of HRP. *Brain research* 382: 305–326, 1986.

Barlow H. Possible principles underlying the transformation of sensory messages. In: *Sensory communication*. 1961, p. 271–274.

Beierlein M, Fall CP, Rinzel J, Yuste R. Thalamocortical bursts trigger recurrent activity in neocortical networks: layer 4 as a frequency-dependent gate. *The Journal of neuroscience : the official journal of the Society for Neuroscience* 22: 9885–94, 2002.

Benucci A, Saleem AB, Carandini M. Adaptation maintains population homeostasis in primary visual cortex. *Nature neuroscience* 16: 724–729, 2013.

Berg RW, Kleinfeld D. Rhythmic whisking by rat: retraction as well as protraction of the vibrissae is under active muscular control. *Journal of neurophysiology* 89: 104–17, 2003.

Berger T, Borgdorff A, Crochet S, Neubauer FB, Lefort S, Fauvet B, Ferezou I, Carleton A, Lüscher H-R, Petersen CCH. Combined voltage and calcium epifluorescence imaging in vitro and in vivo reveals subthreshold and suprathreshold dynamics of mouse barrel cortex. *Journal of neurophysiology* 97: 3751–62, 2007.

Bermejo R, Vyas A, Zeigler HP. Topography of rodent whisking--I. Two-dimensional monitoring of whisker movements. *Somatosensory & motor research* 19: 341–6, 2002.

Birdwell JA, Solomon JH, Thajchayapong M, Taylor MA, Cheely M, Towal RB, Conradt J, Hartmann MJZ, Ja B, Jh S, Thajchayapong M, Ma T, Cheely M, Rb T, Conradt J, Biomechani- HMJZ. Biomechanical Models for Radial Distance Determination by the Rat Vibrissal System. (2007). doi: 10.1152/jn.00707.2006.

Blakemore S, Tavassoli T, Calò S, Thomas RM, Catmur C, Frith U, Haggard P. Tactile sensitivity in Asperger syndrome. 61: 5–13, 2006.

Blakemore SJ, Wolpert DM, Frith CD. Central cancellation of self-produced tickle sensation. *Nature neuroscience* 1: 635–40, 1998.

Boloori A, Jenks R, Desbordes G, Stanley G. Encoding and decoding cortical representations of tactile features in the vibrissa system. *The journal of neuroscience* 30: 9990 –10005, 2010.

Bourassa J, Deschênes M. Corticothalamic projections from the primary visual cortex in rats: a single fiber study using biocytin as an anterograde tracer. *Neuroscience* 66: 253–263, 1995.

Brecht M, Preilowski B, Merzenich MM. Functional architecture of the mystacial vibrissae. *Behavioural brain research* 84: 81–97, 1997.

Briggs F, Mangun GR, Usrey WM. Attention enhances synaptic efficacy and the signal-to-noise ratio in neural circuits. *Nature* 499: 1–8, 2013.

Britten K, Shadlen M. The analysis of visual motion: a comparison of neuronal and psychophysical performance. *The journal of neuroscience* 12: 4745–4765, 1992.

Brumberg JC, Pinto DJ, Simons DJ. Spatial gradients and inhibitory summation in the rat whisker barrel system. *Journal of neurophysiology* 76: 130–40, 1996.

Bruno RM, Khatri V, Land PW, Simons DJ. Thalamocortical angular tuning domains within individual barrels of rat somatosensory cortex. *The Journal of neuroscience : the official journal of the Society for Neuroscience* 23: 9565–74, 2003.

Bruno RM, Sakmann B. Cortex is driven by weak but synchronously active thalamocortical synapses. *Science* 312: 1622–7, 2006.

Bruno RM. Synchrony in sensation. *Current opinion in neurobiology* 21: 701–8, 2011.

Bryant JJL, Roy S, Heck DDH. A technique for stereotaxic recordings of neuronal activity in awake, head-restrained mice. *Journal of neuroscience methods* 178: 75–9, 2009.

Buschman TJ, Miller EK. Top-down versus bottom-up control of attention in the prefrontal and posterior parietal cortices. *Science (New York, N.Y.)* 315: 1860–2, 2007.

Busse L, Ayaz A, Dhruv NT, Katzner S, Saleem AB, Schölvinck ML, Zaharia AD, Carandini M. The detection of visual contrast in the behaving mouse. *The Journal of neuroscience : the official journal of the Society for Neuroscience* 31: 11351–61, 2011.

Butovas S, Schwarz C. Detection psychophysics of intracortical microstimulation in rat primary somatosensory cortex. *The European journal of neuroscience* 25: 2161–9, 2007.

Carandini M, Churchland AK. Probing perceptual decisions in rodents. *Nature Neuroscience* 16: 824–831, 2013.

Carpenter RHS. Contrast, probability, and saccadic latency; evidence for independence of detection and decision. *Current biology : CB* 14: 1576–80, 2004.

Carvell GE, Simons DJ. Biometric Analyses of Vibrissal Tactile Discrimination in the Rat. *The Journal of Neuroscience* 10: 2638–2648, 1990.

Carvell GE, Simons DJ. Task- and subject-related differences in sensorimotor behavior during active touch. *Somatosensory & motor research* 12: 1–9, 1995.

Cascio C, Mcglone ÆF, Folger ÆS, Tannan V, Baranek ÆG, Pelphrey ÆKA. Tactile Perception in Adults with Autism : a Multidimensional Psychophysical Study. (2008). doi: 10.1007/s10803-007-0370-8.

Castro-Alamancos MA. Role of thalamocortical sensory suppression during arousal: focusing sensory inputs in neocortex. *The Journal of neuroscience : the official journal of the Society for Neuroscience* 22: 9651–5, 2002.

Castro-Alamancos MA. Absence of rapid sensory adaptation in neocortex during information processing states. *Neuron* 41: 455–64, 2004.

Chen Y, Geisler WS, Seidemann E. Optimal decoding of correlated neural population responses in the primate visual cortex. *Nature neuroscience* 9: 1412–20, 2006.

Chen Y, Geisler WS, Seidemann E. Optimal Temporal Decoding of Neural Population Responses in a Reaction-Time Visual Detection Task. *Journal of neurophysiology* 99: 1366–1379, 2008.

Cherry E. Some experiments on the recognition of speech, with one and with two ears. *The Journal of the acoustical society of America* 25: 975, 1953.

Chung S, Li X, Nelson SB. Short-term depression at thalamocortical synapses contributes to rapid adaptation of cortical sensory responses in vivo. *Neuron* 34: 437–46, 2002.

Clifford CWG, Webster MA, Stanley GB, Stocker AA, Kohn A, Sharpee TO, Schwartz O. Visual adaptation: neural, psychological and computational aspects. *Vision research* 47: 3125–31, 2007.

Constantinople CM, Bruno RM. Effects and mechanisms of wakefulness on local cortical networks. *Neuron* 69: 1061–8, 2011.

Cook EP, Maunsell JHR. Dynamics of neuronal responses in macaque MT and VIP during motion detection. *Nature neuroscience* 5: 985–94, 2002.

Crane T. The waterfall illusion. *Analysis* 48.3: 142–147, 1988.

Crick F, Koch C. Towards a neurobiological theory of consciousness. *Seminars in the Neurosciences* 2: 275, 1990.

Crick F, Koch C. A framework for consciousness. *Nature neuroscience* 6: 119–26, 2003.

Crick F. Function of the thalamic reticular complex: The searchlight hypothesis. *Proceedings of the National Academy of Sciences of the United States of America* 81: 4586–4590, 1984.

Crochet S, Petersen CCH. Correlating whisker behavior with membrane potential in barrel cortex of awake mice. *Nature neuroscience* 9: 608–10, 2006.

Cullen KE. Sensory signals during active versus passive movement. *Current opinion in neurobiology* 14: 698–706, 2004.

Curtis JC, Kleinfeld D. Phase-to-rate transformations encode touch in cortical neurons of a scanning sensorimotor system. *Nature neuroscience* 12: 492–501, 2009.

Davis DJ, Sachdev R, Pieribone VA. Effect of high velocity, large amplitude stimuli on the spread of depolarization in S1 “barrel” cortex. *Somatosensory & motor research* 28: 73–85, 2011.

Davis H. Underestimating the rat’s intelligence. *Brain research. Cognitive brain research* 3: 291–8, 1996.

Desimone R, Duncan J. Neural mechanisms of selective visual attention. *Annual review of neuroscience* 18: 193–222, 1995.

Diamond ME, Arabzadeh E. Whisker sensory system - From receptor to decision. *Progress in neurobiology* (July 6, 2012). doi: 10.1016/j.pneurobio.2012.05.013.

Diamond ME, von Heimendahl M, Arabzadeh E. Whisker-mediated texture discrimination. *PLoS biology* 6: e220, 2008a.

Diamond ME, von Heimendahl M, Knutsen PM, Kleinfeld D, Ahissar E. "Where" and "what" in the whisker sensorimotor system. *Nature Reviews Neuroscience* 9: 601–12, 2008b.

Dorrn AL, Yuan K, Barker AJ, Schreiner CE, Froemke RC. Developmental sensory experience balances cortical excitation and inhibition. *Nature* 465: 932–6, 2010.

Duda R, Hart P, Stork D. *Pattern Classification and Scene Analysis 2nd ed.* New York: Wiley, 1995.

Ebara S, Kumamoto K, Matsuura T, Mazurkiewicz JE, Rice FL. Similarities and differences in the innervation of mystacial vibrissal follicle-sinus complexes in the rat and cat: a confocal microscopic study. *The Journal of comparative neurology* 449: 103–19, 2002.

Ego-Stengel V, Mello E Souza T, Jacob V, Shulz DE. Spatiotemporal characteristics of neuronal sensory integration in the barrel cortex of the rat. *Journal of neurophysiology* 93: 1450–67, 2005.

Fairhall AL, Lewen GD, Bialek W, de Ruyter Van Steveninck RR. Efficiency and ambiguity in an adaptive neural code. *Nature* 412: 787–92, 2001.

Fanselow EE, Nicolelis MA. Behavioral modulation of tactile responses in the rat somatosensory system. *The Journal of neuroscience : the official journal of the Society for Neuroscience* 19: 7603–16, 1999.

Fanselow EE, Sameshima K, Baccala LA, Nicolelis MA. Thalamic bursting in rats during different awake behavioral states. *Proceedings of the National Academy of Sciences of the United States of America* 98: 15330–5, 2001.

Fenno L, Yizhar O, Deisseroth K. The development and application of optogenetics. *Annual review of neuroscience* 34: 389–412, 2011.

Ferezou I, Bolea S, Petersen CCH. Visualizing the cortical representation of whisker touch: voltage-sensitive dye imaging in freely moving mice. *Neuron* 50: 617–29, 2006.

Ferezou I, Haiss F, Gentet LJ, Aronoff R, Weber B, Petersen CCH. Spatiotemporal dynamics of cortical sensorimotor integration in behaving mice. *Neuron* 56: 907–23, 2007.

Fox K. *Barrel cortex*. Cambridge University Press, 2008.

Fraser G, Hartings JA, Simons DJ. Adaptation of trigeminal ganglion cells to periodic whisker deflections. *Somatosensory & motor research* 23: 111–8, 2006.

Fridman G, Blair H, Blaisdell A, Judy J. Perceived intensity of somatosensory cortical electrical stimulation. *Experimental brain research* 203: 499–515, 2010.

Friedberg MH, Lee SM, Ebner FF. Modulation of receptive field properties of thalamic somatosensory neurons by the depth of anesthesia. *Journal of neurophysiology* 81: 2243–52, 1999.

Frith C. Concluding review A framework for studying the neural basis of attention. *Neuropsychologia* 39: 1367–1371, 2001.

Fründ I, Haenel N, Wichmann F. Inference for psychometric functions in the presence of nonstationary behavior. *Journal of vision* 11: 1–19, 2011.

Gabernet L, Jadhav SPS, Feldman DE DE, Carandini M, Scanziani M. Somatosensory integration controlled by dynamic thalamocortical feed-forward inhibition. *Neuron* 48: 315–27, 2005.

Ganmor E, Katz Y, Lampl I. Intensity-dependent adaptation of cortical and thalamic neurons is controlled by brainstem circuits of the sensory pathway. *Neuron* 66: 273–86, 2010.

Garabedian CE, Jones SR, Merzenich MM, Dale A, Moore CI. Band-pass response properties of rat SI neurons. *Journal of neurophysiology* 90: 1379–91, 2003.

Gardner JL, Sun P, Waggoner RA, Ueno K, Tanaka K, Cheng K. Contrast adaptation and representation in human early visual cortex. *Neuron* 47: 607–20, 2005.

Gerdjikov T V, Bergner CG, Stüttgen MC, Waiblinger C, Schwarz C. Discrimination of vibrotactile stimuli in the rat whisker system: behavior and neurometrics. *Neuron* 65: 530–40, 2010.

Gil Z, Connors BW, Amitai Y. Efficacy of thalamocortical and intracortical synaptic connections: quanta, innervation, and reliability. *Neuron* 23: 385–97, 1999.

Gilbert CD, Li W. Top-down influences on visual processing. *Nature Reviews Neuroscience* 14: 350–363, 2013.

Gilbert CD, Sigman M. Brain states: top-down influences in sensory processing. *Neuron* 54: 677–96, 2007.

Gilja V, Chestek C a, Diester I, Henderson JM, Deisseroth K, Shenoy K V. Challenges and opportunities for next-generation intracortically based neural prostheses. *IEEE transactions on bio-medical engineering* 58: 1891–9, 2011.

Goble A, Hollins M. Vibrotactile adaptation enhances amplitude discrimination. *The Journal of the Acoustical Society of America* 93: 418–24, 1993.

Goble AK, Hollins M. Vibrotactile adaptation enhances frequency discrimination. *The Journal of the Acoustical Society of America* 96: 771–80, 1994.

Gold JI, Shadlen MN. Neural computations that underlie decisions about sensory stimuli. *Trends in cognitive sciences* 5: 10–16, 2001.

Gold JI, Shadlen MN. The neural basis of decision making. *Annual review of neuroscience* 30: 535–74, 2007.

Green DM, Swets JA. Signal detection theory and psychophysics. 1966.

Greenberg DS, Houweling AR, Kerr JND. Population imaging of ongoing neuronal activity in the visual cortex of awake rats. *Nature neuroscience* 11: 749–51, 2008.

Greenlee MW, Georgeson MA, Magnussen S, Harris JP. The time course of adaptation to spatial contrast. *Vision research* 31: 223–36, 1991.

Grinvald A, Hildesheim R. VSDI: a new era in functional imaging of cortical dynamics. *Nature reviews. Neuroscience* 5: 874–85, 2004.

Güell A, Braak L, Gharib C. Cardiovascular deconditioning during weightlessness simulation and the use of lower body negative pressure as a countermeasure to orthostatic intolerance. *The Physiologist* 33: S31–3, 1990.

Guić-Robles E, Valdivieso C, Guajardo G. Rats can learn a roughness discrimination using only their vibrissal system. *Behavioural brain research* 31: 285–9, 1989.

Guido W, Weyand T. Burst responses in thalamic relay cells of the awake behaving cat. *Journal of neurophysiology* 74: 1782–6, 1995.

Guillery RW, Feig SL, Lozsádi DA. Paying attention to the thalamic reticular nucleus. *Trends in neurosciences* 2236: 28–32, 1998.

Gustafson JW, Felbain-Keramidas SL. Behavioral and neural approaches to the function of the mystacial vibrissae. *Psychological bulletin* 84: 477–88, 1977.

Haidarliu S, Ahissar E. Size Gradients of Barreloids. *Journal of comparative neurology* 387: 372–387, 2001.

Haiss F, Butovas S, Schwarz C. A miniaturized chronic microelectrode drive for awake behaving head restrained mice and rats. *Journal of neuroscience methods* 187: 67–72, 2010.

Hardan AY, Girgis RR, Adams J, Gilbert AR, Keshavan MS, Minshew NJ. Abnormal brain size effect on the thalamus in autism. *Psychiatry research* 147: 145–51, 2006.

Harris RM. Morphology of Physiologically Identified Thalamocortical Relay Neurons in the Rat Ventrobasal Thalamus. *The Journal of comparative neurology* 251: 491–505, 1986.

Hartmann MJ, Johnson NJ, Towal RB, Assad C. Mechanical characteristics of rat vibrissae: resonant frequencies and damping in isolated whiskers and in the awake behaving animal. *The Journal of neuroscience : the official journal of the Society for Neuroscience* 23: 6510–9, 2003.

Harvey MA, Bermejo R, Zeigler HP. Discriminative whisking in the head-fixed rat: optoelectronic monitoring during tactile detection and discrimination tasks. *Somatosensory & motor research* 18: 211–22, 2001.

Hayar A, Bryant JL, Boughter JD, Heck DH. A low-cost solution to measure mouse licking in an electrophysiological setup with a standard analog-to-digital converter. *Journal of neuroscience methods* 153: 203–7, 2006.

Haykin S, Chen Z. The cocktail party problem. *Neural computation* 17: 1875–902, 2005.

Heimendahl M von, Itskov PMP, von Heimendahl M, Arabzadeh E, Diamond ME. Neuronal activity in rat barrel cortex underlying texture discrimination. *PLoS biology* 5: e305, 2007.

Heiss JE, Katz Y, Ganmor E, Lampl I. Shift in the balance between excitation and inhibition during sensory adaptation of S1 neurons. *The Journal of neuroscience : the official journal of the Society for Neuroscience* 28: 13320–30, 2008.

Hentschke H, Haiss F, Schwarz C. Central signals rapidly switch tactile processing in rat barrel cortex during whisker movements. *Cerebral cortex (New York, N.Y. : 1991)* 16: 1142–56, 2006.

Higley MJ, Contreras D. Balanced excitation and inhibition determine spike timing during frequency adaptation. *The Journal of neuroscience : the official journal of the Society for Neuroscience* 26: 448–57, 2006.

Histed MH, Carvalho L a, Maunsell JHR. Psychophysical measurement of contrast sensitivity in the behaving mouse. *Journal of neurophysiology* 107: 758–65, 2012.

Houweling AR, Brecht M. Behavioural report of single neuron stimulation in somatosensory cortex. *Nature* 451: 65–8, 2008.

Huber D, Petreanu L, Ghitani N, Ranade S, Hromádka T, Mainen Z, Svoboda K. Sparse optical microstimulation in barrel cortex drives learned behaviour in freely moving mice. *Nature* 451: 61–4, 2008.

Huk AC, Shadlen MN. Neural activity in macaque parietal cortex reflects temporal integration of visual motion signals during perceptual decision making. *The Journal of neuroscience : the official journal of the Society for Neuroscience* 25: 10420–36, 2005.

Hutson KA, Masterton RB. The sensory contribution of a single vibrissa's cortical barrel. *Journal of neurophysiology* 56: 1196–223, 1986.

Izhikevich E. Simple model of spiking neurons. *IEEE transactions on neural networks / a publication of the IEEE Neural Networks Council* 14: 1569–72, 2003.

Izhikevich E. *Dynamical systems in neuroscience*. The MIT Press, 2007.

Jacobs AL, Fridman G, Douglas RM, Alam NM, Latham PE, Prusky GT, Nirenberg S. Ruling out and ruling in neural codes. *Proceedings of the National Academy of Sciences of the United States of America* 106: 5936–41, 2009.

Jadhav SP, Feldman DE. Texture coding in the whisker system. *Current opinion in neurobiology* 20: 313–8, 2010.

Jadhav SP, Wolfe J, Feldman DE. Sparse temporal coding of elementary tactile features during active whisker sensation. *Nature neuroscience* 12: 792–800, 2009.

Jenks RA, Vaziri A, Boloori A-R, Stanley GB. Self-motion and the shaping of sensory signals. *Journal of neurophysiology* 103: 2195–207, 2010.

Jin W, Zhang R, Wu J. Voltage-sensitive dye imaging of population neuronal activity in cortical tissue. *Journal of neuroscience methods* 115: 13–27, 2002.

Johnson KO. Sensory discrimination: decision process. *Journal of neurophysiology* 43: 1771–1792, 1980.

Kandel E, Schwartz J, Jessell T. *Principles of neural science*. 4th Editio. McGraw-Hill, 2000.

Kastner S, Ungerleider LG. Mechanisms of visual attention in the human cortex. *Annual review of neuroscience* 23: 315–41, 2000.

Katz Y, Heiss JE, Lampl I. Cross-whisker adaptation of neurons in the rat barrel cortex. *The Journal of neuroscience : the official journal of the Society for Neuroscience* 26: 13363–72, 2006.

Khatri V, Bermejo R, Brumberg JC, Keller A, Zeigler HP. Whisking in Air : Encoding of Kinematics by Trigeminal Ganglion Neurons in Awake Rats. *Journal of neurophysiology* 101: 1836–1846, 2009a.

Khatri V, Bruno RM, Simons DJ. Stimulus-specific and stimulus-nonspecific firing synchrony and its modulation by sensory adaptation in the whisker-to-barrel pathway. *Journal of neurophysiology* 101: 2328–38, 2009b.

Khatri V, Hartings JA, Simons DJ. Adaptation in thalamic barreloid and cortical barrel neurons to periodic whisker deflections varying in frequency and velocity. *Journal of neurophysiology* 92: 3244–54, 2004.

Kleinfeld D, Ahissar E, Diamond MEM. Active sensation : insights from the rodent vibrissa sensorimotor system. *Current opinion in neurobiology* 16: 435–444, 2006.

Kleinfeld D, Delaney KR. Distributed representation of vibrissa movement in the upper layers of somatosensory cortex revealed with voltage-sensitive dyes. *The Journal of comparative neurology* 375: 89–108, 1996.

Knutsen PM, Derdikman D, Ahissar E. Tracking whisker and head movements in unrestrained behaving rodents. *Journal of neurophysiology* 93: 2294–301, 2005.

Kohn A, Whitsel BL. Sensory cortical dynamics. *Behavioural brain research* 135: 119–26, 2002.

Kok P, Jehee JFM, de Lange FP. Less is more: expectation sharpens representations in the primary visual cortex. *Neuron* 75: 265–70, 2012.

Krupa DJ, Matell MS, Brisben AJ, Oliveira LM, Nicolelis MA. Behavioral properties of the trigeminal somatosensory system in rats performing whisker-dependent tactile discriminations. *The Journal of neuroscience : the official journal of the Society for Neuroscience* 21: 5752–63, 2001.

Krupa DJ, Wiest MC, Shuler MG, Laubach M, Nicolelis MAL. Layer-specific somatosensory cortical activation during active tactile discrimination. *Science (New York, N.Y.)* 304: 1989–92, 2004.

Kyriazi T, Simons J, Kyriazi H, Simons D. Thalamocortical Response Transformations in Simulated Whisker Barrels. *The Journal of neuroscience* 13, 1993.

Lam Y-W, Sherman SM. Functional organization of the somatosensory cortical layer 6 feedback to the thalamus. *Cerebral cortex (New York, N.Y. : 1991)* 20: 13–24, 2010.

Laughlin SB. The role of sensory adaptation in the retina. *The Journal of experimental biology* 146: 39–62, 1989.

Lavallée P, Deschênes M. Dendroarchitecture and lateral inhibition in thalamic barreloids. *The Journal of neuroscience : the official journal of the Society for Neuroscience* 24: 6098–105, 2004.

Lee CJ, Whitsel BL, Tommerdahl M. Mechanisms underlying somatosensory cortical dynamics: II. In vitro studies. *Cerebral cortex (New York, N.Y. : 1991)* 2: 107–33, 1992.

Lee CJ, Whitsel BL. Mechanisms underlying somatosensory cortical dynamics: I. In vivo studies. *Cerebral cortex (New York, N.Y. : 1991)* 2: 81–106, 1992.

Lee S-H, Kwan AC, Zhang S, Phoumthipphavong V, Flannery JG, Masmanidis SC, Taniguchi H, Huang ZJ, Zhang F, Boyden ES, Deisseroth K, Dan Y. Activation of specific interneurons improves V1 feature selectivity and visual perception. *Nature* 488: 379–83, 2012.

Lee S-H, Simons DJ. Angular tuning and velocity sensitivity in different neuron classes within layer 4 of rat barrel cortex. *Journal of neurophysiology* 91: 223–9, 2004.

Leiser SC, Moxon KA. Responses of trigeminal ganglion neurons during natural whisking behaviors in the awake rat. *Neuron* 53: 117–33, 2007.

Lesica NA, Jin J, Weng C, Yeh C-I, Butts DA, Stanley GB, Alonso J-M. Adaptation to stimulus contrast and correlations during natural visual stimulation. *Neuron* 55: 479–91, 2007.

Lesica NA, Stanley GB. Encoding of natural scene movies by tonic and burst spikes in the lateral geniculate nucleus. *The Journal of neuroscience : the official journal of the Society for Neuroscience* 24: 10731–40, 2004.

Lesica NA, Weng C, Jin J, Yeh C-I, Alonso J-M, Stanley GB. Dynamic encoding of natural luminance sequences by LGN bursts. *PLoS biology* 4: e209, 2006.

Lippert MT, Takagaki K, Xu W, Huang X, Wu J-Y. Methods for voltage-sensitive dye imaging of rat cortical activity with high signal-to-noise ratio. *Journal of neurophysiology* 98: 502–12, 2007.

Luna R, Hernández A, Brody CD, Romo R. Neural codes for perceptual discrimination in primary somatosensory cortex. *Nature neuroscience* 8: 1210–9, 2005.

Macmillan N, Creelman C. *Detection theory: A user's guide*. Psychology Press, 2004.

Maddess T, McCourt ME, Blakeslee B, Cunningham RB. Factors governing the adaptation of cells in area-17 of the cat visual cortex. *Biological cybernetics* 59: 229–36, 1988.

Maravall M, Petersen RS, Fairhall AL, Arabzadeh E, Diamond ME. Shifts in coding properties and maintenance of information transmission during adaptation in barrel cortex. *PLoS biology* 5: e19, 2007.

Marsat G, Pollack GS. A behavioral role for feature detection by sensory bursts. *The Journal of neuroscience : the official journal of the Society for Neuroscience* 26: 10542–7, 2006.

Masland R. Neuronal diversity in the retina. *Current opinion in neurobiology* 11: 431–436, 2001.

Mayrhofer JM, Skreb V, von der Behrens W, Musall S, Weber B, Haiss F. Novel two-alternative forced choice paradigm for bilateral vibrotactile whisker frequency discrimination in head-fixed mice and rats. *Journal of neurophysiology* 109: 273–84, 2013.

Mazurek ME, Roitman JD, Ditterich J, Shadlen MN. A role for neural integrators in perceptual decision making. *Cerebral cortex (New York, N.Y. : 1991)* 13: 1257–69, 2003.

McAlonan K, Cavanaugh J, Wurtz RH. Guarding the gateway to cortex with attention in visual thalamus. *Nature* 456: 391–4, 2008.

McManus JNJ, Li W, Gilbert CD. Adaptive shape processing in primary visual cortex. *Proceedings of the National Academy of Sciences of the United States of America* 108: 9739–46, 2011.

Mehta SB, Whitmer D, Figueroa R, Williams B a, Kleinfeld D. Active spatial perception in the vibrissa scanning sensorimotor system. *PLoS biology* 5: e15, 2007.

Meier P, Reinagel P. Rat performance on visual detection task modeled with divisive normalization and adaptive decision thresholds. 11: 1–17, 2011.

Milani H, Steiner H, Huston JP. Analysis of recovery from behavioral asymmetries induced by unilateral removal of vibrissae in the rat. *Behavioral neuroscience* 103: 1067–74, 1989.

Minnery BS, Bruno RM, Simons DJ. Response transformation and receptive-field synthesis in the lemniscal trigeminothalamic circuit. *Journal of neurophysiology* 90: 1556–70, 2003.

Mirabella G, Battiston S, Diamond ME. Integration of multiple-whisker inputs in rat somatosensory cortex. *Cerebral cortex (New York, N.Y. : 1991)* 11: 164–70, 2001.

Mitchinson B, Martin CJ, Grant R a, Prescott TJ. Feedback control in active sensing: rat exploratory whisking is modulated by environmental contact. *Proceedings. Biological sciences / The Royal Society* 274: 1035–41, 2007.

Moore CI, Nelson SB, Sur M. Dynamics of neuronal processing in rat somatosensory cortex. *Trends in neurosciences* 22: 513–20, 1999.

Moore CI. Frequency-dependent processing in the vibrissa sensory system. *Journal of neurophysiology* 91: 2390–9, 2004.

Morita T, Kang H, Wolfe J, Jadhav SP, Feldman DE. Psychometric curve and behavioral strategies for whisker-based texture discrimination in rats. *PloS one* 6: e20437, 2011.

Motter BC. Focal attention produces spatially selective processing in visual cortical areas V1, V2, and V4 in the presence of competing stimuli. *Journal of neurophysiology* 70: 909–19, 1993.

Neimark MA, Andermann ML, Hopfield JJ, Moore CI. Vibrissa resonance as a transduction mechanism for tactile encoding. *The Journal of neuroscience : the official journal of the Society for Neuroscience* 23: 6499–509, 2003.

Niell CM, Stryker MP. Modulation of visual responses by behavioral state in mouse visual cortex. *Neuron* 65: 472–9, 2010.

O'Connor DH, Clack NG, Huber D, Komiyama T, Myers EW, Svoboda K. Vibrissa-based object localization in head-fixed mice. *The Journal of neuroscience : the official journal of the Society for Neuroscience* 30: 1947–67, 2010a.

O'Connor DH, Hires SA, Guo Z V, Li N, Yu J, Sun Q-Q, Huber D, Svoboda K. Neural coding during active somatosensation revealed using illusory touch. *Nature Neuroscience* : 1–11, 2013.

O'Connor DH, Peron SP, Huber D, Svoboda K. Neural activity in barrel cortex underlying vibrissa-based object localization in mice. *Neuron* 67: 1048–61, 2010b.

Ohara PT, Havton LA. Dendritic Architecture of Rat Somatosensory Thalamocortical Projection Neurons. *The Journal of comparative neurology* 341: 159–171, 1994.

Ollerenshaw DR, Bari BA, Millard DC, Orr LE, Wang Q, Stanley GB. Detection of tactile inputs in the rat vibrissa pathway. *Journal of neurophysiology* 108: 479–90, 2012.

Olsen SR, Bortone DS, Adesnik H, Scanziani M. Gain control by layer six in cortical circuits of vision. *Nature* 483: 47–52, 2012.

Pais-Vieira M, Lebedev MA, Wiest MC, Nicolelis MAL. Simultaneous top-down modulation of the primary somatosensory cortex and thalamic nuclei during active tactile discrimination. *The Journal of neuroscience : the official journal of the Society for Neuroscience* 33: 4076–93, 2013.

Paxinos G, Watson C. *The rat brain in stereotaxic coordinates*. San Diego, CA: Academic, 2007.

Petersen CCH, Grinvald A, Sakmann B. Spatiotemporal dynamics of sensory responses in layer 2/3 of rat barrel cortex measured in vivo by voltage-sensitive dye imaging combined with whole-cell voltage recordings and neuron reconstructions. *The Journal of neuroscience : the official journal of the Society for Neuroscience* 23: 1298–309, 2003a.

Petersen CCH, Hahn TTG, Mehta M, Grinvald A, Sakmann B. Interaction of sensory responses with spontaneous depolarization in layer 2/3 barrel cortex. *Proceedings of the National Academy of Sciences of the United States of America* 100: 13638–43, 2003b.

Petersen CCH. The functional organization of the barrel cortex. *Neuron* 56: 339–55, 2007.

Pierret T, Lavalle P, Deschenes M. Parallel Streams for the Relay of Vibrissal Information through Thalamic Barreloids. *The Journal of neuroscience* 20: 7455–7462, 2000.

Pinto DJ, Brumberg JC, Simons DJ. Circuit dynamics and coding strategies in rodent somatosensory cortex. *Journal of neurophysiology* 83: 1158–66, 2000.

Polack P-O, Friedman J, Golshani P. Cellular mechanisms of brain state–dependent gain modulation in visual cortex. *Nature Neuroscience* : 1–11, 2013.

Polikov VS, Tresco PA, Reichert WM. Response of brain tissue to chronically implanted neural electrodes. *Journal of neuroscience methods* 148: 1–18, 2005.

Posner MI, Petersen SE. The attention system of the human brain. *Annual review of neuroscience* 13: 25–42, 1990.

Poulet JFA, Fernandez LMJ, Crochet S, Petersen CCH. Thalamic control of cortical states. *Nature neuroscience* 15: 370–2, 2012.

Poulet JFA, Petersen CCH. Internal brain state regulates membrane potential synchrony in barrel cortex of behaving mice. *Nature* 454: 881–5, 2008.

Quiroga RQ, Reddy L, Kreiman G, Koch C, Fried I. Invariant visual representation by single neurons in the human brain. *Nature* 435: 1102–7, 2005.

Raposo D, Sheppard JP, Schrater PR, Churchland AK. Multisensory decision-making in rats and humans. *The Journal of neuroscience : the official journal of the Society for Neuroscience* 32: 3726–35, 2012.

Ritt JT, Andermann ML, Moore CI. Embodied information processing: vibrissa mechanics and texture features shape micromotions in actively sensing rats. *Neuron* 57: 599–613, 2008.

Roitman JD, Shadlen MN. Response of neurons in the lateral intraparietal area during a combined visual discrimination reaction time task. *The Journal of neuroscience : the official journal of the Society for Neuroscience* 22: 9475–89, 2002.

Romo R, Hernández A, Zainos A, Brody CD, Lemus L. Sensing without touching: psychophysical performance based on cortical microstimulation. *Neuron* 26: 273–8, 2000.

Romo R, Hernández A, Zainos A, Salinas E. Somatosensory discrimination based on cortical microstimulation. *Nature* 392: 387–90, 1998.

Romo R, Salinas E. Touch and go: decision-making mechanisms in somatosensation. *Annual review of neuroscience* 24: 107–37, 2001.

Roy SA, Alloway KD. Coincidence detection or temporal integration? What the neurons in somatosensory cortex are doing. *The Journal of neuroscience : the official journal of the Society for Neuroscience* 21: 2462–73, 2001.

Rubenstein JLR, Merzenich MM. Model of autism : increased ratio of excitation / inhibition in key neural systems. (2003). doi: 10.1046/j.1601-183X.2003.00037.x.

Sagi D, Julesz B. Detection versus discrimination of visual orientation. *Perception* 13: 619–28, 1984.

Sarter M, Givens B, Bruno JP. The cognitive neuroscience of sustained attention: where top-down meets bottom-up. *Brain research. Brain research reviews* 35: 146–60, 2001.

Schall JD, Thompson KG. Neural selection and control of visually guided eye movements. *Annual review of neuroscience* 22: 241–59, 1999.

Schwarz C, Hentschke H, Butovas S, Haiss F, Stüttgen MC, Gerdjikov T V, Bergner CG, Waiblinger C. The head-fixed behaving rat--procedures and pitfalls. *Somatosensory & motor research* 27: 131–48, 2010.

Shadlen MN, Newsome WT. Neural basis of a perceptual decision in the parietal cortex (area LIP) of the rhesus monkey. *Journal of neurophysiology* 86: 1916–36, 2001.

Sherman SM, Guillery RW. Functional organization of thalamocortical relays. *Journal of neurophysiology* 76: 1367–95, 1996.

Sherman SM, Guillery RW. The role of the thalamus in the flow of information to the cortex. *Philosophical transactions of the Royal Society of London. Series B, Biological sciences* 357: 1695–708, 2002.

Sherman SM. Tonic and burst firing: dual modes of thalamocortical relay. *Trends in neurosciences* 24: 122–6, 2001a.

Sherman SM. A wake-up call from the thalamus. *Nature neuroscience* 4: 344–6, 2001b.

Sherman SM. The thalamus is more than just a relay. *Current opinion in neurobiology* 17: 417–22, 2007.

Sheth BR, Moore CI, Sur M. Temporal modulation of spatial borders in rat barrel cortex. *Journal of neurophysiology* 79: 464–70, 1998.

Shipp S. The brain circuitry of attention. *Trends in cognitive sciences* 8: 223–30, 2004.

Shuler MG, Krupa DJ, Nicolelis MAL. Integration of bilateral whisker stimuli in rats: role of the whisker barrel cortices. *Cerebral cortex (New York, N.Y. : 1991)* 12: 86–97, 2002.

Simoncelli EP. Vision and the statistics of the visual environment. *Current Opinion in Neurobiology* 13: 144–149, 2003.

Simons DJ, Woolsey TA. Morphology of Golgi-Cox-impregnated barrel neurons in rat SmI cortex. *The Journal of comparative neurology* 230: 119–32, 1984.

Simons SB, Chiu J, Favorov O V, Whitsel BL, Tommerdahl M. Duration-dependent response of SI to vibrotactile stimulation in squirrel monkey. *Journal of neurophysiology* 97: 2121–9, 2007.

Simons SB, Tannan V, Chiu J, Favorov O V, Whitsel BL, Tommerdahl M. Amplitude-dependency of response of SI cortex to flutter stimulation. *BMC neuroscience* 6: 43, 2005.

Smith PPL, Ratcliff R. Psychology and neurobiology of simple decisions. *Trends in neurosciences* 27: 161–8, 2004.

Sosnik R, Haidarliu S, Ahissar E. Temporal frequency of whisker movement. I. Representations in brain stem and thalamus. *Journal of neurophysiology* 86: 339–53, 2001.

Stanley GB, Jin J, Wang Y, Desbordes G, Wang Q, Black MJ, Alonso J-M. Visual orientation and directional selectivity through thalamic synchrony. *The Journal of neuroscience : the official journal of the Society for Neuroscience* 32: 9073–88, 2012.

Stanley GB, Li FF, Dan Y. Reconstruction of natural scenes from ensemble responses in the lateral geniculate nucleus. *The Journal of neuroscience : the official journal of the Society for Neuroscience* 19: 8036–42, 1999.

Stanley GB. It's not you, it's me. Really. *Nature neuroscience* 12: 374–5, 2009.

Stanley GB. Reading and writing the neural code. *Nature neuroscience* 16: 259–63, 2013.

Steriade M, McCormick DA, Sejnowski TJ. Thalamocortical oscillations in the sleeping and aroused brain. *Science (New York, N.Y.)* 262: 679–85, 1993.

Straube S, Fahle M. Visual detection and identification are not the same: evidence from psychophysics and fMRI. *Brain and cognition* 75: 29–38, 2011.

Stüttgen MC, Rüter J, Schwarz C. Two psychophysical channels of whisker deflection in rats align with two neuronal classes of primary afferents. *The Journal of neuroscience : the official journal of the Society for Neuroscience* 26: 7933–41, 2006.

Stüttgen MC, Schwarz C, Jäkel F. Mapping spikes to sensations. *Frontiers in neuroscience* 5: 125, 2011.

Stüttgen MC, Schwarz C. Psychophysical and neurometric detection performance under stimulus uncertainty. *Nature neuroscience* 11: 1091–9, 2008.

Stüttgen MC, Schwarz C. Integration of vibrotactile signals for whisker-related perception in rats is governed by short time constants: comparison of neurometric and psychometric detection performance. *The Journal of neuroscience : the official journal of the Society for Neuroscience* 30: 2060–9, 2010.

Super H, Roelfsema P. Chronic multiunit recordings in behaving animals: advantages and limitations. *Progress in brain research* 147: 263–282, 2005.

Swadlow H, Gusev A. The impact of "bursting" thalamic impulses at a neocortical synapse. *Nature neuroscience* 4: 402–8, 2001.

Tannan V, Whitsel BL, Tommerdahl MA. Vibrotactile adaptation enhances spatial localization. *Brain research* 1102: 109–16, 2006.

Temereanca S, Brown EN, Simons DJ. Rapid changes in thalamic firing synchrony during repetitive whisker stimulation. *The Journal of neuroscience : the official journal of the Society for Neuroscience* 28: 11153–64, 2008.

Temereanca S, Simons DJ. Local field potentials and the encoding of whisker deflections by population firing synchrony in thalamic barreloids. *Journal of neurophysiology* 89: 2137–45, 2003.

Thomson AM. Neocortical layer 6, a review. *Frontiers in neuroanatomy* 4: 13, 2010.

Tommerdahl M, Favorov O, Whitsel BL. Optical imaging of intrinsic signals in somatosensory cortex. *Behavioural brain research* 135: 83–91, 2002.

Tommerdahl M, Tannan V, Cascio CJ, Baranek GT, Whitsel BL. Vibrotactile adaptation fails to enhance spatial localization in adults with autism. *Brain research* 1154: 116–23, 2007.

Towal R, Quist B, Gopal V. The morphology of the rat vibrissal array: a model for quantifying spatiotemporal patterns of whisker-object contact. *PLoS computational biology* 7, 2011.

Uchida N, Mainen ZF. Speed and accuracy of olfactory discrimination in the rat. *Nature neuroscience* 6: 1224–9, 2003.

Usrey WM, Alonso JM, Reid RC. Synaptic interactions between thalamic inputs to simple cells in cat visual cortex. *The Journal of neuroscience : the official journal of the Society for Neuroscience* 20: 5461–7, 2000.

Vierck CJ, Jones MB. Influences of low and high frequency oscillation upon spatio-tactile resolution. *Physiology & behavior* 5: 1431–5, 1970.

Vincent S. The functions of the vibrissae in the behavior of the white rat. *Behav. Monogr.* 1: 1–85, 1912.

Voigt BC, Brecht M, Houweling AR. Behavioral detectability of single-cell stimulation in the ventral posterior medial nucleus of the thalamus. *The Journal of neuroscience : the official journal of the Society for Neuroscience* 28: 12362–7, 2008.

Wang Q, Millard DC, Zheng HJ V, Stanley GB. Voltage-sensitive dye imaging reveals improved topographic activation of cortex in response to manipulation of thalamic microstimulation parameters. *Journal of neural engineering* 9: 026008, 2012.

Wang Q, Webber RM, Stanley GB. Thalamic synchrony and the adaptive gating of information flow to cortex. *Nature neuroscience* 13: 1534–41, 2010.

Wark B, Lundstrom BN, Fairhall A. Sensory adaptation. *Current opinion in neurobiology* 17: 423–9, 2007.

Webber RM, Stanley GB. Nonlinear encoding of tactile patterns in the barrel cortex. *Journal of neurophysiology* 91: 2010–22, 2004.

Webber RM, Stanley GB. Transient and steady-state dynamics of cortical adaptation. *Journal of neurophysiology* 95: 2923–32, 2006.

Wolfe J, Hill DN, Pahlavan S, Drew PJ, Kleinfeld D, Feldman DE. Texture coding in the rat whisker system: slip-stick versus differential resonance. *PLoS biology* 6: e215, 2008.

Wong-Riley M. Changes in the visual system of monocularly sutured or enucleated cats demonstrable with cytochrome oxidase histochemistry. *Brain research* 171: 11–28, 1979.

Woolsey TA, Van der Loos H. The structural organization of layer IV in the somatosensory region (SI) of mouse cerebral cortex. The description of a cortical field composed of discrete cytoarchitectonic units. *Brain research* 17: 205–42, 1970.

Woolsey TA. Mouse SmI cortex: qualitative and quantitative classification of Golgi-impregnated barrel neurons. *Proceedings of the National Academy of Sciences of the United States of America* 72: 2165–2169, 1975.

Wurtz RH, Goldberg ME, Robinson DL. Brain mechanisms of visual attention. *Sci Am* 246: 124–135, 1982.

Xu Y. Distinctive neural mechanisms supporting visual object individuation and identification. *Journal of cognitive neuroscience* 21: 511–8, 2009.

Yu C, Derdikman D, Haidarliu S, Ahissar E. Parallel thalamic pathways for whisking and touch signals in the rat. *PLoS biology* 4: e124, 2006.

Yu X-J, Xu X-X, He S, He J. Change detection by thalamic reticular neurons. *Nature neuroscience* 12: 1165–70, 2009.